AIRCRAFT CONTROL USING NONLINEAR DYNAMIC INVERSION IN CONJUNCTION WITH ADAPTIVE ROBUST CONTROL

A Thesis

by

JAMES ROBERT FISHER

Submitted to the Office of Graduate Studies of
Texas A&M University
in partial fulfillment of the requirements for the degree of

MASTER OF SCIENCE

December 2004

Major Subject: Mechanical Engineering

AIRCRAFT CONTROL USING NONLINEAR DYNAMIC INVERSION IN CONJUNCTION WITH ADAPTIVE ROBUST CONTROL

A Thesis

by

JAMES ROBERT FISHER

Submitted to Texas A&M University
in partial fulfillment of the requirements
for the degree of

MASTER OF SCIENCE

Approved as to style and content by:

S. Craig Smith (Co-Chair of Committee)	D.V.A.H.G Swaroop (Co-Chair of Committee)
John Valasek (Member)	Dennis O'Neal (Head of Department)

December 2004

Major Subject: Mechanical Engineering

ABSTRACT

Aircraft Control Using Nonlinear Dynamic Inversion in Conjunction with Adaptive Robust Control. (December 2004)

James Robert Fisher, B.S., Texas A&M University

Co–Chairs of Advisory Committee: Dr. S. Craig Smith
Dr. D.V.A.H.G. Swaroop

This thesis describes the implementation of Yao's adaptive robust control to an aircraft control system. This control law is implemented as a means to maintain stability and tracking performance of the aircraft in the face of failures and changing aerodynamic response. The control methodology is implemented as an outer loop controller to an aircraft under nonlinear dynamic inversion control.

The adaptive robust control methodology combines the robustness of sliding mode control to all types of uncertainty with the ability of adaptive control to remove steady state errors. A performance measure is developed in to reflect more subjective qualities a pilot would look for while flying an aircraft. Using this measure, comparisons of the adaptive robust control technique with the sliding mode and adaptive control methodologies are made for various failure conditions. Each control methodology is implemented on a full envelope, high fidelity simulation of the F-15 IFCS aircraft as well as on a lower fidelity full envelope F-5A simulation. Adaptive robust control is found to exhibit the best performance in terms of the introduced measure for several different failure types and amplitudes.

To Marin’

ACKNOWLEDGMENTS

The material in this thesis is based upon work supported by NASA under NGT4-52435. Any opinions, findings, and conclusions or recommendations expressed in this publication are those of the author and do not necessarily reflect the views of NASA.

Thanks are in order for all of the people at NASA Dryden who have served as mentors and have donated their time to aide in this work. They have also allowed the use of their resources as well as their aircraft simulation tools. In particular, I want to thank John Burken for all the time he has spent mentoring me.

I also want to thank my advisor, Dr. Craig Smith. Thank you for helping me broaden my thinking and for helping me learn to always take a step back and truly analyze the problem.

I want to thank my family and friends for all of their support and their prayers and encouragement.

Finally, I have to give thanks to God for the blessings that He has given me. I know that all that I have comes from Him and pray that all that I do is for His glory.

TABLE OF CONTENTS

CHAPTER Page

LIST OF FIGURES

FIGURE Page

FIGURE Page

FIGURE Page

FIGURE Page

FIGURE Page

FIGURE Page

FIGURE Page

CHAPTER I

INTRODUCTION/MOTIVATION

Aircraft control problems pose a unique challenge to a control designer because of the large variation in their dynamics over many different flight conditions as well as their tendency to be non-minimum phase. The performance requirements may vary as functions of flight condition (speed, altitude, etc.) and/or pilot commands. Meeting performance specifications can be particularly challenging when one wants an extremely maneuverable aircraft (e.g. F-15). A common method of dealing with the variations in dynamics and performance objectives is to schedule the controller using relevant parameters. Dynamic Inversion (DI) is a form of feedback linearization used to force a nonlinear system to behave linearly from a synthetic input to a desired output. This allows the designer of an outer control loop to treat the aircraft under DI control as one linear system over the entire flight envelope (in many cases a system of decoupled integrators).

For an aircraft under dynamic inversion control, modeling errors and component failures lead to a departure from nominal behavior. In such a case the response of the aircraft under dynamic inversion control alone is unpredictable. Though a pilot may be able to maintain level flight, attempting a maneuver may cause loss of control due to an unexpected transient response of the aircraft due to a pilot command. An additional outer control loop can be designed to deal with failures and mismatch in the dynamic inversion control law.

There are many approaches that seek to add robustness to the dynamic inversion control law. These emphasize either achieving steady state performance or transient performance. For the discussion in this thesis, the term *transient performance* will refer to the exponential convergence of the tracking error of the system to zero. Techniques such as

---

This thesis follows the style and format of *IEEE Transactions on Automatic Control.*

neural networks or adaptive control are concerned with asymptotic command tracking performance. Typically, there are no guarantees on the rate of convergence to the commanded trajectory. This lack of a guaranteed convergence rate often translates to sluggish responses or undamped oscillation, hindering maneuverability. The other end of the spectrum involves techniques such as sliding mode control which emphasize rate of convergence of the actual response to the commanded response, or what will be referred to as transient performance. This type of control can have the same drawbacks as linear high gain control when applied to a system with actuator rate and position limits.

Adaptive robust control is utilized as a means to control the aircraft in the presence of modeling uncertainties and actuator failures. This control combines the transient performance of sliding mode control with the steady state performance of adaptive control methods.

CHAPTER II

BACKGROUND

Gain scheduling has proven to be a successful approach to controlling aircraft over a large range of operating conditions. Many approaches schedule the parameters of a linear controller based on measured variables such as Mach number, angle-of-attack, or dynamic pressure. This can be accomplished by linear interpolation between pre-computed controllers. Methods such as Linear Parameter Varying Control (LPV) allow continuous dependence of the control law on the scheduling parameters [1, 2]. Dynamic Inversion may also be used to schedule control actions. The dynamics of an aircraft can be represented by the following dynamic differential equation:

$$\dot{x} = f(x,t,\Gamma) + g(x,t,\Gamma)\,u \qquad\qquad x \in \mathbb{R}^{n\times 1},\ u \in \mathbb{R}^{p\times 1},\ (p > n) \tag{II.1}$$

The vector x represents aircraft states and u represents a vector of control inputs. Only the case where $p > n$ will be considered, although many aircraft have $p = n$ or even $p < n$. The vector Γ consists of measurements including flight condition and states which are not control variables. A control of the following form may be used to render the system dynamics unobservable and set the input/output behavior to that of decoupled integrators.

$$u = \bar{g}^{\dagger}(x,t,\Gamma)\left[\dot{x}_d - \bar{f}(x,t,\Gamma)\right] \tag{II.2}$$

In the above expression, $\bar{g}(x,t,\Gamma)$ and $\bar{f}(x,t,\Gamma)$ indicate the best approximations of $g(x,t,\Gamma)$ and $f(x,t,\Gamma)$ respectively. The $(\cdot)^{\dagger}$ term indicates the generalized inverse. The desired state evolution is given by x_d (work done on creating designs for this desired evolution is described by [3]). Further information on choosing states for inversion and designing the dynamic inversion controller can be found in [4]. If the system is modeled perfectly,

$f(x,t,\Gamma) = \bar{f}(x,t,\Gamma)$. The input-output dynamics will be:

$$\dot{x} = \dot{x}_d \tag{II.3}$$

In aircraft models, sources of uncertainty may arise due to imprecise knowledge of aerodynamic coefficients, damaged or ineffective control surfaces, etc. In the presence of such modeling errors, an expression such as the following can be used to describe the system including the control from Equation (II.2).

$$\dot{x} = \tilde{f}(x,t,\Gamma) + \tilde{g}(x,t,\Gamma)\dot{x}_d \tag{II.4}$$

Where $\tilde{g} = g(x,t,\Gamma)\bar{g}^{\dagger}(x,t,\Gamma)$ and $\tilde{f} = f(x,t,\Gamma) - \tilde{g}(x,t,\Gamma)\bar{f}(x,t,\Gamma)$. If control authority over an actuator is lost, the resulting mismatch between modeled and observed behavior can be attributed to an additional disturbance (denoted Δ below).

$$\dot{x} = \tilde{f}(x,t,\Gamma) + \tilde{g}(x,t,\Gamma)\dot{x}_d + \Delta(x,t,\Gamma,\dot{x}_d) \tag{II.5}$$

A variety of approaches deal with the problem of uncertain (and nonlinear) aircraft dynamics as well as failures. In the literature, two approaches seem to dominate. A common approach is to detect a failure and then respond with a precalculated control. This research is usually devoted to detecting failures or precalculating responses given a detection. Once the fault has been identified, there are various approaches to dealing with the problem. In [5], with knowledge of which actuator is failed, two approaches are taken. In one approach, a servomechanism problem is solved for each failure case and the controller is switched based on what has failed. In the other approach, an adjustment to the control is calculated based upon the difference between the dynamic models of the healthy and faulty aircraft. An optimization problem is solved online to find the adjusted control which minimizes the difference in behavior from that of the healthy aircraft.

Another approach to dealing with actuator failures is to create a control that provides

robust tracking response in the face of failures without any type of “reconfiguration” or failure detection. This will be the focus of the proposed research. A variety of methodologies have been employed. Interest has been shown in the usage of adaptive Neural Nets [6, 7, 8] whereby a network adds robustness to the dynamic inversion control law. The neural network uses data about the system to “learn” the inversion errors (for example $\tilde{f}$ and $\tilde{g}$ in Equation (II.4)). Robustness of the scheme to unmodeled dynamics is addressed in [9]. While this neural network approach is considered an adaptive approach, more traditional adaptive approaches have been taken in [10, 11]. A structured adaptive model inversion approach to dealing with failures is discussed in [12]. Traditional adaptive approaches assume uncertainty lies only in the magnitude of the parameters in the model (which are assumed to be constant). If the magnitude of these parameters vary, or there is uncertainty that has not been modelled, there is no guarantee that the control will stabilize the aircraft. There are also no clear guarantees on the rate of convergence to a commanded trajectory. This could potentially limit the maneuverability of the aircraft.

Sliding Mode Control (SMC) has also been used to address the problem. This control requires less information about the model structure, only bounds on uncertainties. Sliding mode control has been used to account for modeling uncertainties and actuator failures in [13, 14, 15, 16, 17, 18]. Sliding mode control exhibits incredible robustness to all types of uncertainty. To compensate for uncertainty and reject constant disturbances, SMC must be high gain, which can result in saturation of actuator rate and position limits.

CHAPTER III

PROBLEM FORMULATION

A. Aircraft Equations of Motion

This thesis will be concerned with the application of control methodologies to the aircraft control problem. These problems provide a unique challenge to a control designer because of the large variation in their dynamics over many different flight conditions. Aircraft by nature behave nonlinearly, making traditional linear control designs suitable only over small regions. Aircraft behavior also exhibits strong coupling between the three axes of rotation, further reducing the range over which linear approximations hold. This issue will be discussed in more detail later in this document. The aircraft dynamic models themselves are not the only source of nonlinearity in the problem. Implementing controls on a real aircraft requires consideration of other factors, namely rate and position limits on the actuators. These are present for reasons such as preventing the excitation of structural modes, preserving structural integrity of the aircraft (i.e. preventing surfaces from being damaged), and limits on the performance of the actuators themselves. These limits have a large impact on performance of the aircraft and severely restrict the control strategies that one is able to employ. Destabilizing and limit-cycle behavior can result from strategies that are too "high gain". It is the opinion of the author that the rate and position limits on an aircraft are the most significant inhibitors to any control strategy.

Two models of an aircraft will be utilized in this thesis. In its most general form, an aircraft can be modeled by the following differential equation.

$$\begin{aligned} \dot{x} &= f(t,x,\nu,\Gamma) \\ y &= h(t,x,\Gamma) \end{aligned} \tag{III.1}$$

In the above expression, $x \in \mathbb{R}^n$ represents the states of the aircraft, $y \in \mathbb{R}^m$ is a vector containing the states of interest, $\nu \in \mathbb{R}^p$ is a vector of controls, and $\Gamma \in \mathbb{R}^l$ is a vector containing additional parameters that influence the equations of motion. This vector may also contain the states of unmodeled dynamics. A more specific representation for the dynamics is given by:

$$\begin{aligned} \dot{x} &= f(t,x,\Gamma) + g(t,x,\Gamma)\nu \\ y &= h(t,x,\Gamma) \end{aligned} \tag{III.2}$$

In the above expression, $f\colon \mathbb{R} \times \mathbb{R}^n \times \mathbb{R}^l \mapsto \mathbb{R}^n$, $g\colon \mathbb{R} \times \mathbb{R}^n \times \mathbb{R}^l \mapsto \mathbb{R}^{n \times p}$, and $h\colon \mathbb{R} \times \mathbb{R}^n \times \mathbb{R}^l \mapsto \mathbb{R}^m$. In this representation, the evolution of the state is affine with respect to the control. This will become useful when we begin to look at the implementation of a dynamic inversion controller. The first form is included because the controller implementations that will be discussed are not restricted to systems of the class in III.2, but apply to a broader class of systems that are described by III.1. More assumptions about the dimensionality of these vectors will be discussed in Section VII along with the implementation of the dynamic inversion.

B. Failure Modeling

The response of a system in the presence of a failure is one of the largest motivations for the current research. For simulation purposes, the control schemes being tested will have no knowledge of a failure. No control reconfiguration will be utilized. For example, if two actuators are being commanded, the control scheme will attempt to command the same two actuators in the same manner both before and after the failure. The outer loop control schemes will seek to account for the map of the failure location and plant control reconfiguration as it maps through the DI inner loop control. It is important to clarify

the different types of failures that will be addressed and how these will be modeled in simulation.

1. Loss of surface effectiveness

This type of failure can occur when an aircraft is damaged by enemy fire or if part of a surface is removed from a collision. Essentially, a loss of surface failure results in the effectiveness of the surface declining. If half of the stabilator is missing for example, the achievable control moment is reduced by a percentage. The damaged surface is still operaable (if it does not go completely missing), but it's effectiveness is reduced. This will be modeled in simulation by reducing the moment induced by the surface by a certain percentage. This failure mode will be the easiest for the control methodologies to handle, so it warrants only a small amount of discussion.

2. Floating actuator

A floating actuator failure occurs when control of an actuator is lost and it begins to move based on parameters other than the pilot command. For this case, not only is control authority over the actuator lost, but a disturbance is induced based on some other variable. For the discussion in this thesis, the case where a stabilator begins to vary with α (angle-of-attack) will be considered. This type of failure will only be considered briefly for the F-5A aircraft as well as for the linearized F-15 aircraft model. The modeling of this failure will be accomplished by commanding the left or right stabilator actuator with the angle-of-attack of the aircraft after the failure time. Of the failure types considered, this type of failure is the most difficult for the controllers to handle. Not only must the control perform in the face of a large modelling uncertainty, but it must also deal with a time varying disturbance.

3. Hard-over failure

Hard-Over failures will receive the most attention in this work, partially because these types of failures were the initial motivation of the research. This type of failure occurs when an actuator fails to respond to actuator commands, moves to some set position, and locks in place. Often, the actuator will lock in its current position at the time of the failure. In this work, the actuator will be commanded to some final position (not necessarily at trim) and remain locked there for the duration of the maneuver. This is much more difficult for the control scheme to handle than a “lock-in-place” failure, so this is the type of failure which will be considered. To model this, at the time of the failure the actuator will be commanded to a set failure position and remain there. This type of failure will result in a constant disturbance on the system proportional to the failure amplitude.

CHAPTER IV

ADAPTIVE CONTROL

The behavior of dynamic systems are usually modelled using a set of ordinary differential equations. The dynamics of the actual system may correspond closely to that of the model, but errors will always exist. These errors may be the result of unmodelled dynamics and/or inaccuracies in the model parameters. In this way, the uncertainty may be of known form, or it may not. The adaptive control methodology is geared toward handling inaccuracies in the parameters of the model, or uncertanties that take on known form. Adaptive control was initially developed as a means to deal with large parameter variations in aircraft [19]. Since its development it has branched into many other areas such as robotic manipulation, power systems, and process control. The objective of this scheme is to dynamically adjust the magnitudes of known model parameters in such a way that the "true" representation of the system will result.

The systems expressed in Section III may have a known description, but modelling errors such as those previously described may be inherent. To begin our discussion of the adaptive control laws, let us begin by assuming the system described by (III.1) has the following form.

$$\dot{x} = f(t,x,\Gamma,\nu) = \varphi(t,x,\Gamma)\,\vartheta + \nu + \Delta(t,x,\Gamma,\nu) \tag{IV.1}$$

For the purposes of this section, we assume that the output of the system is the state, x ($y = x$ in (III.1)). The variable, $\vartheta \in \mathbb{R}^a$, is a vector of parameters. These are assumed to be constant, or at the worst, slowly varying with time. The function,
$\varphi(t,x,\Gamma) : \mathbb{R} \times \mathbb{R}^n \times \mathbb{R}^l \mapsto \mathbb{R}^{n\times a}$, will be designated as a *regressor*. A disturbance term, $\Delta(t,x,\Gamma,\nu) : \mathbb{R} \times \mathbb{R}^n \times \mathbb{R}^l \times \mathbb{R}^m \mapsto \mathbb{R}^n$, is included as well. The regressor (φ) is made up of a series of functions that describe the evolution of the states. As an illustrative example,

consider the differential equation,

$$\dot{x} = \theta_1 x + \theta_2 \sin(\omega x) \tag{IV.2}$$

The regressor is given by the following:

$$\varphi(t,x,\omega) = \begin{bmatrix} x & \sin(\omega x) \end{bmatrix} \tag{IV.3}$$

The parameter vector, ϑ, given by $\begin{bmatrix} \theta_1 & \theta_2 \end{bmatrix}^T$ in the previous example, is made up of the (generally unknown) magnitudes of the shape function elements. For the purposes of this paper, we will denote the uncertainties of this form as *parametric uncertainties*. All of the unknown dynamics and disturbances are lumped in the $\Delta(t,x,\Gamma,\nu)$ term. These may include the effects of a failure on the aircraft or higher frequency behavior for example. Uncertainties in the dynamics that arise from this term will be defined as *unstructured uncertainties*.

A conventional adaptive control law that addresses the above problem will now be discussed [19, 20]. For our discussion of adaptive control, we will assume that there are no unmodelled dynamics or disturbances ($\Delta = 0$). Define x_d as a signal that it is desired for output of the system in (IV.1) to track. Define $e = x - x_d$ as the tracking error between the desired state trajectory and the actual states. Consider the following control law (notation adapted from [21]):

$$\begin{aligned} \nu &= \nu_{fa} + \nu_{sa} \\ \nu_{fa} &= \dot{x}_d(t) - \varphi(t,x,\Gamma)\,\hat{\vartheta} \\ \nu_{sa} &= -ke \end{aligned} \tag{IV.4}$$

The $\hat{\vartheta}$ term is an estimated value of the true parameter value ϑ. The update law providing the value for $\hat{\vartheta}$ is given below. The ν_{fa} portion of the control law contains the adaptive in-

version of the dynamics and their replacement with desired dynamics ($\dot{x}_d$). The ν_{sa} portion of the control contains error feedback which will help ensure assymptotic stability.

$$\dot{\hat{\vartheta}} = \gamma\varphi(t,x,\Gamma)^T e \qquad\qquad \gamma > 0 \tag{IV.5}$$

In this way, the estimated parameter is adjusted based on the error between the actual state and the desired state trajectories. The *learning rate*, or the sensitivity of the estimated parameter to the tracking error can be adjusted via the positive definite γ matrix.

Theorem IV.1 *Using the adaptive control law given by Equation (IV.4) and the update law given by Equation (IV.5) the output of the system in Equation (IV.1) with* $\Delta(t,x,\Gamma,\nu) = 0$ *tracks the desired output,* x_d*, asymptotically, i.e.,* $e \to 0$ *as* $t \to \infty$*.*

Proof: If we substitute Equation (IV.4) into Equation (IV.1), the following error dynamics result:

$$\dot{e} + ke = -\varphi(t,x,\Gamma)\,\tilde{\vartheta} \tag{IV.6}$$

To asses the stability of the control law, we use the following positive definite function as a Lyapunov candidate function, where $\tilde{\vartheta} \triangleq \hat{\vartheta} - \vartheta$.

$$V_a = \frac{1}{2}e^T e + \frac{1}{2}\tilde{\vartheta}^T\gamma^{-1}\tilde{\vartheta} \tag{IV.7}$$

The time derivative of this funtion is given below.

$$\dot{V}_a = e^T\left[-ke - \varphi(t,x,\Gamma)\,\tilde{\vartheta}\right] + \tilde{\vartheta}^T\gamma^{-1}\dot{\tilde{\vartheta}} \tag{IV.8}$$

Using the update law given in Equation (IV.5), we arrive at

$$\dot{V}_a = -e^T ke \tag{IV.9}$$

This implies that $e \in \mathcal{L}_2 \cap \mathcal{L}_\infty$. Furthermore, we can make the assumption that $\Gamma \in \mathcal{L}_\infty \cap \mathcal{L}_2$ since $e \in \mathcal{L}_\infty \cap \mathcal{L}_2$. This allows us to conclude that $\hat{\vartheta} \in \mathcal{L}_\infty$. Thus, $\dot{e}$ is uniformly

continuously bounded, which allows us to conlude that $e \rightarrow 0$ asymptotically (as a result of Barbalat's Lemma [19]). $\triangle$

Theorem IV.2 *Under the conditions of Theorem IV.1, if a trajectory satisfies the following Persistence of Excitation (PE) condition, where T, t_0, and ε_p are some positive scalars, then the estimated parameter, $\hat{\vartheta}$, in (IV.4) converges to its true value ($\tilde{\vartheta} \rightarrow 0$ as $t \rightarrow \infty$).*

$$\int_t^{t+T} \varphi(\tau, x_d(\tau), \Gamma(\tau))\, \varphi(\tau, x_d(\tau), \Gamma(\tau))^T\, d\tau \geq \varepsilon_p I \tag{IV.10}$$

Proof: While this theorem is important, the PE condition may be tough to verify for nonlinear systems, and is therefore not utilized in this thesis. The interested reader should see proof in Sastry [22]. $\triangle$

These theorems show the ability of the adaptive control law given in Equation (IV.4) to guarantee asymptotic tracking of the desired input signal. It is important to note that no guarantees have been made (in this work) for adaptive control in the presence of the unstructured uncertainty term, $\Delta(t, x, \Gamma, \nu)$. This will become crucial in the implementation of the controller in later sections.

CHAPTER V

SLIDING MODE CONTROL (SMC)

Sliding mode control (also known as Deterministic Robust Control) is another means to address the uncertainties that arise in the system given in (IV.1). Unlike the adaptive control implemntation discussed above, SMC does not contain dynamic feedback. In other words, the control response does not depend directly on the time history, but simply on the current values of certain signals. In this section, we will be concerned with the implementation of this control methodologies on the type systems presented in Equation (IV.1).

The backbone of the SMC methodology is the *sliding surface*. The sliding surface is defined by a stable transfer function that relates the tracking error, e, to some filtered error term, z. In other words, the surface is the solution of a stable differential equation in terms of the error. The control will depend on this filtered tracking error term. Before we go into more depth on this subject, we will define our sliding surface. As mentioned previously, in the system given by (IV.1), it is desired that the output variable, x, should track a reference $x_d(t)$. Again, define the tracking error, $e = x(t) - x_d(t)$. Auxillary variables x_c, z, y_c, and x_r are defined as follows:

x_c : filter states

x_r : filtered reference

z : filtered error

$$\begin{aligned} \dot{x}_c &= A_c x_c + B_c e & & x_c \in \mathbb{R}^{n_c}, A_c \in \mathbb{R}^{n_c \times n_c}, B_c \in \mathbb{R}^{n_c} \\ z &= C_c x_c + e = y_c + e & & C_c \in \mathbb{R}^{1 \times n_c} \\ &= x - x_r & & x_r \stackrel{\triangle}{=} x_d(t) - y_c \end{aligned} \tag{V.1}$$

The system given by (A_c, B_c, C_c) is a filter for the tracking error. The sliding surface is described by the stable solution to the differential equation, $z = 0$. A filtered version of

the reference command x_d is given by x_r. This will constitute the feedforward portion of the control. Its form is important for proving the stability of the system. The dynamics on the sliding surface are designed using (A_c, B_c, C_c). The transfer function from e to z has relative degree zero, meaning that tracking errors affect the SMC without delay. This is also important in any real implementation of sliding mode control. In the traditional SMC implementation (for example, that described by [19]), a structure such as the following is used to describe the stable differential equation which defines the sliding surface.

$$z = \left(\frac{d}{dt} + \lambda\right)^n e \tag{V.2}$$

Implementing this control in practice relies on the availability of nth order derivative information. Usually, this requires taking numerical derivatives of signals which can result in large amounts of noise. Using a filter implementation such as that in (V.1) prevents the usage of approximate derivative information which means it does not have the drawback of the noise that arises from taking the derivative of a signal. The purpose of the filtered reference command signal, x_r, will be made clear when we begin proving the stability of the control law.

We can put the sliding surface in transfer function form.

$$T_{ze} = \left(I_n + C_c\left(sI_{n_c} - A_c\right)^{-1} B_c\right) e \tag{V.3}$$

Where I_{n_c} is the identity matrix of dimension $n_c \times n_c$. The control problem will be framed in terms of the filtered error term, z, defined above. The objective of the control will be to force the output of the transfer function, T_{ze} to be zero. Once this "surface" is achieved, the stable filter guarantees that the tracking error will be forced to zero as well. Many approaches can be taken to the design of T_{ze}. This transfer function can be designed so that the system response has a desirable convergence rate for example. Design of T_{ze} can also be carried out in terms of its inverse, T_{ze}. This is possible since the transfer function

has relative degree zero. For example, the design can be carried out so that high frequency changes in z do not affect e, but low frequency changes do. This can be very helpful since sliding mode control is known to be "high gain". Further study of the design process of a sliding mode controller is conducted in [13].

Now that a sliding surface has been designed, we must now select a control law that will drive the response of the system onto the surface and therefore achieve track the desired signal. But before we do this, we must place a few limitations on the system. We must make the following assumptions about ϑ and $\Delta(t,x,\Gamma,\nu)$ from (IV.1). If we denote $\vartheta = \begin{bmatrix} \vartheta_1 & \vartheta_2 & \cdots & \vartheta_a \end{bmatrix}^T$ and $\Delta(t,x,\Gamma,\nu) = \begin{bmatrix} \Delta_1 & \Delta_2 & \cdots & \Delta_n \end{bmatrix}^T$

$$\begin{aligned} \vartheta_i \in \Omega_{\vartheta_i} &\triangleq \left\{ \vartheta_i : \vartheta_{min,i} \leq \vartheta_i \leq \vartheta_{max,i} \right\} \\ \left| \Delta_i(t,x,\Gamma,\nu) \right| &\leq \delta_i(t,x) \end{aligned} \tag{V.4}$$

These assumptions essentially place bounds on the amount of uncertainty that is present in the system. Specifically, $\delta_i(t,x)$ is a bounded function of time such that $\delta_i(t,x) \in \mathcal{L}_\infty$ when $x(t) \in \mathcal{L}_\infty$. We will find later that the stability of the system requires these bounds being met. These bounds can also be thought of as a measure of the robustness of the control to the magnitude of the disturbances and uncertainties.

A control law that can achieve stability (and performance) in the presence of uncertaintes in the above form is given by the following:

$$\begin{aligned} \nu &= \nu_f + \nu_s \\ \nu_f &= \dot{x}_r - \varphi(t,x,\Gamma)\,\hat{\vartheta} \\ \nu_s &= -kz - h(t,x,\Gamma)\,\mathrm{sgn}(z) \end{aligned} \tag{V.5}$$

Essential to this control law are the assumptions that there exists a bound on the uncertainty and that this bound is known (i.e. $h(t,x,\Gamma)$ is known. In the above control law, $\hat{\vartheta}$ is the best

estimate of the vector ϑ. The function, $\operatorname{sgn}(z)$ is the signum function operating elementwise on z. In other words, when $z_i > 0$, $\operatorname{sgn}(z)_i = 1$, when $z_i < 0$, $\operatorname{sgn}(z)_i = -1$, and when $z_i = 0$, $\operatorname{sgn}(z)_i = 0$. The ν_f portion of the control can be thought of as a feedforward portion of the control, and the ν_s portion can be thought of as the feedback portion. This is not entirely true as $\dot{x}_r$ depends on the tracking error. Finally, some assumptions need to be made about the function $h(t,x,\Gamma)$. This function is a *bounding function* that must meet the following requirement.

$$h(t,x,\Gamma) \geq \left| -\varphi(t,x,\Gamma)\tilde{\vartheta} + \Delta(t,x,\Gamma,\nu) \right| \tag{V.6}$$

Again, define $\tilde{\vartheta} \triangleq \hat{\vartheta} - \vartheta$ as the error in the estimated parameter vector. A simple choice of h is the following:

$$h(t,x,\Gamma) = \left|\varphi(t,x,\Gamma)\right| (\vartheta_{max} - \vartheta_{min}) + \delta(t,x) \tag{V.7}$$

where $\vartheta_{max} \triangleq \begin{bmatrix} \vartheta_{1,max} & \vartheta_{2,max} & \cdots & \vartheta_{a,max} \end{bmatrix}^T$ and ϑ_{min} is defined similarly. Chosing h in this way may be simple, but overly conservative as it is a worst case estimate. A variety of other choices can be made so long as the requirement in (V.6) is met.

Now that the control law has been defined and the groundwork laid, the following theorems will provide stability and performance information regarding the choice of control law. One important point must be made before continuing. For methods such as Lyapunov's Direct Method, the evolution of the state is required to be continuously differentiable. While it is common in practice for control laws such as the one given in (V.5) to be used and stability proved via Lyapunov, it is important to note that strictly speaking this methodology makes this assumption.

Theorem V.1 *The control law given in (V.5) guarantees that the system given in (IV.1) tracks the desired input exponentially with respect to time.*

Proof: Choose the following postive definite Lyapunov function:

$$V_s = \frac{1}{2} z^T z \tag{V.8}$$

The time derivative of this function is given by:

$$\begin{aligned} \dot{V}_s &= z^T \left[-\varphi(t,x,\Gamma)\,\tilde{\vartheta} + \Delta(t,x,\Gamma) - kz - h(t,x,\Gamma)\,\mathrm{sgn}(z) \right] \\ &\leq |z^T| \left| -\varphi(t,x,\Gamma)\,\tilde{\vartheta} + \Delta(t,x,\Gamma) \right| - z^T kz - h(t,x,\Gamma)\,|z| \\ &\leq -z^T kz \end{aligned} \tag{V.9}$$

In the above expressions, the operation $|\cdot|$ is elementwise when operating on a vector. This proves that z is exponentially stable. Exponential stability of z implies exponential stability of the tracking error, e. $\triangle$

The above control law (V.5), while stabilizing the response of the system, is discontinuous across the sliding surface as a result of the $\mathrm{sgn}(z)$ term. This can lead to chattering in the response. In the aircraft control problem, this can lead to instability due to rate limiting. The result of the chattering coupled with the rate limiting is a limit-cycle behavior. This can lead to instability and what is called PIO (pilot-induced-oscillations) [23]. The response is very undesirable for performance as well as for a pilot. As a result, the discontinuous portion of the control, $\mathrm{sgn}(z)$, is replaced with a different function $\mu\left(h(t,x,\Gamma),z\right)$. This gives us the following updated control law.

$$\begin{aligned} \nu &= \nu_f + \nu_s \\ \nu_f &= \dot{x}_r - \varphi(t,x,\Gamma)\,\hat{\vartheta} \\ \nu_s &= -kz - \mu\left(h(t,x,\Gamma),z\right) \end{aligned} \tag{V.10}$$

Theorem V.2 *If the control law given in (V.10) is applied, the tracking error converges exponentially and has some guaranteed transient performance and final tracking accuracy.*

Proof: Substituing the control law in (V.10) into (IV.1), we obtain the following error dynamics.

$$\dot{z} = -kz - \mu\left(h\left(t,x,\Gamma\right),z\right) - \varphi\left(t,x,\Gamma\right)\tilde{\vartheta} + \Delta\left(t,x,\Gamma\right) \tag{V.11}$$

We can again use the same Lyapunov function from above, $V_s\left(t\right) = \frac{1}{2}z^T z$ The time derivative of this function is given by

$$\dot{V}_s \leq \left|z^T\right|\left|-\varphi\left(t,x,\Gamma\right)\tilde{\vartheta} + \Delta\left(t,x,\Gamma\right)\right| - z^T kz - z^T\mu\left(h\left(t,x,\Gamma\right),z\right) \tag{V.12}$$

Before we can go any further, we must make the following assumptions.

$$\begin{array}{ll} \text{i.} & z^T\mu\left(h\left(t,x,\Gamma\right),z\right) \geq 0 \\ \text{ii.} & \left|z^T\right|h\left(t,x,\Gamma\right) - z^T\mu\left(h\left(t,x,\Gamma\right),z\right) \leq \varepsilon(t) \end{array} \tag{V.13}$$

Using the above assumptions, we arrive at the following:

$$\begin{aligned} \dot{V}_s &\leq \left|z^T\right|h\left(t,x,\Gamma\right) - z^T kz - z^T\mu\left(h\left(t,x,\Gamma\right),z\right) \\ \dot{V}_s &\leq -z^T kz + \varepsilon(t) \end{aligned} \tag{V.14}$$

If we use $-z^T kz \leq -\lambda_{min}(k)z^T z$, where $\lambda_{min}(k)$ is the smallest eigenvalue of the matrix k, then the above expression simplifies to the following.

$$\dot{V}_s \leq -2\lambda_{min}(k)V_s + \varepsilon(t) \tag{V.15}$$

We can integrate this expression to get the following result.

$$\begin{aligned} V_s(t) &\leq e^{-2\lambda_{min}(k)t}V_s(0) + \int_0^t \exp -2\lambda_{min}(k)\left(t-\tau\right)\varepsilon\left(\tau\right)d\tau \\ V_s(t) &\leq e^{-2\lambda_{min}(k)t}V_s(0) + \frac{\varepsilon_{max}}{2\lambda_{min}(k)}\left[1 - e^{-2\lambda_{min}(k)t}\right] \end{aligned} \tag{V.16}$$

This implies that the system converges exponentially to the region where $z^T z \leq \frac{\varepsilon_{max}}{\lambda_{min}(k)}$. This region is called a *boundary layer*. There are no guarantees about the behavior of the

system inside the boundary layer. The final tracking error can be freely adjusted by tuning the controller parameters ε and k. $\triangle$

The SMC law allows the control designer to not only guarantee stability, but guarantee exponential convergence to the sliding surface. In this sense, SMC allows the designer to have performance guarantees. The function, $\mu(h(t,x,\Gamma),z)$ can be selected in a variety of ways. In most of the literature, the $\text{sgn}(\cdot)$ function is replaced with a $\text{sat}(\cdot)$ (saturation) function [13, 14, 15, 16, 17, 18, 21, 24]. The saturation function ($\text{sat}(z)$) can be defined as follows.

$$\text{sat}(z) = \begin{cases} 1 & z > 1 \\ z & -1 \leq z \leq 1 \\ -1 & z < -1 \end{cases} \tag{V.17}$$

To create a continuous (but still nonlinear) control law, we use the following μ.

$$\mu\left(h(t,x,\Gamma),z\right) = h(t,x,\Gamma)\,\text{sat}\left(\frac{z}{\varepsilon}\right) \tag{V.18}$$

This function causes the controller to behave linearly in some region around the sliding surface, $z \leq \varepsilon(t)$. Outside of this region, the controller performs exactly as it would if it contatined a signum function.

CHAPTER VI

ADAPTIVE ROBUST CONTROL (ARC)

The motivation for using Adaptive Robust Control in a particular application is to achieve a combination of the transient performance and robustness of sliding mode control (Section V) with the steady state error guarantees of adaptive control (Section IV). When the adaptive control law presented previously is employed, it may suffer from parameter drift and may become unstable in the presence of disturbances and measurement noise if certain PE conditions are not satistfied [25]. In addition, the stability of a system under adaptive control is not guaranteed in the face of unmodeled dynamics and disturbances. Several modifications can be made that give guarantees in the face of disturbances. These usually guarantee boundedness in the mean squared sense with respect to various parameters. Discussion of these methods as well as references to their discussion in literature can be found in [20]. The form of the adaptive law presented stabilizes the system in the presence of parametric uncertainties, but makes no guarantees in the face of unstructured uncertainty. Sliding mode control is still able to guarantee the stability of the system in the face of both types of uncertainty. This quality makes it desirable for use in the systems that this thesis will address. Furthermore, using SMC, a measure of the speed of convergence of the system is provided as well. The two major drawbacks to SMC are the high gains needed to acheive good tracking accuracy as well as the requirement that the magnitude of the uncertainty have an upper bound (note: the bound may not necessarily be constant). As mentioned previously, the high gains required to acheive accuracy may be detrimental to performance due to the aircraft's actuator rate limits. If some form of parameter adaption can be included as part of the SMC, this might help to improve tracking accuracy without the requirement of resorting to higher gains.

Adaptive Robust Control (ARC) as outlined by Yao [21] is a marriage of sliding mode

control to adaptive control. The result is a control law that maintains the robustness properties of SMC to all types of uncertainty with the ability of adaptive control to adapt to parametric uncertainties. The methodology starts with SMC as a backbone and adds on a parameter adaptation law. In order to accomplish this, a few conflicts must be resolved. Sliding mode control requires the system uncertainties to be bounded (see equation (V.4)). In order to ensure exponential stability, the parameter estimates generated by the adaptation law must be bounded. This should not hinder the ability of the adaptive law to converge to the true estimates if the PE condition is satisfied. In order to meet this boundedness requirement we assume that the true value of the estimated parameter $\vartheta_i \in \Omega_{\vartheta_i} \stackrel{\triangle}{=} [\vartheta_{i,min}, \vartheta_{i,max}]$ (in general, Ω_{ϑ_i} must be convex). With this in mind, we introduce the following projection map.

$$\vartheta_{\pi i} = \begin{cases} \vartheta_i & \vartheta_i \in \Omega_{\vartheta_i} \\ \vartheta_{i,max} & \vartheta_i > \vartheta_{i,max} \\ \vartheta_{i,min} & \vartheta_i < \vartheta_{i,min} \end{cases} \tag{VI.1}$$

This map differs from [21, 24]. We are not concerned about the projection being smooth because we will only be addressing systems with relative degree one.

The adaptive robust control law which ensures the convergence of the system given by Equation (IV.1) to the sliding surface ($z = 0$) is given below.

$$\begin{aligned} \nu &= \nu_s + \nu_a \\ \nu_a &= \dot{x}_r - \varphi(t,x)\,\hat{\vartheta}_\pi \\ \nu_s &= -kz - \mu\left(h(t,x,\Gamma),z\right) \end{aligned} \tag{VI.2}$$

The ν_s portion of the control can be thought of as the sliding mode portion, providing stability in the face of disturbances and transient performance guarantees (through selection of k) [21]. The ν_a term is the adaptive portion of the control law. It consists of an approximate inversion of the dynamics, $\varphi(t,x,\Gamma)\,\hat{\vartheta}_\pi$, as well as feedforward control, $\dot{x}_r$. If

$\hat{\vartheta}_\pi$ is replaced with a nominal approximation or best guess for ϑ, SMC is recovered. The vector $\hat{\vartheta}_\pi = \begin{bmatrix} \hat{\vartheta}_{\pi 1} & \hat{\vartheta}_{\pi 2} & \cdots & \hat{\vartheta}_{\pi a} \end{bmatrix}^T$ where the function $(\cdot)_{\pi i}$ denotes the elementwise projection mapping discussed above.

As discussed in section V, $h(t,x,\Gamma)$ must meet certain requirements. For the control law given in (VI.2), the following requirement is placed on h.

$$h(t,x,\Gamma) \geq \left|\varphi(t,x,\Gamma)\left(\vartheta - \hat{\vartheta}_\pi\right) + \Delta(t,x,\Gamma\nu)\right| \tag{VI.3}$$

These requirement requires uncertainty to be bounded and for this bound to be known. A simple choice for $h(t,x,\Gamma)$ which will ensure that the above bound is met is the following

$$h(t,x,\Gamma) = \left|\varphi(t,x,\Gamma)\right|(\vartheta_{max} - \vartheta_{min}) + \delta(t,x) \tag{VI.4}$$

where the function $|\cdot|$ operates elementwise on the vector (or matrix) $\varphi(t,x,\Gamma)$.

The function $\mu\left(h(t,x,\Gamma),z\right)$ is the effective sliding mode portion of the control. If $\mu(h,z) = h(t,x,\Gamma)\,\mathrm{sgn}(z)$, one is assuming infinitely fast switching and a discontinous control law (standard SMC). A continuous approximation may be made for the signum function, resulting in $\mu(h,z) = h(t,x,\Gamma)\,\mathrm{sat}(z/\varepsilon)$.

The evolution of the parameter estimates will be governed by the following parameter update law.

$$\dot{\hat{\vartheta}} = \gamma\varphi(t,x,\Gamma)^T z \tag{VI.5}$$

This update law is essentially the same as that found in (IV.5). The ARC update law is driven by the value of the filtered error, z, as opposed to depending on e directly. We are now ready to examine the properties of the control law.

Theorem VI.1 *In the presence of parametric uncertainties only, ($\Delta(t,x,\Gamma,\nu) = 0$), the control law given in (VI.2) along with the update law given by (VI.5) regulates the tracking error, e, to zero. In other words, the ARC control law forces the system in (IV.1) to be*

uniformly asymptotically stable with respect to e.

Proof: We start by defining the following Lyapunov function:

$$V_t = \frac{1}{2} z^T z + V_\vartheta\left(\vartheta, \hat{\vartheta}\right) \tag{VI.6}$$

Let

$$V_\vartheta\left(\vartheta, \hat{\vartheta}\right) = \sum_{i=1}^{a} \gamma_i^{-1} \int_0^{\tilde{\vartheta}_i} \left((\vartheta_i + \tau)_\pi - \vartheta_i\right) d\tau \tag{VI.7}$$

As a consequence, the following is true.

$$\frac{\partial}{\partial \tilde{\vartheta}_i} V_\vartheta\left(\vartheta, \hat{\vartheta}\right) = \gamma^{-1}\left(\hat{\vartheta}_{\pi i} - \vartheta_i\right) \tag{VI.8}$$

Now we can begin to examine the stability of the system. Define $\tilde{\vartheta}_\pi \stackrel{\triangle}{=} \hat{\vartheta}_\pi - \vartheta$ as the error between the value of ϑ projected onto Ω_ϑ. We start by finding an expression for $\dot{z}$.

$$\dot{z} = -kz - \varphi(t,x,\Gamma)\,\tilde{\vartheta}_\pi - \mu\left(h(t,x,\Gamma), z\right) + \Delta(t,x,\Gamma,\nu) \tag{VI.9}$$

Taking the time derivative of V_t yields.

$$\dot{V}_t = z^T\left[-kz - \varphi(t,x,\Gamma)\,\tilde{\vartheta}_\pi - \mu\left(h(t,x,\Gamma), z\right) + \Delta(t,x,\Gamma,\nu)\right] + \tilde{\vartheta}_\pi^T \gamma^{-1} \dot{\tilde{\vartheta}} \tag{VI.10}$$

where the matrix, γ, is a square matrix given by $\gamma = \mathtt{diag}\begin{bmatrix} \gamma_1 & \gamma_2 & \cdots & \gamma_a \end{bmatrix}$. As is done in adaptive control, assuming slowly varying ϑ parameters, we set $\dot{\tilde{\vartheta}} = \dot{\hat{\vartheta}}$. Assuming $\Delta = 0$ and utilizing the update law in (VI.5), we arrive at the following.

$$\begin{aligned} \dot{V}_t &= -z^T kz - z^T \mu\left(h(t,x,\Gamma), z\right) \\ &\leq -z^T kz \end{aligned} \tag{VI.11}$$

A similar argument to that used in Theorem IV.1 is used to show stability here. Positive definiteness of V_t and negative definiteness of $\dot{V}_t$ implies that it has a limit as $t \to \infty$, $\tilde{\vartheta}_\pi \in \mathcal{L}_\infty$, and that $z \in \mathcal{L}_\infty \cap \mathcal{L}_2$ (It is not necessary to show that $\tilde{\vartheta}_\pi \in \mathcal{L}_\infty$ because it is bounded

by definition). In turn, from (VI.9) it can be shown that $\dot{z} \in \mathcal{L}_\infty$. Therefore, from Barbalat's Lemma, $z \to 0$ as $t \to 0$. $\triangle$

This result has the same impact as that of Theorem IV.1. Now we examine the stability of the system in the presence of disturbances ($\Delta \neq 0$).

Theorem VI.2 *The control law given in (VI.2), when applied to (IV.1), regulates tracking error to within some boundary layer region around $z = 0$ in the presence of unstructured uncertainty ($\Delta \neq 0$) given some restrictions on $h(t,x,\Gamma)$.*

Proof: We can utilize the same V_s from Theorem V.2.

$$V_s = \frac{1}{2} z^T z \tag{VI.12}$$

Taking the time derivative of this Lyapunov function yields.

$$\dot{V}_s = z^T \dot{z} = z^T \left(-kz - \varphi(t,x,\Gamma)\,\tilde{\vartheta}_\pi - \mu\left(h(t,x,\Gamma),z\right) + \Delta(t,x,\Gamma,\nu) \right) \tag{VI.13}$$

As in Theorem V.2, assumptions about $h(t,x,\Gamma)$ must be satisfied.

$$\begin{aligned} &\text{i.} \quad z^T \mu\left(h(t,x,\Gamma),z\right) \geq 0 \\ &\text{ii.} \quad \left|z^T\right| \left| -\varphi(t,x,\Gamma)\,\tilde{\vartheta}_\pi + \Delta(t,x,\Gamma,\nu) \right| - z^T \mu\left(h(t,x,\Gamma),z\right) \leq \varepsilon(t) \end{aligned} \tag{VI.14}$$

We can use this information to simplify $\dot{V}_s$.

$$\dot{V}_s \leq -z^T k z + \left|z^T\right| \left| -\varphi(t,x,\Gamma)\,\tilde{\vartheta}_\pi + \Delta(t,x,\Gamma,\nu) \right| - z^T \mu\left(h(t,x,\Gamma),z\right) \tag{VI.15}$$

Using the above assumptions, the above expression simplifies to the following.

$$\dot{V}_s \leq -z^T k z + \varepsilon(t) \tag{VI.16}$$

Integrate this expression arrives at the following result (See Theorem V.2).

$$V_s(t) \leq e^{-2\lambda_{min}(k)t} V_s(0) + \frac{\varepsilon_{max}}{2\lambda_{min}(k)} \left[1 - e^{-2\lambda_{min}(k)t} \right] \tag{VI.17}$$

This implies that the system converges exponentially to the boundary layer region where $z^T z \leq \frac{\varepsilon_{max}}{\lambda_{min}(k)}$. As with sliding mode control, there are no guarantees about the behavior of the system inside the boundary layer. The final tracking error can be freely adjusted by tuning the controller parameters ε and k. $\triangle$

This theorem is important because it shows that stability is guaranteed even in the presence of unstructured uncertainty. Theorem VI.2 shows that the tracking error of the system decays exponentially to some boundary layer region regardless of the nature of the uncertainty in the system. Theorem VI.1 shows that if there is no unstructured uncertainty present in the system, the tracking error will not only decay to some boundary layer exponentially, but will assymptotically decay to zero inside of this boundary layer. If the form of a disturbance is known and it can be included as part of the parametric uncertainty set, then ARC can regulate tracking error to within a boundary layer exponentially, and to zero assymptotically. It is simple to extend this theorem to the case where $\mu(h(t,x,\Gamma),z) = h(t,x,\Gamma)\,\mathrm{sgn}(z)$.

CHAPTER VII

DYNAMIC INVERSION CONTROL

Dynamic inversion control (DI) is a form of feedback linearization that can be employed to render the dynamics of a system (both linear and nonlinear) unobservable. If the exact form of a system of dynamic equations is known, and all states can be measured, a controller can be formulated to make the input-output behavior of the system that of a set of integrators.

We start our discussion of Dynamic Inversion by outlining feedback linearization theory. The discussion will center around theory presented by Khalil [26]. We start by making some assumptions about the system given in (III.2). First, to simplify the discussion, we assume that there is no explicit dependence of y on time. In addition, there will be no dependence of y on Γ. We define the new system:

$$\begin{aligned} \dot{x} &= f(t,x,\Gamma) + g(t,x,\Gamma)\nu \\ y &= h(x) \end{aligned} \tag{VII.1}$$

Furthermore, the discussion in this section will be centered on systems that have relative degree one. In terms of the system given by (VII.1):

$$\frac{\partial h}{\partial x} g(t,x,\Gamma) \neq 0 \tag{VII.2}$$

This condition ensures that the input is present in the derivative of the output. For a single-input-single-output system, this is the only condition needed to ensure that the system is relative degree one. For a system with multiple inputs and outputs, there are a few more conditions that must be satisfied.

- $\frac{\partial h}{\partial x} g(t,x,\Gamma)$ must be square
- $\frac{\partial h}{\partial x} g(t,x,\Gamma)$ must be full rank $\forall\, t,x,\Gamma$

To place further restrictions on the systems to be considered, we use a state transformation for x and Γ. Before doing this, we define the new state variable $\bar{x} = \begin{bmatrix} x & \Gamma \end{bmatrix}^T$ so that:

$$\dot{\bar{x}} = \begin{bmatrix} \dot{x} \\ \dot{\Gamma} \end{bmatrix} = \begin{bmatrix} f(t,x,\Gamma) \\ f_1(t,x,\Gamma) \end{bmatrix} + \begin{bmatrix} g(t,x,\Gamma) \\ g_1(t,x,\Gamma) \end{bmatrix} \nu = \bar{f}(t,x,\Gamma) + \bar{g}(t,x,\Gamma)\nu \qquad \text{(VII.3)}$$

The functions f_1 and g_1 describe the evolution of the parameter states. These functions will not be necessary for the DI control, but they will be important in analyzing the properties of the control law. To formulate the control law and begin examining the stability, we start with the following state transformation.

$$z = T(\bar{x}) = \begin{bmatrix} \phi_1(x,\Gamma) \\ \vdots \\ \phi_{n-p}(x,\Gamma) \\ h(x) \end{bmatrix} = \begin{bmatrix} \eta \\ \xi \end{bmatrix} \qquad \text{(VII.4)}$$

where $\eta = \begin{bmatrix} \phi_1(x,\Gamma) & \cdots & \phi_{n-p}(x,\Gamma) \end{bmatrix}^T$ and $\xi = h(x)$. The function $h(x)$ in the transformation causes the outputs to become states of the system. The functions $\phi_i(x,\Gamma)$ are selected so that

$$\frac{\partial \phi_i}{\partial \bar{x}} \bar{g}(t,x,\Gamma) = 0 \quad \forall i = 1,\ldots,n-p \qquad \text{(VII.5)}$$

This state transformation allows us to rewrite our state equations in terms of the new variables. We start by examining the time derivative of η.

$$\begin{aligned} \dot{\eta} &= \frac{\partial \phi}{\partial \bar{x}} \dot{\bar{x}} \qquad \text{(VII.6)} \\ &= \frac{\partial \phi}{\partial \bar{x}} \left[\bar{f}(t,x,\Gamma) \right] \end{aligned}$$

Thus, the η vector is selected so that the input does not show up in its first derivative. If we

compute the time derivative of ξ, we arrive at the following.

$$\begin{aligned} \dot{\xi} &= \frac{\partial h}{\partial \bar{x}} \dot{\bar{x}} \\ &= \frac{\partial h}{\partial \bar{x}} \bar{f}(t,x,\Gamma) + \frac{\partial h}{\partial \bar{x}} \bar{g}(t,x,\Gamma)\,\nu \end{aligned} \tag{VII.7}$$

We know that h is a function of x only, so $\frac{\partial h}{\partial \bar{x}} = \begin{bmatrix} \frac{\partial h}{\partial x} & 0 \end{bmatrix}^T$. Thus, the expression above simplifies to.

$$\begin{aligned} \dot{\xi} &= \frac{\partial h}{\partial x} f(t,x,\Gamma) + \frac{\partial h}{\partial x} g(t,x,\Gamma)\,\nu \\ &= A\xi + \gamma(t,x,\Gamma)\,[\nu - \alpha(t,x,\Gamma)] \end{aligned} \tag{VII.8}$$

where

$$\begin{aligned} \alpha(t,x,\Gamma) &\triangleq \left(\frac{\partial h}{\partial x} g(t,x,\Gamma)\right)^{-1} f(t,x,\Gamma) \\ \gamma(t,x,\Gamma) &\triangleq \frac{\partial h}{\partial x} g(t,x,\Gamma) \end{aligned} \tag{VII.9}$$

The matrix $A \in \mathbb{R}^{p\times p}$ is the zero matrix. This gives us what is refered to as the *normal form*. It has been developed by many different authors, but the presentation in this thesis will follow that of Khalil [26, 27, 28, 29, 30].

$$\begin{aligned} \dot{\eta} &= \frac{\partial \phi}{\partial \bar{x}} \left[\bar{f}(t,x,\Gamma)\right] \\ \dot{\xi} &= A\xi + \gamma(t,x,\Gamma)\,[\nu - \alpha(t,x,\Gamma)] \\ y &= \xi \end{aligned} \tag{VII.10}$$

Note that in Khalil, the definition is more general and includes cases where the relative degree of the system is more than one.

The goal of the dynamic inversion control law is to let the A matrix be the governing input-output dynamics of the system. By selecting the proper control law we can “zero”

the other dynamics of the system leaving only integrator dynamics. The control law that accomplishes this is given by:

$$\nu = \alpha(t,x,\Gamma) + \gamma^{-1}(t,x,\Gamma)\,\rho \tag{VII.11}$$

The result of the application of this control law (with no modeling errors) is the following:

$$\dot{\xi} = \rho \tag{VII.12}$$

In order for this control law to be useful, we must also guarantee internal stability. Thus we define *zero dynamics* as the dynamics of the system given by

$$\dot{\eta} = \frac{\partial \phi}{\partial \bar{x}}\left[\bar{f}(t,x,\Gamma)\right]\Big|_{x,\Gamma=T^{-1}(z_0)} \tag{VII.13}$$

where $z_0 = \begin{bmatrix} \phi_1 & \cdots & \phi_{n-p} & 0 \end{bmatrix}^T$. If these dynamics are stable, then the system is said to be minimum phase. This coupled with the conditions presented earlier guarantee that the control law will stabilize the system given a proper ρ as defined in (VII.11). This generalized dynamic inversion control law can now be applied to a linearized aircraft model as well as a full nonlinear aircraft model.

A. Pitch Axis Example

In this section, the application of dynamic inversion to an aircraft problem is demonstrated for a single input single output (SISO) system. For this example, the pitch axis will be considered. A dynamic model for an aircraft can be put into the form described in Section VI. A block diagram showing how the control would be implemented on the pitch axis (including the ARC) is given in Figure VII.1. Linear dynamic models are considered for simplicity in this section. For small variations around a single trimmed flight condition, the

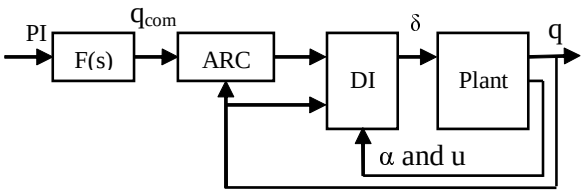

Fig. VII.1. ARC Implementation on Aircraft Pitch Axis

longitudinal dynamics of an aircraft can be modeled as follows.

$$\begin{bmatrix} \dot{u} \\ \dot{\alpha} \\ \dot{q} \end{bmatrix} = A_q \begin{bmatrix} u \\ \alpha \\ q \end{bmatrix} + B_q \delta_e \qquad y = C_q \begin{bmatrix} u \\ \alpha \\ q \end{bmatrix} = q \tag{VII.14}$$

In the above expression, the state variables u, α, and q represent the velocity of the aircraft along the body axis x-direction, the aircraft angle-of-attack, and the body axis pitch rate. It is assumed that there is a one dimensional synthetic control, δ_e, which will be allocated to the pitch actuators (for the F-15 IFCS aircraft it is the stabilators only). The stick input is considered as the source of a pitch rate command. In this example, it is desired to control the pitch rate, q, of the aircraft. The synthetic elevator input for the DI controller is given by:

$$\delta_e = \left(C_q \hat{B}_q\right)^{\dagger} \left(\dot{q}_{des} - C_q \hat{A}_q \begin{bmatrix} u \\ \alpha \\ q \end{bmatrix} \right) \tag{VII.15}$$

In the above expression, $\hat{B}_q$, $\hat{A}_q$ are the nominal values of B_q and A_q respectively. The $(\cdot)^{\dagger}$ function is used to represent a generalized inverse. The control requires feedback of u, q, and α. Measurements for q and α are easily obtained, but this may not be the case for u.

In practice, the short period approximation can be used to eliminate u at the expense of inversion error.

The dynamic inversion control (with respect to the dynamics of q) given in (VII.15) applied to the system with dynamics given by Equation (VII.14), results in the following dynamic equations for the closed loop.

$$\dot{q} = C_q \left(A_q - B_q \left(C_q \hat{B}_q \right)^{\dagger} C_q \hat{A}_q \right) \begin{bmatrix} u \\ \alpha \\ q \end{bmatrix} + C_q B_q \left(C_q \hat{B}_q \right)^{\dagger} \dot{q}_{des} \tag{VII.16}$$

For the SISO case, $C_q \in \mathbb{R}^{1\times 3}$ and $\hat{B}_q \in \mathbb{R}^{3\times 1}$. The resulting product is a scalar and is therefore invertable provided $\hat{B}_q$ is not in the null space of C_q. Furthermore, if the plant is modeled perfectly ($\hat{B}_q = B_q$ and $\hat{A}_q = A_q$), the expression simplifies to the following:

$$\begin{aligned} \dot{q} &= \left(C_q A_q - C_q B_q \left(C_q B_q \right)^{-1} C_q A_q \right) \begin{bmatrix} u \\ \alpha \\ q \end{bmatrix} + C_q B_q \left(C_q B_q \right)^{-1} \dot{q}_{des} \qquad \text{(VII.17)} \\ &= \left(C_q A_q - C_q A_q \right) \begin{bmatrix} u \\ \alpha \\ q \end{bmatrix} + \dot{q}_{des} \\ &= \dot{q}_{des} \end{aligned}$$

Thus for the pitch axis, the DI control law results in the dynamics of q being that of an integrator. This will not be the case in the presence of either modeling errors or disturbances. Modeling errors ($A_q \neq \hat{A}_q$, $B_q \neq \hat{B}_q$, etc.) result in governing (closed loop) equations of the form:

$$\dot{q} = \theta_u u + \theta_\alpha \alpha + \theta_q q + \theta_{\dot{q}_{des}} \dot{q}_{des} \tag{VII.18}$$

where θ_u, θ_α, θ_q, and $\theta_{\dot{q}_{des}}$ depend on the modeling errors. If the aircraft were to experience

an actuator failure where an actuator became unresponsive we might model the closed loop as the following:

$$\dot{q} = \theta_u u + \theta_\alpha \alpha + \theta_q q + \theta_{\dot{q}_{des}} \dot{q}_{des} + \Delta(t) \tag{VII.19}$$

where $\Delta(t)$ is a disturbance term resulting from non-symmetric actuator response.

In flight, variations in q generally have larger amplitude than those of α or u. Additionally, in the face of a constant exogenous disturbance such as a stuck control surface, we will have a new non-zero equilibrium point in terms of the states α and u (q will track a reference command). Define the new trim points as α_t and u_t. Let $\tilde{\alpha} = \alpha - \alpha_t$ and $\tilde{u} = u - u_t$. Now define

$$\theta_u u + \theta_\alpha \alpha = \theta_c + \theta_u \tilde{u} + \theta_\alpha \tilde{\alpha} \tag{VII.20}$$

Where $\theta_c = \theta_u u_t + \theta_\alpha \alpha_t$. This allows us to model the unknown constant perturbation as part of our regressor. The $\theta_u \tilde{u}$ and $\theta_\alpha \tilde{\alpha}$ terms can be used to capture the perturbations from the new trim. As an example consider a stuck stabilitor. This stuck control surface will result in more drag on the aircraft. For the aircraft to maintain a pitch rate of 0 deg/s the angle of attack, α, and velocity, u, must now differ from their trims to account for this new disturbance. The dynamics can be expressed as follows:

$$\begin{aligned} \dot{q} &= \theta_q q + \theta_c + \theta_u \tilde{u} + \theta_\alpha \tilde{\alpha} + \dot{q}_{des} + \left(\theta_{\dot{q}_{des}} - 1\right) \dot{q}_{des} + \Delta(t) \\ &= \theta_q q + \theta_c + \dot{q}_{des} + \Delta\left(t, \dot{q}_{des}, \tilde{\alpha}, \tilde{u}\right) \end{aligned} \tag{VII.21}$$

The regressor associated with the parameter vector $\begin{bmatrix} \theta_q & \theta_c \end{bmatrix}^T$ (denoted as $\varphi(x,t)$ in Equation (IV.1)) for the longitudinal dynamics is $\begin{bmatrix} q & 1 \end{bmatrix}$. From this point, the three methods described previously, adaptive control, sliding mode control, and adaptive robust control, can be applied.

B. MIMO DI

The analysis performed in Section A is good only for a single flight condition. As the aircraft moves away from the operating point, the modeling errors in the DI law become larger. It is therefore important to alter the dynamic inversion law parameters with the flight condition. This can be accomplished by scheduling linear models around a series of flight conditions. While this can be effective, it requires the determination of many factors such as the spacing between operating points, the scheduling parameters, and then of course the interpolation between models. The dynamics of an aircraft are well known and the nonlinear behavior it exhibits can be modeled fairly accurately. This knowledge can be used to nonlinearly invert the dynamics of the aircraft. The rotational equations of motion for an aircraft can be represented by the following differential equations of motion [31].

$$\begin{bmatrix} \dot{p} \\ \dot{q} \\ \dot{r} \end{bmatrix} = \begin{bmatrix} \frac{1}{I_{zz}I_{xx}-I_{xz}^2}\left(I_{xz}N + I_{zz}L + I_{xz}\left(I_{xx}+I_{zz}-I_{yy}\right)pq + \left(\left(I_{yy}-I_{zz}\right)I_{zz}-I_{xz}^2\right)qr\right) \\ \frac{1}{I_{yy}}\left(M + \left(I_{zz}-I_{xx}\right)pr + I_{xz}\left(r^2-p^2\right)\right) \\ \frac{1}{I_{xx}I_{zz}-I_{xz}^2}\left(I_{xz}L + I_{xx}N + \left(\left(I_{xx}-I_{yy}\right)I_{xx}+I_{xz}^2\right)pq + I_{xz}\left(I_{yy}-I_{xx}-I_{zz}\right)qr\right) \end{bmatrix} \tag{VII.22}$$

where

$$\begin{aligned} \frac{L}{\bar{q}Sb} &= C_{l\beta}\beta + C_{lp}\left(\frac{pb}{2U}\right) + C_{lr}\left(\frac{rb}{2U}\right) + C_{l\delta_a}\delta_a + C_{l\delta_r}\delta_r \\ \frac{M}{\bar{q}S\bar{c}} &= C_{mu}u + C_{m\alpha}\alpha + C_{mq}\left(\frac{q\bar{c}}{2U}\right) + C_{m\delta_e}\delta_e \\ \frac{N}{\bar{q}Sb} &= C_{n\beta}\beta + C_{np}\left(\frac{pb}{2U}\right) + C_{nr}\left(\frac{rb}{2U}\right) + C_{n\delta_a}\delta_a + C_{n\delta_r}\delta_r \end{aligned} \tag{VII.23}$$

The $C_{(\cdot)}$ terms are aerodynamic coefficients. These are nonlinear functions of the flight condition and are usually found by collecting wind tunnel data and/or flight test data. The terms S, b, and $\bar{c}$ are positive constants corresponding to aircraft geometry parameters. The $\bar{q}$ term is the dynamic pressure and U is the speed at which the aircraft is travelling.

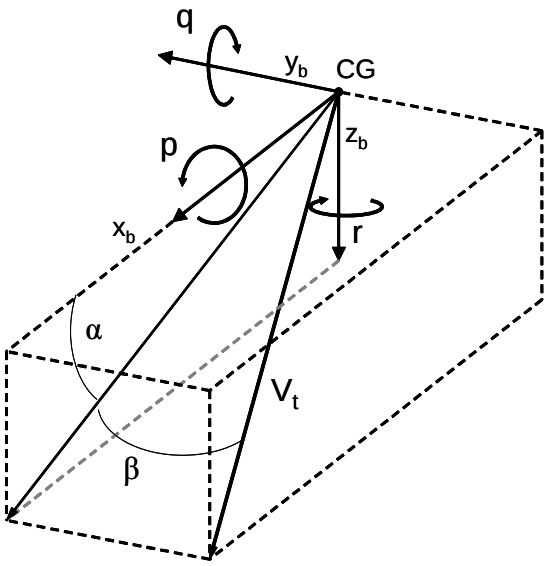

Fig. VII.2. Diagram of the aircraft body axis coordinate system along with angular rotation rates, angle-of-attack (α), and sideslip angle (β)

The $\delta_{(.)}$ terms are control moments induced by displacement of the control surfaces of the aircraft. The variables *p*, *q*, and *r* represent the roll, pitch, and yaw rates of the aircraft (see figure VII.2). These are the angular rotation rates expressed in the body axis coordinate frame as displayed in figure VII.2 (adapted from [12]). The point of origin of the coordinate system in figure VII.2 is the center of mass of the aircraft. The figure also shows the velocity vector of the center of mass of the aircraft in the body frame (V_t) and how angle-of-attack and sideslip angle are measured in terms of this velocity vector.

The terms in Equation (VII.22) can be used to invert the inherent rotational dynamics and "replace" them with the desired rotational dynamics. Figure VII.3 shows a block diagram of this implementation. The preprocessor, or $F(s)$, takes pilot stick commands and converts them to $\dot{p}$, $\dot{q}$, and $\dot{r}$ reference signals. The evolution of the remaining states can be modeled by a set of differential equations which are not included here [31].

To simplify the representation of the dynamics of the aircraft, define the following

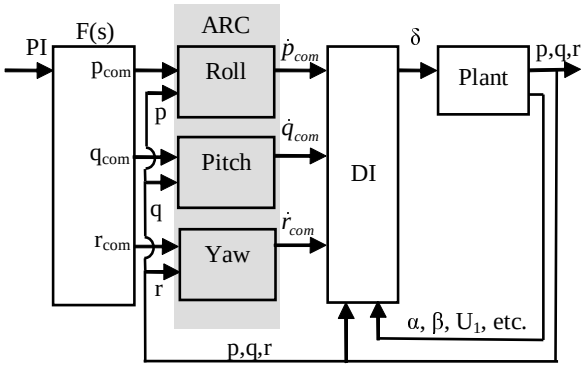

Fig. VII.3. ARC Implementation on 6-DOF Aircraft

quantities for the roll and yaw axes:

$$
\begin{aligned}
C_{p\beta} &= \frac{\bar{q}Sb\left(I_{xz}C_{n\beta}+I_{zz}C_{l\beta}\right)}{I_{zz}I_{xx}-I_{xz}^2} & C_{r\beta} &= \frac{\bar{q}Sb\left(I_{xx}C_{n\beta}+I_{xz}C_{l\beta}\right)}{I_{zz}I_{xx}-I_{xz}^2}\\
C_{pp} &= \frac{\bar{q}Sb^2\left(I_{xz}C_{np}+I_{zz}C_{lp}\right)}{2U\left(I_{zz}I_{xx}-I_{xz}^2\right)} & C_{rp} &= \frac{\bar{q}Sb^2\left(I_{xx}C_{np}+I_{xz}C_{lp}\right)}{2U\left(I_{zz}I_{xx}-I_{xz}^2\right)}\\
C_{pr} &= \frac{\bar{q}Sb^2\left(I_{xz}C_{nr}+I_{zz}C_{lr}\right)}{2U\left(I_{zz}I_{xx}-I_{xz}^2\right)} & C_{rr} &= \frac{\bar{q}Sb^2\left(I_{xx}C_{nr}+I_{xz}C_{lr}\right)}{2U\left(I_{zz}I_{xx}-I_{xz}^2\right)}\\
C_{p\delta_a} &= \frac{\bar{q}Sb\left(I_{xz}C_{n\delta_a}+I_{zz}C_{l\delta_a}\right)}{I_{zz}I_{xx}-I_{xz}^2} & C_{r\delta_a} &= \frac{\bar{q}Sb\left(I_{xx}C_{n\delta_a}+I_{xz}C_{l\delta_a}\right)}{I_{zz}I_{xx}-I_{xz}^2}\\
C_{p\delta_r} &= \frac{\bar{q}Sb\left(I_{xz}C_{n\delta_r}+I_{zz}C_{l\delta_r}\right)}{I_{zz}I_{xx}-I_{xz}^2} & C_{r\delta_r} &= \frac{\bar{q}Sb\left(I_{xx}C_{n\delta_r}+I_{xz}C_{l\delta_r}\right)}{I_{zz}I_{xx}-I_{xz}^2}\\
I_{p1} &= \frac{I_{xz}\left(I_{xx}+I_{zz}-I_{yy}\right)}{I_{zz}I_{xx}-I_{xz}^2} & I_{p2} &= \frac{\left(\left(I_{yy}-I_{zz}\right)I_{zz}-I_{xz}^2\right)}{I_{zz}I_{xx}-I_{xz}^2}\\
I_{r1} &= \frac{\left(\left(I_{xx}-I_{yy}\right)I_{xx}+I_{xz}^2\right)}{I_{zz}I_{xx}-I_{xz}^2} & I_{r2} &= -I_{p1}
\end{aligned}
\qquad \text{(VII.24)}
$$

Similarly, we define the following for the pitch axis.

$$\begin{aligned} C_{q\alpha} &= \frac{1}{I_{yy}}\bar{q}S\bar{c}C_{m\alpha} \\ C_{qu} &= \frac{1}{I_{yy}}\bar{q}S\bar{c}C_{mu} \\ C_{qq} &= \frac{\bar{q}S\bar{c}^2C_{mq}}{2UI_{yy}} \\ C_{q\delta_e} &= \frac{1}{I_{yy}}\bar{q}S\bar{c}C_{m\delta_e} \\ I_{q1} &= \frac{I_{zz}-I_{xx}}{I_{yy}} \\ I_{q2} &= \frac{I_{xz}}{I_{yy}} \end{aligned} \tag{VII.25}$$

These quantities allow us to write the following rotational equations of motion for the aircraft.

$$\begin{bmatrix} \dot{p} \\ \dot{q} \\ \dot{r} \end{bmatrix} = \begin{bmatrix} C_{p\beta}\beta + C_{pp}p + C_{pr}r + I_{p1}pq + I_{p2}qr \\ C_{qu}u + C_{q\alpha}\alpha + C_{qq}q + I_{q1}pr + I_{q2}\left(r^2 - p^2\right) \\ C_{r\beta}\beta + C_{rp}p + C_{rr}r + I_{r1}pq + I_{r2}qr \end{bmatrix} + \begin{bmatrix} C_{p\delta_a} & 0 & C_{p\delta_r} \\ 0 & C_{q\delta_e} & 0 \\ C_{r\delta_a} & 0 & C_{r\delta_r} \end{bmatrix} \begin{bmatrix} \delta_a \\ \delta_e \\ \delta_r \end{bmatrix} \tag{VII.26}$$

This representation will be important for examining the implementation of the various outer loop control schemes previously mentioned. The dynamics needed for inversion (p, q, and r) can be simplified and represented by the following.

$$\begin{aligned} \dot{x} &= A(x,y) + B(x,y)\,\delta \\ x &= \begin{bmatrix} p & q & r \end{bmatrix}^T \end{aligned} \tag{VII.27}$$

The variable, y, is made up of the other state variables whose dynamic equations of motion are not explicitly utilized in the inversion (α, β, etc).

The objective of the DI inner loop is to control the values of p, q, and r. The controls come in the form of the δ vector which are synthetic control commands for roll, pitch, and

yaw. These synthetic controls are then allocated to the actuators. In our example, this is done through a static control allocation of the form.

$$\bar{\delta} = T\delta \tag{VII.28}$$

The actual surface commands are the elements of the $\bar{\delta}$ vector. The control allocation (be it static or dynamic) must be included as part of $B(x,y)$. $B(x,y) \in \mathbb{R}^{3\times 3}$ is invertible. As the true values for the coefficients $C_{p\beta}, C_{r\beta}, C_{q\delta_e}$, etc. are not known, they can be approximated with the estimates $\bar{C}_{p\beta}, \bar{C}_{r\beta}, \bar{C}_{q\delta_e}$, etc. These estimates are functions of the estimates of the aerodynamic coefficients, aircraft parameters such as S and b, and inertia value estimates. These terms make up the estimates of $A(x,y)$ and $B(x,y)$ given by $\hat{A}(x,y)$ and $\hat{B}(x,y)$ respectively. The dynamic inversion control law given in more general terms in (VII.11) takes the form:

$$\delta_{des} = \hat{B}(x,y)^{-1}\left(\dot{x}_{des} - \hat{A}(x,y)\right) \tag{VII.29}$$

where $\dot{x}_{des} = [\dot{p}_{des}, \dot{q}_{des}, \dot{r}_{des}]^T$. If $\hat{A}(x,y) = A(x,y)$ and $\hat{B}(x,y) = B(x,y)$, it follows that

$$\dot{x} = \dot{x}_{des} \tag{VII.30}$$

However, if this is not the case

$$\dot{x} = A(x,y) - B(x,y)\hat{B}(x,y)^{-1}\hat{A}(x,y) + B(x,y)\hat{B}(x,y)^{-1}\dot{x}_{des} \tag{VII.31}$$

At this stage it is difficult to see how this model can be put into the form given in (IV.1).

This will be accomplished utilizing (VII.26). To simplify things,

$$
\begin{aligned}
B\hat{B}^{-1} &= \begin{bmatrix} C_{p\delta_a} & 0 & C_{p\delta_r} \\ 0 & C_{q\delta_e} & 0 \\ C_{r\delta_a} & 0 & C_{r\delta_r} \end{bmatrix} \begin{bmatrix} \frac{\bar{C}_{r\delta_r}}{\bar{C}_{p\delta_a}\bar{C}_{r\delta_r}-\bar{C}_{p\delta_r}\bar{C}_{r\delta_a}} & 0 & -\frac{\bar{C}_{p\delta_r}}{\bar{C}_{p\delta_a}\bar{C}_{r\delta_r}-\bar{C}_{p\delta_r}\bar{C}_{r\delta_a}} \\ 0 & \frac{1}{\bar{C}_{q\delta_e}} & 0 \\ -\frac{\bar{C}_{r\delta_a}}{\bar{C}_{p\delta_a}\bar{C}_{r\delta_r}-\bar{C}_{p\delta_r}\bar{C}_{r\delta_a}} & 0 & \frac{\bar{C}_{p\delta_a}}{\bar{C}_{p\delta_a}\bar{C}_{r\delta_r}-\bar{C}_{p\delta_r}\bar{C}_{r\delta_a}} \end{bmatrix} \\
&= \begin{bmatrix} \frac{C_{p\delta_a}\bar{C}_{r\delta_r}-C_{p\delta_r}\bar{C}_{r\delta_a}}{\bar{C}_{p\delta_a}\bar{C}_{r\delta_r}-\bar{C}_{p\delta_r}\bar{C}_{r\delta_a}} & 0 & \frac{C_{p\delta_a}\bar{C}_{p\delta_r}-C_{p\delta_r}\bar{C}_{p\delta_a}}{\bar{C}_{p\delta_a}\bar{C}_{r\delta_r}-\bar{C}_{p\delta_r}\bar{C}_{r\delta_a}} \\ 0 & \frac{C_{q\delta_e}}{\bar{C}_{q\delta_e}} & 0 \\ \frac{C_{r\delta_a}\bar{C}_{r\delta_r}-C_{r\delta_r}\bar{C}_{r\delta_a}}{\bar{C}_{p\delta_a}\bar{C}_{r\delta_r}-\bar{C}_{p\delta_r}\bar{C}_{r\delta_a}} & 0 & \frac{C_{r\delta_a}\bar{C}_{p\delta_r}-C_{r\delta_r}\bar{C}_{p\delta_a}}{\bar{C}_{p\delta_a}\bar{C}_{r\delta_r}-\bar{C}_{p\delta_r}\bar{C}_{r\delta_a}} \end{bmatrix}
\end{aligned}
\tag{VII.32}
$$

From the above expression, it follows that if the $\bar{C}_{(\cdot)}$ terms are exactly equal to the $C_{(\cdot)}$ terms, the above matrix will be the Identity Matrix. When there are modelling errors in the parameters, the matrix can be expressed as the following.

$$
B(x,y)\hat{B}(x,y)^{-1} = \begin{bmatrix} \tilde{B}_{11} & 0 & \tilde{B}_{13} \\ 0 & \tilde{B}_{22} & 0 \\ \tilde{B}_{31} & 0 & \tilde{B}_{33} \end{bmatrix} \tag{VII.33}
$$

Next we examine the $B(x,y)\hat{B}(x,y)^{-1}\hat{A}(x,y)$ term.

$$
B\hat{B}^{-1}\hat{A} = \begin{bmatrix} \tilde{B}_{11} & 0 & \tilde{B}_{13} \\ 0 & \tilde{B}_{22} & 0 \\ \tilde{B}_{31} & 0 & \tilde{B}_{33} \end{bmatrix} \begin{bmatrix} \bar{C}_{p\beta}\beta + \bar{C}_{pp}p + \bar{C}_{pr}r + \bar{I}_{p1}pq + \bar{I}_{p2}qr \\ \bar{C}_{qu}u + \bar{C}_{q\alpha}\alpha + \bar{C}_{qq}q + \bar{I}_{q1}pr + \bar{I}_{q2}\left(r^2 - p^2\right) \\ \bar{C}_{r\beta}\beta + \bar{C}_{rp}p + \bar{C}_{rr}r + \bar{I}_{r1}pq + \bar{I}_{r2}qr \end{bmatrix} \tag{VII.34}
$$

Now, we make the following definitions.

$$\begin{aligned}
\hat{C}_{p(\cdot)} &= \tilde{B}_{11}\bar{C}_{p(\cdot)} + \tilde{B}_{13}\bar{C}_{r(\cdot)} \\
\hat{I}_{p(\cdot)} &= \tilde{B}_{11}\bar{I}_{p(\cdot)} + \tilde{B}_{13}\bar{I}_{r(\cdot)} \\
\hat{C}_{q(\cdot)} &= \tilde{B}_{22}\bar{C}_{q(\cdot)} \\
\hat{I}_{q(\cdot)} &= \tilde{B}_{22}\bar{I}_{q(\cdot)} \\
\hat{C}_{r(\cdot)} &= \tilde{B}_{31}\bar{C}_{p(\cdot)} + \tilde{B}_{33}\bar{C}_{r(\cdot)} \\
\hat{I}_{r(\cdot)} &= \tilde{B}_{31}\bar{I}_{p(\cdot)} + \tilde{B}_{33}\bar{I}_{r(\cdot)}
\end{aligned} \tag{VII.35}$$

where the $(\cdot)$ labels correspond to β, α, etc. for the $\hat{C}$ terms and to 1 or 2 for the $\hat{I}$ terms. This enables us to write the following expression.

$$B\hat{B}^{-1}\hat{A} = \begin{bmatrix} \hat{C}_{p\beta}\beta + \hat{C}_{pp}p + \hat{C}_{pr}r + \hat{I}_{p1}pq + \hat{I}_{p2}qr \\ \hat{C}_{qu}u + \hat{C}_{q\alpha}\alpha + \hat{C}_{qq}q + \hat{I}_{q1}pr + \hat{I}_{q2}\left(r^2 - p^2\right) \\ \hat{C}_{r\beta}\beta + \hat{C}_{rp}p + \hat{C}_{rr}r + \hat{I}_{r1}pq + \hat{I}_{r2}qr \end{bmatrix} \tag{VII.36}$$

Note that while the $\hat{C}$ and $\hat{I}$ terms are nonlinear compositions of various estimated parameters, these quantities vary linearly with the "regressor" p, pq, α, etc. This is essential for adaptive control methodologies. Finally, by defining $\tilde{C}_{(\cdot)} \triangleq C_{(\cdot)} - \hat{C}_{(\cdot)}$ and $\tilde{I}_{(\cdot)} \triangleq I_{(\cdot)} - \hat{I}_{(\cdot)}$, the following expression results.

$$A(x,y) - B(x,y)\hat{B}(x,y)^{-1}\hat{A}(x,y) = \begin{bmatrix} \tilde{C}_{p\beta}\beta + \tilde{C}_{pp}p + \tilde{C}_{pr}r + \tilde{I}_{p1}pq + \tilde{I}_{p2}qr \\ \tilde{C}_{qu}u + \tilde{C}_{q\alpha}\alpha + \tilde{C}_{qq}q + \tilde{I}_{q1}pr + \tilde{I}_{q2}\left(r^2 - p^2\right) \\ \tilde{C}_{r\beta}\beta + \tilde{C}_{rp}p + \tilde{C}_{rr}r + \tilde{I}_{r1}pq + \tilde{I}_{r2}qr \end{bmatrix} \tag{VII.37}$$

Now, we can write the full equations of motion for the dynamics of an aircraft under dy-

namic inversion control.

$$\begin{aligned}\dot{x} &= A(x,y) - B(x,y)\hat{B}(x,y)^{-1}\hat{A}(x,y) + B(x,y)\hat{B}(x,y)^{-1}\dot{x}_{des} \\ &= \begin{bmatrix} \tilde{C}_{p\beta}\beta + \tilde{C}_{pp}p + \tilde{C}_{pr}r + \tilde{I}_{p1}pq + \tilde{I}_{p2}qr \\ \tilde{C}_{qu}u + \tilde{C}_{q\alpha}\alpha + \tilde{C}_{qq}q + \tilde{I}_{q1}pr + \tilde{I}_{q2}\left(r^2 - p^2\right) \\ \tilde{C}_{r\beta}\beta + \tilde{C}_{rp}p + \tilde{C}_{rr}r + \tilde{I}_{r1}pq + \tilde{I}_{r2}qr \end{bmatrix} + \begin{bmatrix} \tilde{B}_{11} & 0 & \tilde{B}_{13} \\ 0 & \tilde{B}_{22} & 0 \\ \tilde{B}_{31} & 0 & \tilde{B}_{33} \end{bmatrix} \begin{bmatrix} \dot{p}_{des} \\ \dot{q}_{des} \\ \dot{r}_{des} \end{bmatrix}\end{aligned} \tag{VII.38}$$

We can represent this system of equations in the following form. In addition to any dynamic mismatch, a failure would result in a perturbation, Δ, in each of the equations of motion. This could be a function of any of the state variables, or simply a constant.

$$\dot{p} = \vartheta_{p\beta}\beta + \vartheta_{pp}p + \vartheta_{pr}r + \vartheta_{p1}pq + \vartheta_{p2}qr + \vartheta_{p\dot{p}}\dot{p}_{des} + \vartheta_{p\dot{r}}\dot{r}_{des} + \Delta_p \tag{VII.39}$$

$$\dot{q} = \vartheta_u u + \vartheta_\alpha \alpha + \vartheta_q q + \vartheta_{q1}pr + \vartheta_{q2}\left(r^2 - p^2\right) + \vartheta_{\dot{q}}\dot{q}_{des} + \Delta_q \tag{VII.40}$$

$$\dot{r} = \vartheta_{r\beta}\beta + \vartheta_{rp}p + \vartheta_{rr}r + \vartheta_{r1}pq + \vartheta_{r2}qr + \vartheta_{r\dot{p}}\dot{p}_{des} + \vartheta_{r\dot{r}}\dot{r}_{des} + \Delta_r \tag{VII.41}$$

If the modeling of the DI control law is perfect, the $\vartheta_{(\cdot)}$ terms will all be zero with the exception of $\vartheta_{p\dot{p}}$, $\vartheta_{q\dot{q}}$, and $\vartheta_{r\dot{r}}$, which will be equal to a constant value, 1. If each $\Delta_i = 0$, the dynamic inversion control results in $\dot{p} = \dot{p}_{des}$, $\dot{q} = \dot{q}_{des}$, and $\dot{r} = \dot{r}_{des}$. Now consider the equilibrium behavior of the system around p=r=q=0. At the equilibrium, the state derivatives will be zero as well.

$$\begin{aligned}\dot{p} = 0 &= \vartheta_{p\beta}\beta + \vartheta_{p\dot{p}}\dot{p}_{des} + \vartheta_{p\dot{r}}\dot{r}_{des} + \Delta_p \\ \dot{q} = 0 &= \vartheta_u u + \vartheta_\alpha \alpha + \vartheta_{\dot{q}}\dot{q}_{des} + \Delta_q \\ \dot{r} = 0 &= \vartheta_{r\beta}\beta + \vartheta_{r\dot{p}}\dot{p}_{des} + \vartheta_{r\dot{r}}\dot{r}_{des} + \Delta_r\end{aligned} \tag{VII.42}$$

In other words,

$$\begin{aligned} \vartheta_{p\dot{p}}\dot{p}_{des} + \vartheta_{p\dot{r}}\dot{r}_{des} &= -\vartheta_{p\beta}\beta - \Delta_p \\ \vartheta_{q\dot{q}}\dot{q}_{des} &= -\vartheta_u u - \vartheta_\alpha \alpha - \Delta_q \\ \vartheta_{r\dot{p}}\dot{p}_{des} + \vartheta_{r\dot{r}}\dot{r}_{des} &= -\vartheta_{r\beta}\beta - \Delta_r \end{aligned} \tag{VII.43}$$

At an equilibrium point, β, α, and u will be constant. Thus

$$\begin{aligned} \vartheta_{p\dot{p}}\dot{p}_{des} + \vartheta_{p\dot{r}}\dot{r}_{des} &= -\vartheta_{pc} - \Delta_p \\ \vartheta_{q\dot{q}}\dot{q}_{des} &= -\vartheta_{qc} - \Delta_q \\ \vartheta_{r\dot{p}}\dot{p}_{des} + \vartheta_{r\dot{r}}\dot{r}_{des} &= -\vartheta_{rc} - \Delta_r \end{aligned} \tag{VII.44}$$

where ϑ_{pc}, ϑ_{qc}, and ϑ_{rc} are constant at the equilibrium point p=r=q=0. Furthermore, if we assume Δ_i is constant at an equilibrium point, it follows that zero steady state error in the presence of modeling mismatch or failures, requires some form of integral control in an outer loop. In terms of adaptive control this means having a constant included as part of the regressor.

To put the aircraft dynamic model in the form of (IV.1), define the following variables (similar to Section A).

$$\begin{aligned} \tilde{\beta} &= \beta - \beta_c \\ \tilde{\alpha} &= \alpha - \alpha_c \\ \tilde{u} &= u - u_c \end{aligned} \tag{VII.45}$$

where α_c, β_c, and u_c are the values at equilibrium. Applying this back to the model yields

$$\begin{aligned}
\dot{p} &= \vartheta_{p\beta}\tilde{\beta} + \vartheta_{pp}p + \vartheta_{pr}r + \vartheta_{p1}pq + \vartheta_{p2}qr + \vartheta_{p\dot{p}}\dot{p}_{des} + \vartheta_{p\dot{r}}\dot{r}_{des} + \vartheta_{p\beta}\beta_c + \Delta_p \\
\dot{q} &= \vartheta_u\tilde{u} + \vartheta_\alpha\tilde{\alpha} + \vartheta_q q + \vartheta_{q1}pr + \vartheta_{q2}\left(r^2 - p^2\right) + \vartheta_{\dot{q}}\dot{q}_{des} + \vartheta_{q\alpha}\alpha_c + \vartheta_{qu}u_c + \Delta_q \\
\dot{r} &= \vartheta_{r\beta}\tilde{\beta} + \vartheta_{rp}p + \vartheta_{rr}r + \vartheta_{r1}pq + \vartheta_{r2}qr + \vartheta_{r\dot{p}}\dot{p}_{des} + \vartheta_{r\dot{r}}\dot{r}_{des} + \vartheta_{r\beta}\beta_c + \Delta_r
\end{aligned} \tag{VII.46}$$

Also, we can write

$$\begin{aligned}
\vartheta_{p\dot{p}}\dot{p}_{des} + \vartheta_{p\dot{r}}\dot{r}_{des} &= \dot{p}_{des} + (\vartheta_{p\dot{p}} - 1)\dot{p}_{des} + \vartheta_{p\dot{r}}\dot{r}_{des} \\
\vartheta_{q\dot{q}}\dot{q}_{des} &= \dot{q}_{des} + \left(\vartheta_{q\dot{q}} - 1\right)\dot{q}_{des} \\
\vartheta_{r\dot{p}}\dot{p}_{des} + \vartheta_{r\dot{r}}\dot{r}_{des} &= \dot{r}_{des} + (\vartheta_{r\dot{r}} - 1)\dot{r}_{des} + \vartheta_{r\dot{p}}\dot{p}_{des}
\end{aligned} \tag{VII.47}$$

The $\vartheta_{p\dot{p}}$, $\vartheta_{q\dot{q}}$, and $\vartheta_{r\dot{r}}$ terms will take on values close to 1. It is desired to suppress any difference from 1 in these variables. We therefore lump the difference from 1 in the Δ_i terms. The cross terms, $\vartheta_{p\dot{r}}$ and $\vartheta_{r\dot{p}}$ will have values close to zero. Cross coupling between DI inputs is not desired, so these terms are also lumped into the Δ_i terms. The $\tilde{\alpha}$, $\tilde{\beta}$, and $\tilde{u}$ variables from (VII.46) will remain fairly small about an operating point, these are lumped into the Δ_i terms as well.

This leaves us with the following system.

$$\begin{aligned}
\dot{p} &= \vartheta_{pp}p + \vartheta_{pr}r + \vartheta_{p1}pq + \vartheta_{p2}qr + \vartheta_{pc} + \dot{p}_{des} + \Delta_{pt} \\
\dot{q} &= \vartheta_q q + \vartheta_{q1}pr + \vartheta_{q2}\left(r^2 - p^2\right) + \vartheta_{qc} + \dot{q}_{des} + \Delta_{qt} \\
\dot{r} &= \vartheta_{rp}p + \vartheta_{rr}r + \vartheta_{r1}pq + \vartheta_{r2}qr + \vartheta_{rc} + \dot{r}_{des} + \Delta_{rt}
\end{aligned} \tag{VII.48}$$

The Δ_{pt}, Δ_{qt}, and Δ_{rt} terms include the uncertainty in the cross coupling on the control input, the transient behavior of the α, β and u terms as well as any other modelling uncer-

tainties or exogenous disturbances. Futhermore, this system can be written as the following.

$$\dot{x} = \varphi(t,x)\,\vartheta + \dot{x}_{des} + \Delta(t,x,\dot{x}_{des}) \tag{VII.49}$$

where

$$\varphi(t,x) = \begin{bmatrix} p & r & pq & qr & 1 & 0 & 0 & 0 & 0 & 0 & 0 & 0 & 0 & 0 \\ 0 & 0 & 0 & 0 & 0 & q & pr & \left(r^2 - p^2\right) & 1 & 0 & 0 & 0 & 0 & 0 \\ 0 & 0 & 0 & 0 & 0 & 0 & 0 & 0 & 0 & p & r & pq & qr & 1 \end{bmatrix} \tag{VII.50}$$

and

$$\vartheta = \begin{bmatrix} \vartheta_{pp} & \vartheta_{pr} & \vartheta_{p1} & \vartheta_{p2} & \vartheta_{pc} & \vartheta_{q} & \vartheta_{q1} & \vartheta_{q2} & \vartheta_{qc} & \vartheta_{rp} & \vartheta_{rr} & \vartheta_{r1} & \vartheta_{r2} & \vartheta_{rc} \end{bmatrix}^T \tag{VII.51}$$

This system is of the same form as (IV.1). The regressor, $\varphi(t,x)$, can be altered by grouping terms into the Δ_i terms. At this point, the system is ready for any of the outer loop control laws mentioned in previous sections.

CHAPTER VIII

EVALUATION CRITERIA

To analyze the results some sort of criteria must be developed to determine the quality of the response generated with respect to the desired response. This is generally fairly challenging with aircraft because much of the evaluation of aircraft response depends on pilot feel. While a large part of the evaluation is non-deterministic, there are some quantifiable response characteristics we can use for evaluation.

- The pilot should not be required to maintain pressure on the stick to hold the aircraft in straight and level flight. In other words a large amount of steady state error is considered to be poor performance.
- High frequency oscillations can result in excitation of structural modes and can also lead to rate limiting behavior that can destabilize the aircraft.
- Reaching rate and position limits in normal operation should be avoided.
- Oscillation about an equilibrium should be kept to a minimum. A pilot does not like to feel like he/she is fighting the aircraft to make it settle at an operating point.

Most of these criteria involve examining the error between the aircraft response and the desired response. In general, the $\mathcal{L}_2$ norm of the error is a good measure for the quality of the response. While this norm alone may be sufficient to tell the difference between a response with large steady state error and one that has small errors, it may be difficult to distinguish between a response with small steady state errors and a response with a small oscillating error. Most pilots would prefer to have to apply a small amount of pressure to keep the aircraft straight and level than be required to deal with oscillatory behavior that cannot be controlled. This must be reflected in a measure of response quality. For this

reason we can utilize a weighted $\mathcal{L}_2$ norm. (Note that the reference to the $\mathcal{L}_2$ space is more correctly a reference to the extended $\mathcal{L}_2$ space ($\mathcal{L}_{2e}$). We are examining the response over a finite time, not over infinite time. Thus, while the $\mathcal{L}_2$ norm of a constant steady state error would not exist, it would exist when evaluating over a finite time). We select the norm so that high frequency errors are penalized more than constant errors of the same magnitude. This is accomplished by designing a filter for the input signal and tuning it so that sufficient penalty is applied.

In the absence of a frequency weight on the norm, the $\mathcal{L}_2$ norm of an oscillating signal will be approximately one half that of a constant signal of the same magnitude (for a pure sinusoid). For this reason, using an unweighted norm to measure the quality of the response would penalize a constant error more than any oscillating error. To alleviate this problem and to have the ability to tune the value of the norm to reflect the frequencies present in the signal, we utilize the following filter.

$$\frac{\hat{y}(s)}{y(s)} = W_{\mathcal{L}_2}(s) = k\frac{(s+z_1)(s+z_2)\cdots(s+z_m)}{(s+p_1)(s+p_2)\cdots(s+p_n)} \tag{VIII.1}$$

Let the impulse response of the filter be given by $w_{\mathcal{L}_2}(t)$. Our weighted $\mathcal{L}_2$ norm is defined to be the following.

$$\|y\|^2_{\mathcal{L}_{2W}} = \int_0^T \left(\left(w_{\mathcal{L}_2} \circ y\right)(\tau)\right)^2 d\tau \tag{VIII.2}$$

where $\circ$ denotes the convolution operator and T is some finite time over which the norm is taken. As was mentioned before, the goal of this norm is to penalize errors of unfavorable frequency content. The discussion of the aircraft problem presented in this thesis revolves around the ability of the aircraft response to accurately track the response of a reference model. The reference model defines the desired speed of response of the aircraft. In light of this it makes sense to penalize error responses of higher frequency content than that of the reference model. A sample frequency response of the weighting function is given

in figure VIII.1. A weighting function of this type would place a large penalty on any

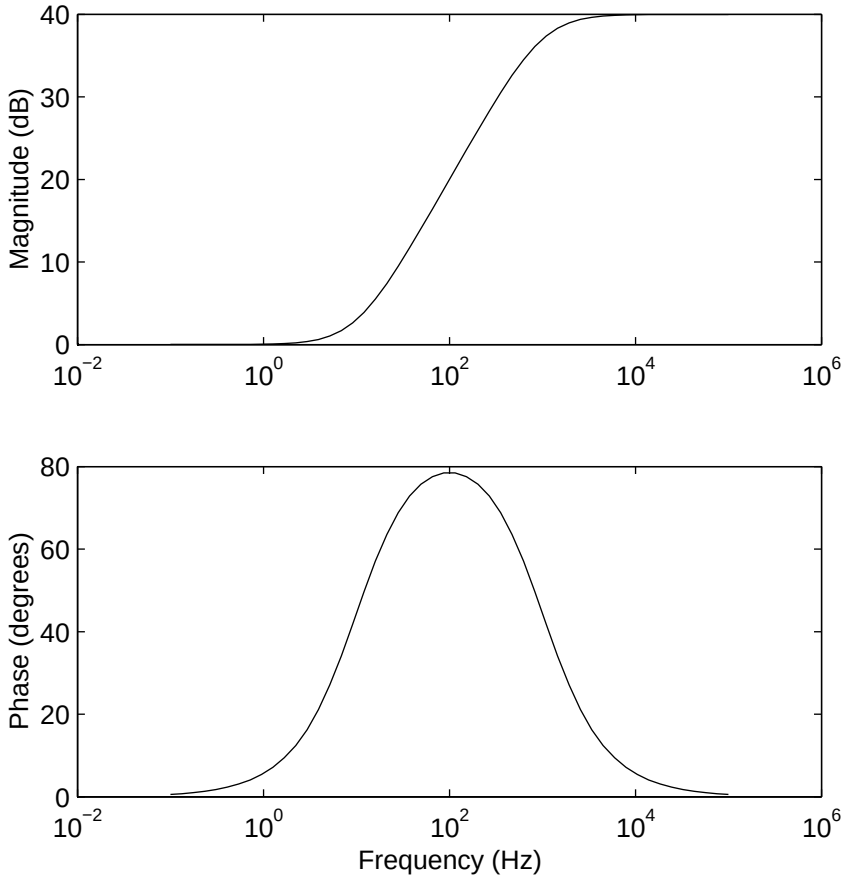

Fig. VIII.1. Sample frequency response of weighting funciton

high frequency error behavior and would not penalize any low frequency behavior. This type of simple filter will be the best approach to weighting the error appropriately. It will be adjusted based on the speed of the reference model. Some simple examples for the norm values that will result for different input signals are given in figures VIII.2, VIII.3, and VIII.4. For these examples, a first order filter with a pole at 100Hz and a zero at 0.1Hz will be considered. We can consider figure VIII.2 as the “optimal” error response. We see that of the three figures, it has the lowest norm. Figure VIII.3 shows the response of the system in the presence of an error decay accompanied by a steady state error. We see

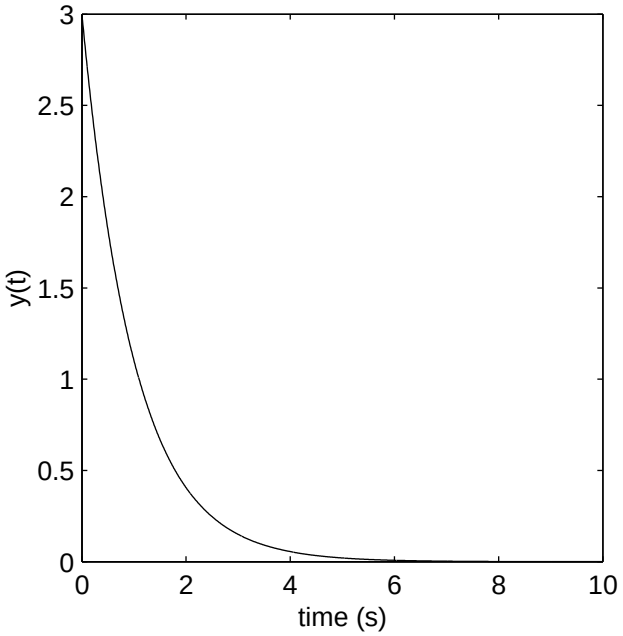

Fig. VIII.2. Example of function with $\|y\|_{\mathcal{L}_{2W}} = 1.3068$

that the norm is increased from the first case. The final case shows a decaying error signal with high frequency oscillations. The norm is highest for this case even though the high frequency component is damped out after about 2 seconds.

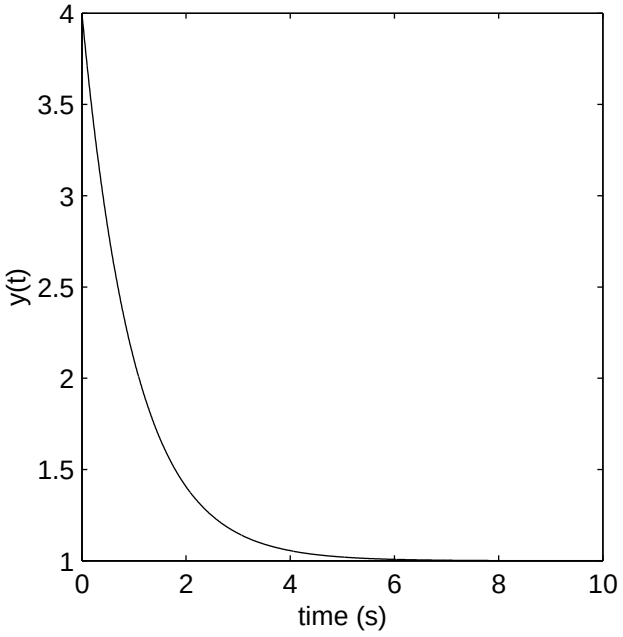

Fig. VIII.3. Example of function with $\|y\|_{\mathcal{L}_{2W}} = 2.907$

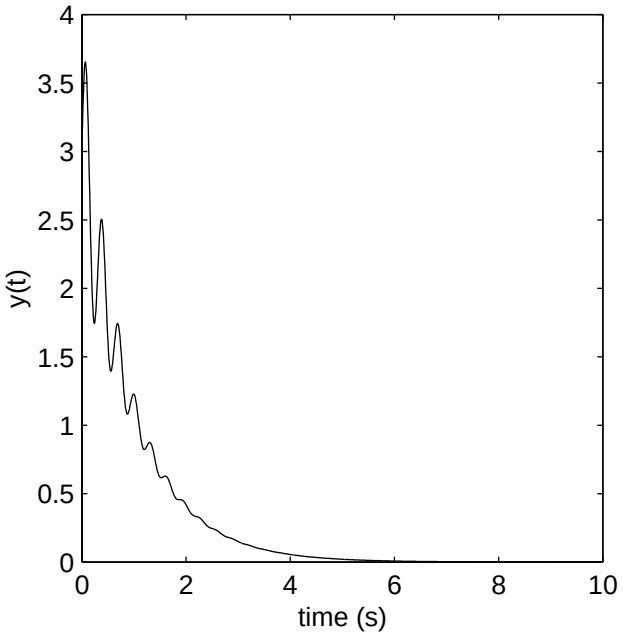

Fig. VIII.4. Example of function with $\|y\|_{\mathcal{L}_{2W}} = 11.4715$

From these simple examples, the weighted norm seems to provide a good measure of the quality of the error response as it relates to more subjective desirable flying qualities. This frequency weighted norm, however, does not take the aggressiveness of a maneuver into account. If the aircraft is given slowly varying inputs, we expect its response to track the desired outputs much more accurately than with quickly varying inputs. This is because the response of the aircraft has structural as well as actuator limitations that limit the speed at which it can respond to an input. To account for this, a performance measure based on the derivative of the reference signal is proposed. The error between the output signals (p, q, and r) and their corresponding reference signals will be normalized by the derivatives of their reference signals, which is also the feedforward portion of the dynamic inverstion control (i.e. $\dot{p}_{des}$, $\dot{q}_{des}$, and $\dot{r}_{des}$). We therefore define the following norm to capture this.

$$\|e\|^2_{\mathcal{L}_{2\dot{u}}} = \int_0^T \frac{e(\tau)^2}{1+\dot{u}(\tau)^2} d\tau \tag{VIII.3}$$

It is important to note that this quantity is no longer a norm, but a performance measure. Although it has many similarities to a norm, it does not satisfy norm definitions. For a purely linear system, increasing the input by a constant gain will increase the output, e, by the same constant gain. As this gain gets large, $\frac{e(\tau)^2}{1+\dot{u}(\tau)^2} \rightarrow \frac{e(\tau)^2}{\dot{u}(\tau)^2}$. As a result, for inputs with magnitude larger than one, the measure will have only a small change. This type of measure is particulary useful in a dynamic inversion because the input supplied into the DI is actually the derivative of the reference model output. In the reference model tracking problem, the error signal closely resembles the derivative signal. Testing of various normalizing signals showed that normalizing using the derivative of the reference signal provided the best results. The following simple example shows why this is the case.

Consider the block diagram shown in figure VIII.5. The transfer function $P(s)$ represents the plant to be controlled. If this transfer function is the DI + Plant, then it might nominally be $\frac{1}{s}$. The $G(s)$ transfer function is the control. For the purposes of this thesis,

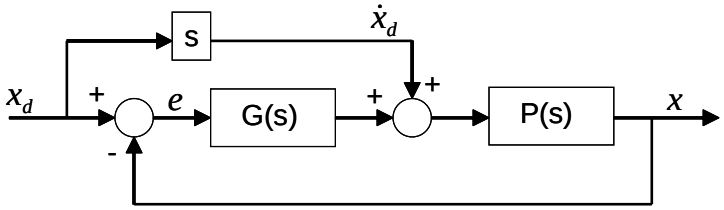

Fig. VIII.5. Block diagram of general system implementation for performance measure

this might be ARC, AC, or SMC. All of these control laws include a feedforward term given by $\dot{x}_d$ (although for SMC and ARC there is some filtered addition to this term that can be included in $G(s)$). The transfer function of this system from the tracking error, *e*, to the feedforward input into the plant, $\dot{x}_d$, is given below.

$$e(s) = \left(\frac{1}{1+G(s)P(s)}\right)\left(\frac{1}{s} - P(s)\right)\dot{x}_d(s) \tag{VIII.4}$$

This example shows that the transfer function from *e* to the derivative of the reference command signal ($\dot{x}_d$) depends on the error between the response of $P(s)$, and that of an integrator. If the plant + DI deviates from this behavior, then the error normalized by $\dot{x}_d$ should give some measure of the difference in the response. For the case of a pure sinusoid, normalizing by $\dot{x}_d$ would leave just an amplitude term (if phase were not considered). The transfer function gain can also be made small when $G(s)$ is large. Therefore, it also provides a measure of how well the controller eliminates the error caused by deviation of $P(s)$ from $\frac{1}{s}$.

This simple example shows that the choice of performance measure in equation (VIII.3) is capable of providing a measure of the error present in the system response regardless of the size of the command inputs.

The two approaches to creating some measure of system performance do not account for cross coupling between axes. While this is something that the control seeks to avoid, error due to cross coupling between axes is more desirable than error when no commands

are being given. For example, if the aircraft were to experience some roll due to a pilot-commanded pitch input, this would not be unexpected (particularly in the presence of a failure). However, if the plane were to pitch up when no commands were given, or if the pilot had to continually fight to keep the aircraft from pitching in one direction, this would be undesirable. Therefore, some distinction must be made between error arising from cross coupling and other undesirable errors. While cross coupling errors will still be penalized (the point of dynamic inversion control as well as the outer loop controllers is to eliminate it), it will be penalized less than in the other cases. The penalty should vary based on the size of the commands (or size of the command rates) in the other axes. The effect of commands in other axes will be added in a similar manner to that of the measure given in equation (VIII.3). The following measure is proposed to provide an adequate gauge of the aircraft response due to variable size command inputs as well as due to cross coupling in its axes.

$$\|y_j\|^2_{\mathcal{L}_{2cc}} = \int_0^t \frac{y_j(\tau)^2}{1+\dot{u}_j(\tau)^2+\sum_{i=1,\neq j}^{n}\dot{u}_i(\tau)^2}d\tau \qquad \text{(VIII.5)}$$

In the above expression, the index j represents the axis for which the data is being taken. If there is only one axis, the $\|\cdot\|_{\mathcal{L}_{2\dot{u}}}$ is reproduced.

CHAPTER IX

APPLICATION

In this section, the various systems to which the control methodologies have been applied will be discussed. Each system provides a unique perspective to the difficulties that are both encountered and overcome by the various control methodologies. A dynamic inversion control law is applied to each system, and three types of outer loop control schemes are tested. These are adaptive control, sliding mode control, and adaptive robust control as discussed previously in Sections IV, V, and VI. Each of these methodologies is applied to a linearized F-15 model, a full nonlinear simulation of the F-15 IFCS aircraft, and to a simulation of the F-5A aircraft.

Each of these aircraft produce different challenges for the control schemes to overcome. The following list indicates the challenges associated with each problem and the reasons each model was chosen for analysis.

- Linearized F-15 Model
  - Provides simplified system for proof of concept
  - Uncertainty in dynamics due to inversion error and actuator failures easily analyzed
  - Response limited to one axis, so coupling is not a problem
  - Actuator rate and position limits create performance limitations
- Full nonlinear model of F-15 IFCS aircraft
  - Full nonlinear,high fidelity model allows testing over a variety of flight conditions in the presence of unknown uncertainties

  - Commands in multiple axes create unique coupling problems the controller must overcome
  - Utilizes nonlinear dynamic inversion, making inversion error more difficult to quantify
  - High-performance aircraft places large demands on speed and quality of response
  - Aircraft must perform well with large amplitude, quickly changing pilot inputs
  - Actuator rate and position limits place limitations on controller gains
  - Failure tests limited to hard-over failures

- Nonlinear model of F-5A aircraft
  - Allows simulation of response over a large range of flight conditions
  - The aircraft does not have the high performace level of the F-15 which creates a unique problem for the implementation of the various control methodologies
  - Allows testing of various types of actuator failures
  - Actuator rate and position limits play a larger role than in the F-15 aircraft

The following sections detail the implementation of control laws onto the three models described above.

A. SISO: Linearized F-15 Model

The implementation of Adaptive Robust Control on a single-input-single-output system is now considered. For this example, a linearized model of the pitch axis dynamics for an F-15 aircraft will be considered. For this example, the state variables are angle-of-attack, α, body axis pitch rate, q, body axis forward velocity, u, altitude, h, and pitch angle, θ. The

dynamics of the aircraft are linearized about 0.75 Mach and 20,000 ft of altitude. The model has been provided by NASA Dryden and is obtained by linearizing a nonlinear model of the F-15 at straight and level flight. The linearized model applies for small deviations around the operating condition (0.75 Mach and 20,000 ft) as well as for small values of the roll angle, angle-of-attack, and sideslip angle. The linearized model is given below:

$$\begin{bmatrix} \dot{u} \\ \dot{\alpha} \\ \dot{q} \\ \dot{\theta} \\ \dot{h} \end{bmatrix} = \begin{bmatrix} -0.0112 & -0.0365 & 0 & -0.5601 & 0.0001 \\ -0.0065 & -1.1182 & 1.0000 & 0.0001 & 0.0001 \\ 0.0015 & 8.3089 & -0.9412 & 0 & -0.0001 \\ 0 & 0 & 1.0000 & 0 & 0 \\ -0.0017 & -13.5803 & 0 & 13.5803 & 0 \end{bmatrix} \begin{bmatrix} u \\ \alpha \\ q \\ \theta \\ h \end{bmatrix} \quad \text{(IX.1)}$$

$$+ \begin{bmatrix} -0.0811 & -0.0811 \\ -0.0688 & -0.0688 \\ -5.9799 & -5.9799 \\ 0 & 0 \\ 0 & 0 \end{bmatrix} \begin{bmatrix} \delta_{sl} \\ \delta_{sr} \end{bmatrix}$$

$$y = \begin{bmatrix} 0 & 0 & 1 & 0 & 0 \end{bmatrix} \begin{bmatrix} u \\ \alpha \\ q \\ \theta \\ h \end{bmatrix}$$

The output that we will be concerned with is body axis pitch rate, q. To set up the dynamic inversion control law, the input vector and output vector must be of the same dimension. To accomplish this, a control allocation is performed which applies equal control to each of the actuators. The allocation is introduced as a transformation of a synthetic control

variable into the two actuators.

$$\begin{bmatrix} \delta_{sl} \\ \delta_{sr} \end{bmatrix} = \begin{bmatrix} 1 \\ 1 \end{bmatrix} \delta_s = T\delta_s \tag{IX.2}$$

If this transformation is applied, then we have a single-input-single-output system that we can dynamically invert. A dynamic inversion control law similar to that given in (VII.15) is applied to the system. If we represent the system given (IX.1) as the following:

$$\begin{aligned} \dot{x} &= A_q x + B_q T \delta_s \\ q &= C_q x \end{aligned} \tag{IX.3}$$

The dynamics of this single-input-single-output system can be inverted by the following control law.

$$\delta_s = \left(C_q \hat{B}_q T\right)^{-1} \left(-C_q \hat{A}_q x + \dot{q}_{des}\right) \tag{IX.4}$$

In section A it is shown that this type of control law can be put into a form condusive to the adaptive, sliding mode, and adaptive robust control laws described previously. To implement these outer loop controls, a regressor ($\varphi(t,x,\Gamma)$ in (IV.1)) must be chosen. For this example, choosing a regressor that includes the terms α, u, etc. does not necessarily aide the performance of the controller. Therefore, the regressor is chosen simply to be $\varphi(t,x,\Gamma) = 1$. The sliding surface is chosen to be a first order transfer function of the form:

$$\begin{aligned} \dot{x}_c &= -a_c x_c + b_c e \\ z_q &= e_q + c_c x_c \end{aligned} \tag{IX.5}$$

where $a_c, b_c, c_c > 0$ and $e_q \triangleq q - q_{des}$. The variable, q is the output variable that we wish to control and q_{des} is the desired pitch rate as provided by the reference model. The output variable, z_q, is the sliding surface that will be used in the adaptive robust and sliding mode control methodologies. The adaptive control technique will use the tracking error directly

(e_q). The results will utilize the pilot input shown in figure IX.1. This input is passed

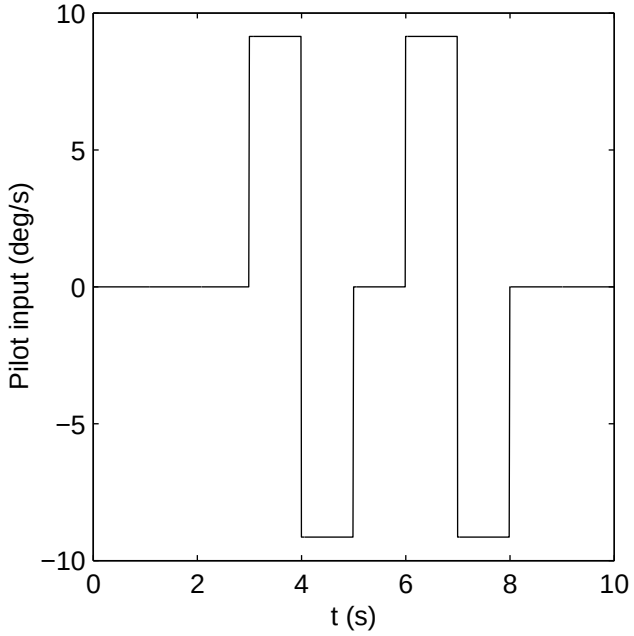

Fig. IX.1. Pilot inputs into the reference model for linearized F-15

into the reference model as shown in figure VII.1. The resulting signal becomes the desired pitch rate for the aircraft to follow. The reference model is chosen so that the pitch dynamics of the aircraft exhibit desirable flying qualities. Figure IX.2 shows the "smoothed" version of the inputs from figure IX.1. This input will allow the evaluation of the adaptive robust control methodology as an outer loop around the dynamic inversion controller. It will also allow the comparison of this control methodology to that of adaptive control and sliding mode control.

B. MIMO: F-15 and F-5A

This section describes the implementation of control laws on the multi-input-multi-output systems, i.e. the F-15 and the F-5. The dynamic inversion implementation is the same for both aircraft and is the one described in Section B. The models will not be given here, but

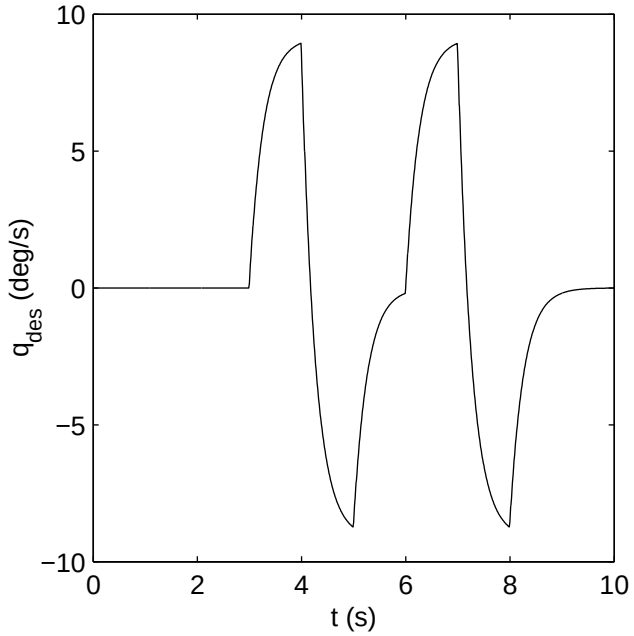

Fig. IX.2. Reference model rate command inputs into DI for linearized F-15

it is important to note that the implementation of the DI results in a system of the form given in (VII.48). The outer loop control implementations differ for each of these aircraft in terms of their sliding surfaces and regressor. There are some common factors in both aircraft. In each case, the outer loop controls are implemented independently of each other. This is illustrated in figure VII.3. Any coupling between control inputs is handled in the dynamic inversion law itself. From an outer loop standpoint, coupling is undesired and is grouped in the Δ terms as disturbances that are to be rejected.

1. F-15

For the F-15 IFCS aircraft, the following system form was used for the outer loop controllers.

$$\dot{x} = \varphi(t,x)\,\vartheta + \dot{x}_{des} + \Delta(t,x,\dot{x}_{des}) \tag{IX.6}$$

where

$$\varphi(t,x) = \begin{bmatrix} p & 1 & 0 & 0 & 0 \\ 0 & 0 & 1 & 0 & 0 \\ 0 & 0 & 0 & r & 1 \end{bmatrix} \tag{IX.7}$$

and

$$\vartheta = \begin{bmatrix} \vartheta_{pp} & \vartheta_{pc} & \vartheta_{qc} & \vartheta_{rr} & \vartheta_{rc} \end{bmatrix} \tag{IX.8}$$

The state variable, x, is defined previously as $\begin{bmatrix} p & q & r \end{bmatrix}^T$. The reference models that the aircraft is desired to follow are second order for pitch and yaw, and first order for the roll axis. Pilot stick inputs are fed into a preprocessor which converts these commands into roll, pitch, and yaw rate commands. This is implemented as shown in figure VII.3. The sliding surfaces used for the sliding mode and adaptive robust control methods are second order and are of the form:

$$\begin{aligned} \dot{x}_{ci} &= A_{ci}x_{ci} + B_{ci}e_i \\ z_i &= C_{ci}x_{ci} + e_i \end{aligned} \tag{IX.9}$$

where $i = p,q,r$ corresponds to each of the command axes, $A_{ci} \in \mathbb{R}^{2\times 2}$, $B_{ci} \in \mathbb{R}^{2\times 1}$, $x_{ci} \in \mathbb{R}^2$, $C_{ci} \in \mathbb{R}^{1\times 2}$, and $z_i, e_i \in \mathbb{R}$. Furthermore, A_{ci} must be Hurwitz. The pair (A_{ci}, B_{ci}) is chosen to be controllable and the pair (A_{ci}, C_{ci}) is chosen to be observable. The adaptive control technique does not use the sliding surface. The adaptive update law for pure adaptive control is a function of the error, e_i.

The control implementation on the F-15 is tested using a variety of different pilot inputs which are designed evaluate the ability of the control laws to handle large inputs, coupling between axes, and create situations where actuators will be performing near or at their rate and position limits. Each input profile was tested for four different command amplitudes and different failure positions as well. The failure tested is a right stabilator

lock. Four seperate command profiles are used to perform the testing. The first set of commands is a simple series of doublet maneuvers. These are designed to demonstrate the ability of each controller to track a reference command in each axis without being required to deal with commands in other axes. This input profile is designed to be a baseline in demonstrating the ability of the aircraft to recover from a failure, and execute simple maneuvers. The input profile is given in figure IX.3 and will be labeled as **PD** (plain doublets) for short when discussing the results. Once passed through the reference models, these commands become those shown in figure IX.4. These will be the reference commands that the combination DI and outer loop control will attempt to track.

The next several sets of commands are intended to be more aggressive and test the ability of the aircraft to handle inputs in two axes at the same time. In particular, when there is a failure, an actuator might be required to move in opposite directions to track the doublets being input simultaneously. These types of inputs are important because it is simple to fall into the trap of tuning a controller to work with a simple set of inputs. These inputs are designed to cause a system experiencing a failure to hit actuator and position limits in order to keep up. It is important that when this occurs, the system does not go unstable. The objective is to track aggressive inputs as closely as possible, but to stay as far away from high destabilizing gains as possible. The first of these sets of commands will be labeled **CD** (coupled doublets). This set of commands performs simultaneous doublets in each of the axes in order to test coupling in the axes. The pilot inputs are given in figure IX.5 and the p, q, and r reference commands are given in figure IX.6.

The final set of inputs is a further expansion of the two cases above. This set of inputs is designed to push the system and test the ability of the controller to keep from lagging too far behind and falling into a limit cycle induced by actuator rate and position limits. This set of maneuvers, while a little unrealistic, nonetheless test the ability of the controller to respond to an agressive, multi-axis input. This set of inputs will be denoted

AD (aggressive doublets). The pilot inputs are shown in figure IX.7 and the commanded body rates are shown in figure IX.8.

2. F-5

For the F-5 aircraft, the system form given in (IX.6) is again used. The only difference lies in the choice of regressor, $\varphi(t,x,\Gamma)$, and in the parameter vector, ϑ. These are given by the following.

$$\varphi(t,x) = \begin{bmatrix} \beta & 1 & 0 & 0 & 0 & 0 \\ 0 & 0 & \alpha & 1 & 0 & 0 \\ 0 & 0 & 0 & 0 & \beta & 1 \end{bmatrix} \tag{IX.10}$$

and

$$\vartheta = \begin{bmatrix} \vartheta_{p\beta} & \vartheta_{pc} & \vartheta_{q\alpha} & \vartheta_{qc} & \vartheta_{r\beta} & \vartheta_{rc} \end{bmatrix} \tag{IX.11}$$

The reference models used were first order for each axis. The implementation shown in figure VII.3 is used in this case as well. The sliding surface was chosen to be first order. The only input profile tested for this aircraft is the PD set of inputs.

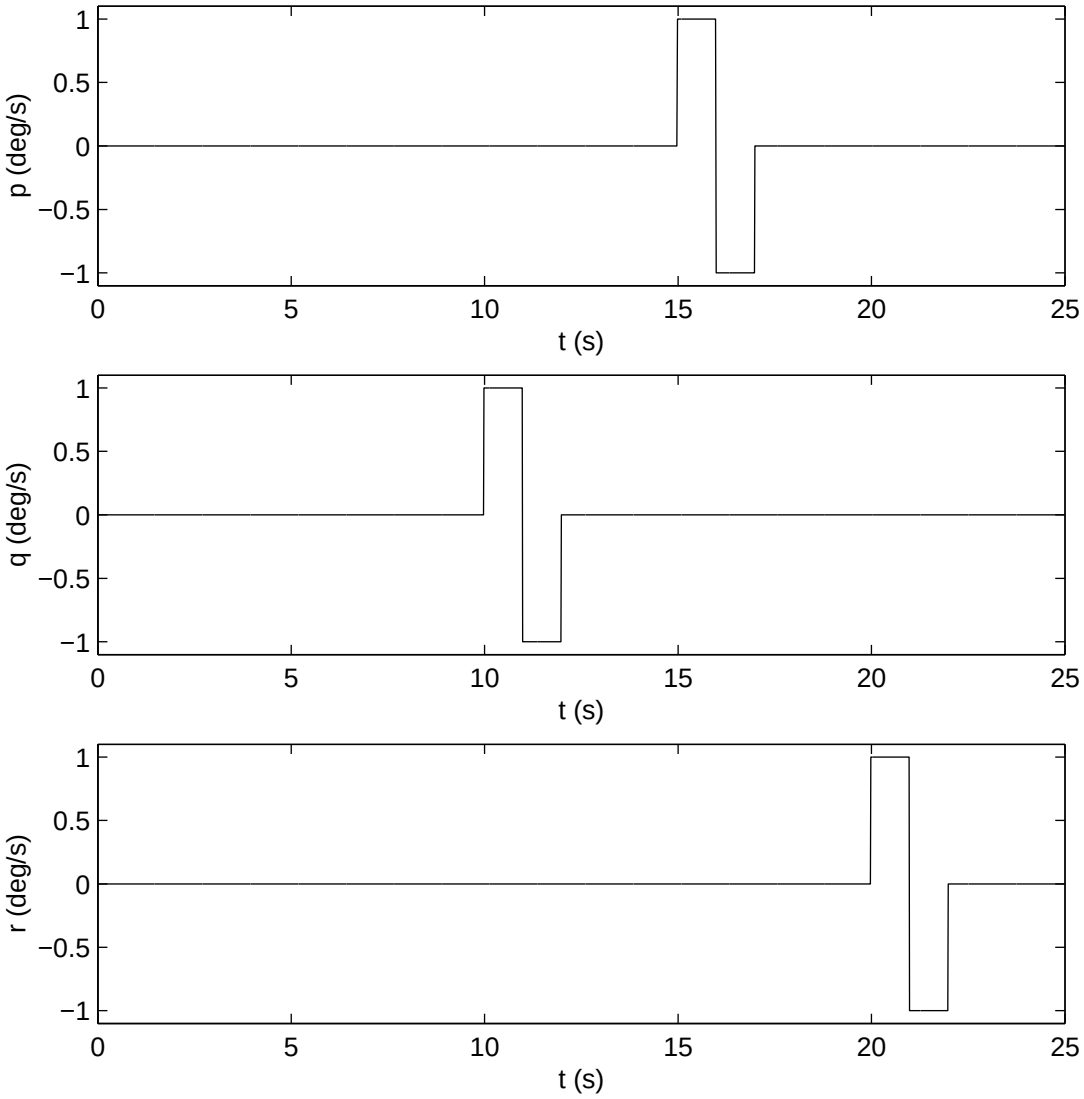

Fig. IX.3. Simple doublet command inputs for F-15 model

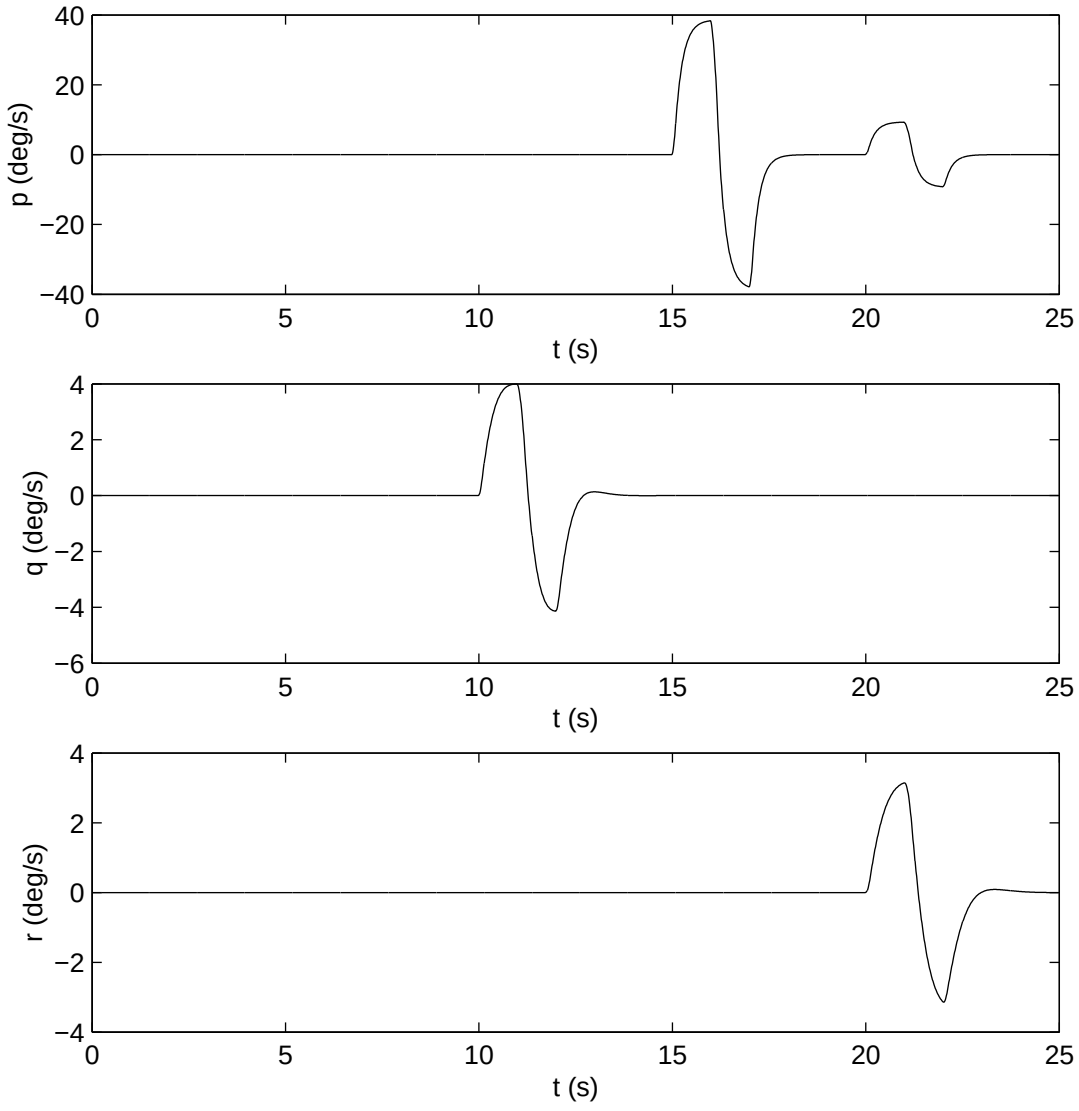

Fig. IX.4. Roll, pitch, and yaw rate commands determined from PD input profile

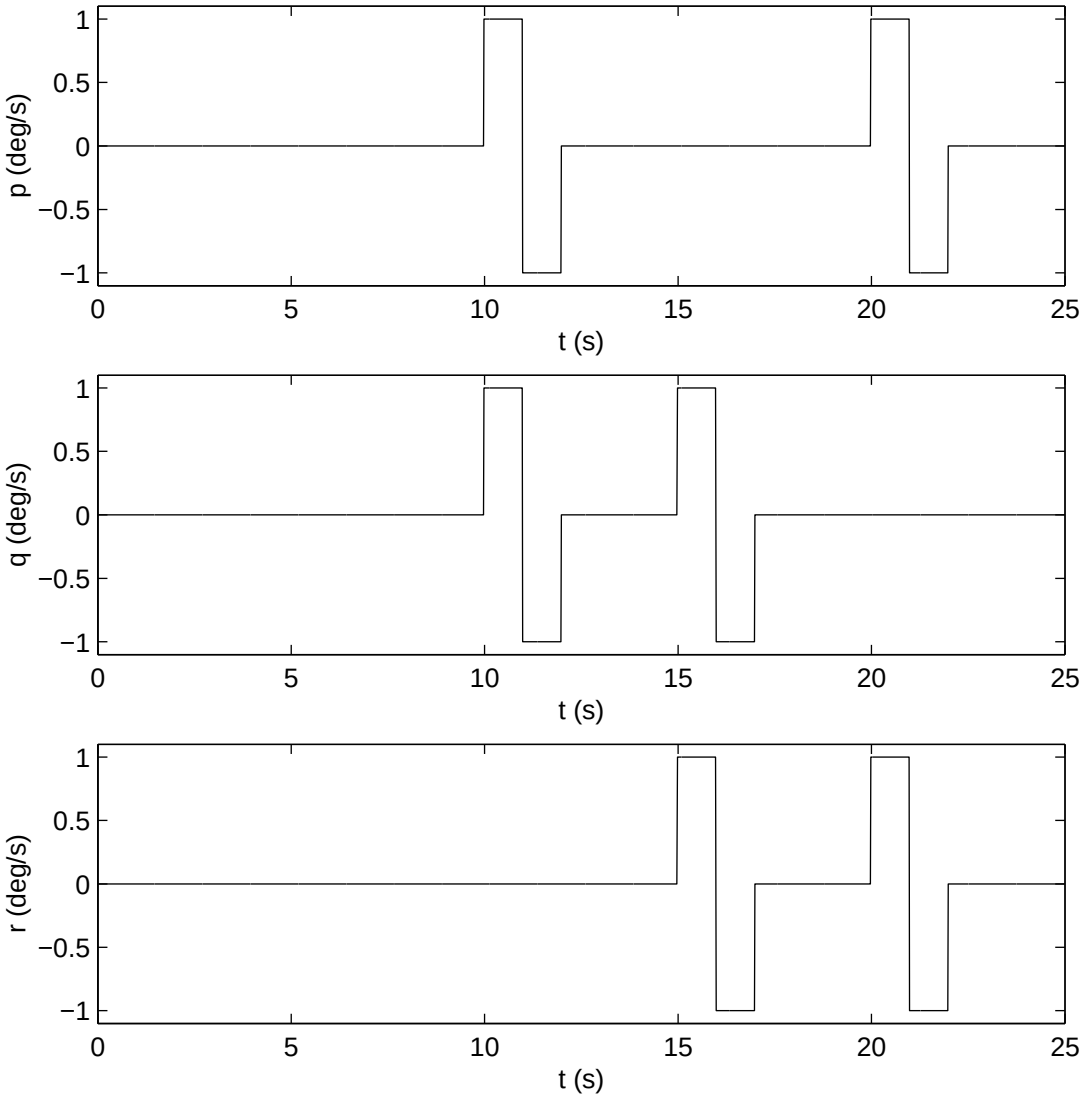

Fig. IX.5. Coupled doublet command inputs for F-15 model

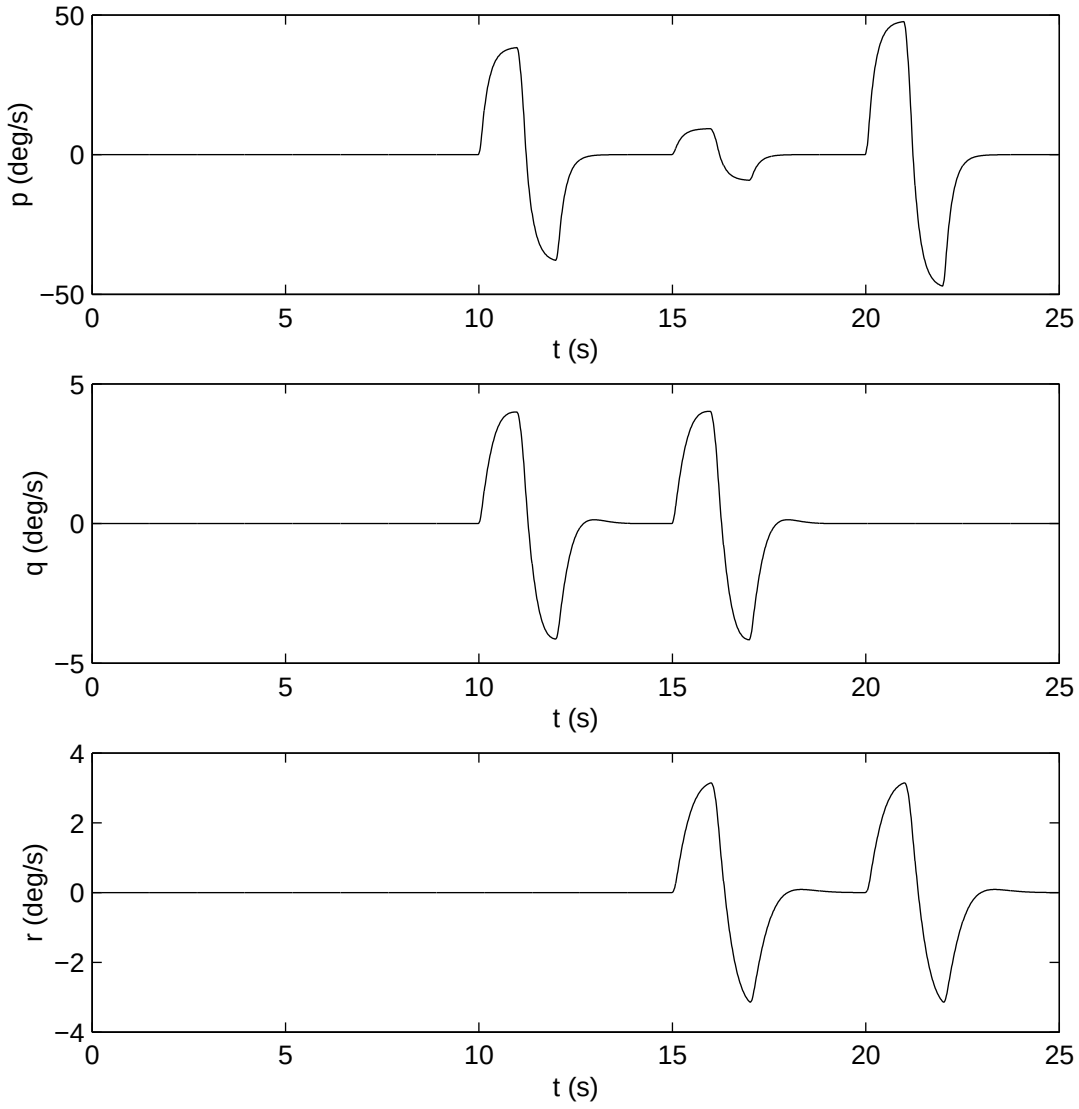

Fig. IX.6. Roll, pitch, and yaw rate commands determined from CD input profile

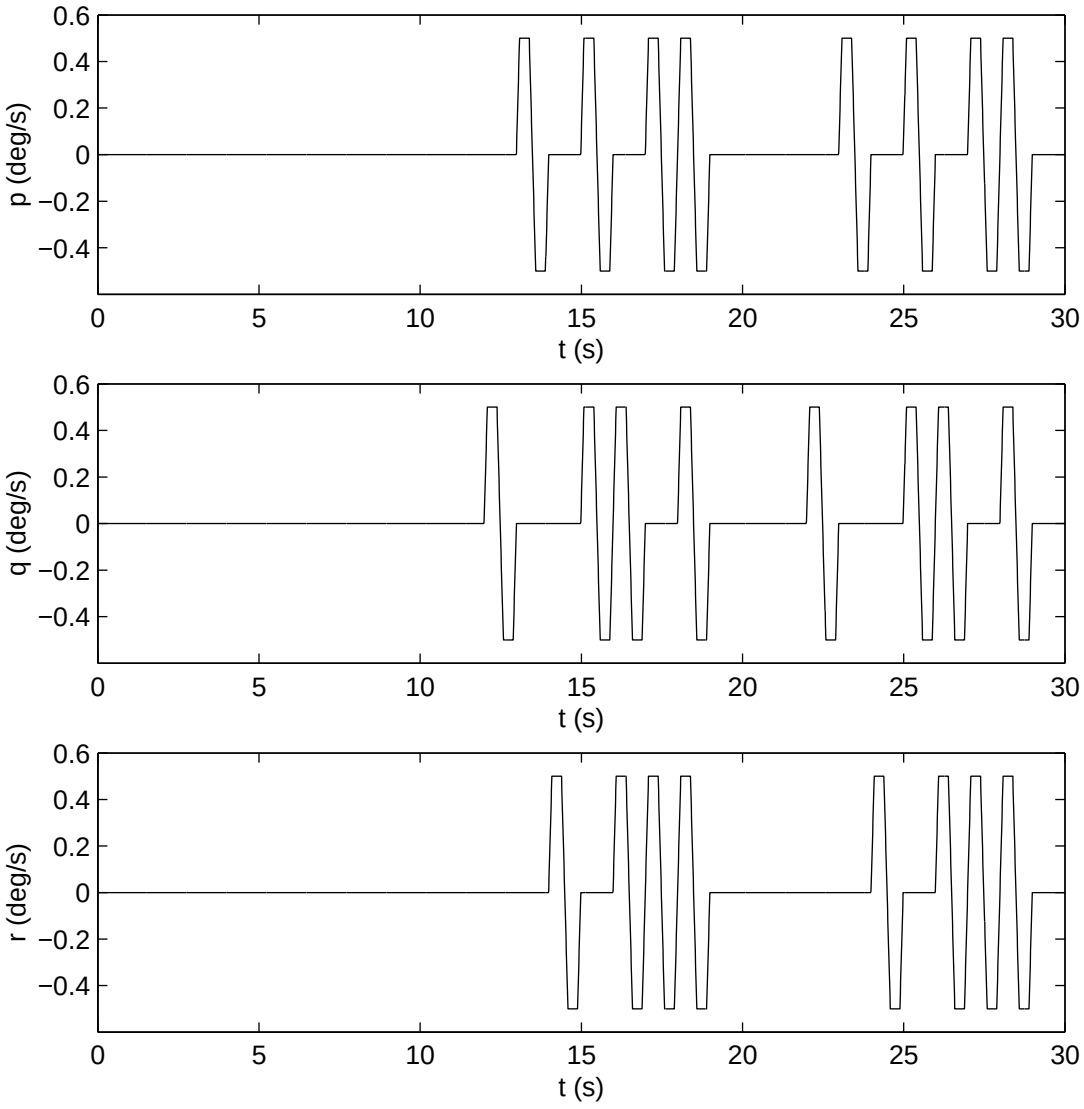

Fig. IX.7. Agressive doublet command inputs for F-15 model

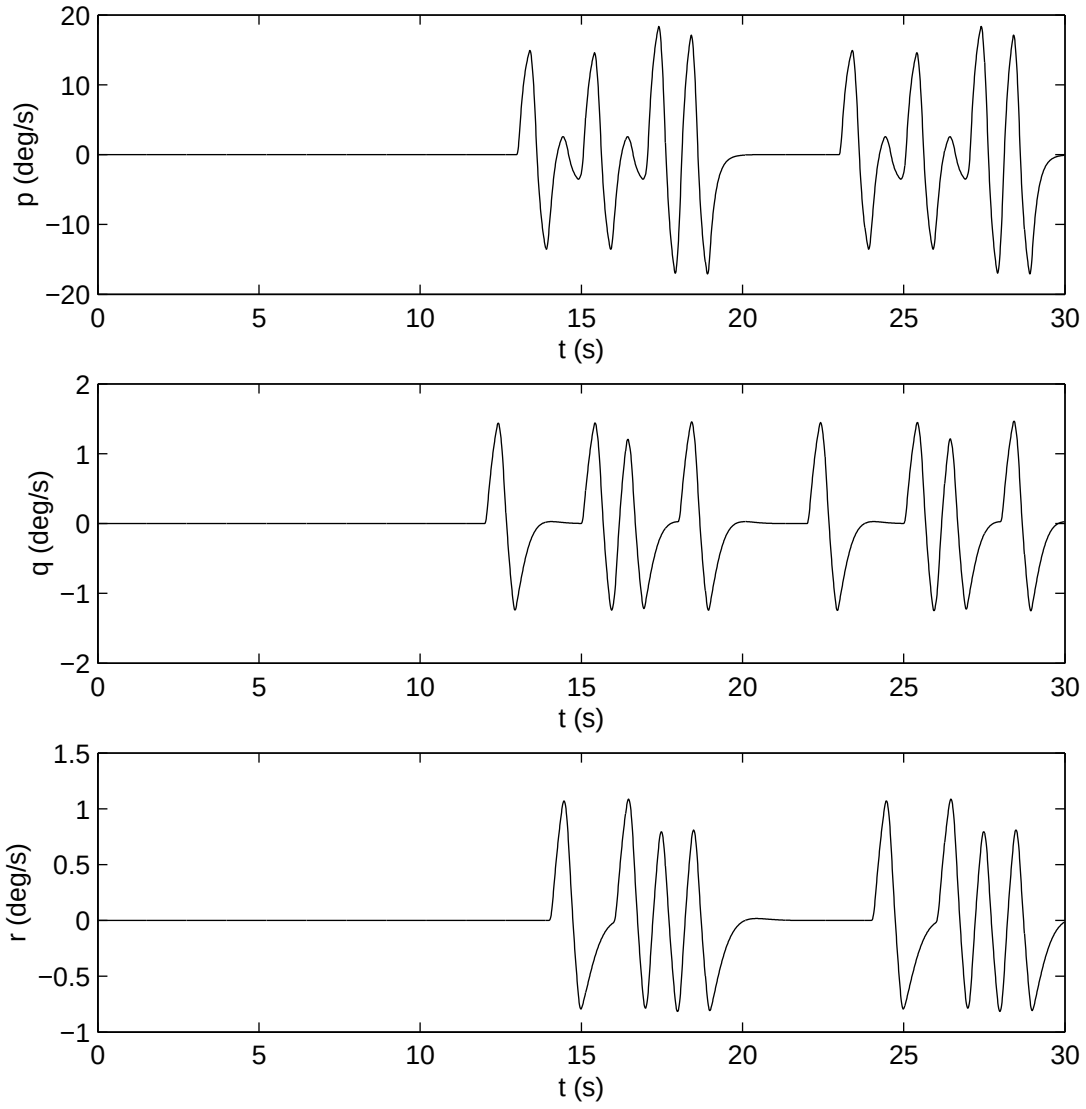

Fig. IX.8. Roll, pitch, and yaw rate commands determined from AD input profile

CHAPTER X

HARD-OVER FAILURE RESULTS

In this section, the responses of the outer loop controllers will be examined in terms of the linearized F-15 model, the full nolinear F-15 simulation and the nonlinear F-5 simulation. This discussion will be conducted with respect to the following areas.

- Transient response to failures

  This type of analysis is designed to assess how quickly the aircraft returns to commanded *p*, *q*, and *r* after a failure occurs. This is important because it desirable for the pilot to be required to do the smallest amount of work possible in attempting to arrest the failure. A large transient at the onset of a failure may result in the aircraft losing stability, or if at low altitude for example, loss of the aircraft. The response will be assesed in terms of how magnitude of the error in the body rate.

- Tracking response in the presence of failures

  The analysis in this section will be devoted to assessing the ability of the aircraft to track *p*, *q*, and *r* commands in the presence of failures and with a variety of command profiles and amplitudes. A pilot will want the least amount of cross-coupling between axes as possible, but will also want the aircraft to perform. This analysis is intended to determine the ability of each controller to track commands as well as limit the amount of cross coupling between axes so that the aircraft is still performs as well as possible and is easily manageable from a pilot's perspective. Performance will be measured in terms of a combination of the performance measures defined in section VIII.

- Steady state response

The ability of each control methodology to eliminate steady state errors will be examined as well. While small steady state errors might be accounted for in terms of retrimming the airplane, there might be failures for which the required trim value is outside the allowable actuator limits for trim. If this were to happen far from home, it would be very difficult for a pilot to maintain stick and pedal pressure for an extended period of time. It is therefore desirable to have any steady state errors as small as possible.

- Overall response

  Not only will the response of the aircraft be weighed in terms of its transient, tracking, and steady state response, but its overall performance will be evaluated as well. Each of the three analysis criteria listed evaluate the performance of the aircraft in one area. In actuality, all of these three things will be related to one another and the pilot will have to deal with the performance of the control laws in each of the three areas simultaneously. If a control performs poorly in one area, but very well in another, it is important to make some overall quantification of how this relates to a controller that demonstrates average performance in both areas. The frequency rated cross-coupling measure discussed in section VIII will be utilized for the overall analysis.

A. Transient Response Analysis

When an actuator failure occurs while an aircraft is in operation, the first few seconds can mean the difference betweeen life and death for the pilot. Any number of situations can make these first few seconds critical. If the pilot is in close formation with other aircraft, a sudden failure may cause the the aircraft experiencing the failure to collide with other aircraft it is not addressed quickly enough. When landing, or in low altitude flight, a sudden

failure could result in the aircraft hitting the ground. It becomes critical for the aircraft to be stabilized in the shortest time possible in these situations. In this section, the transient response of each control methodology with respect to each outer loop controller will be examined.

1. Linearized F-15

The discussion of the transient response characteristics begins with the linearized model of the F-15. Figures X.1, X.2, and X.3 show the response of the aircraft to a failure of the right stabilator to 10 degrees from trim. The figures depict the response under adaptive control, sliding mode control, and adaptive robust control respectively. When evaluating

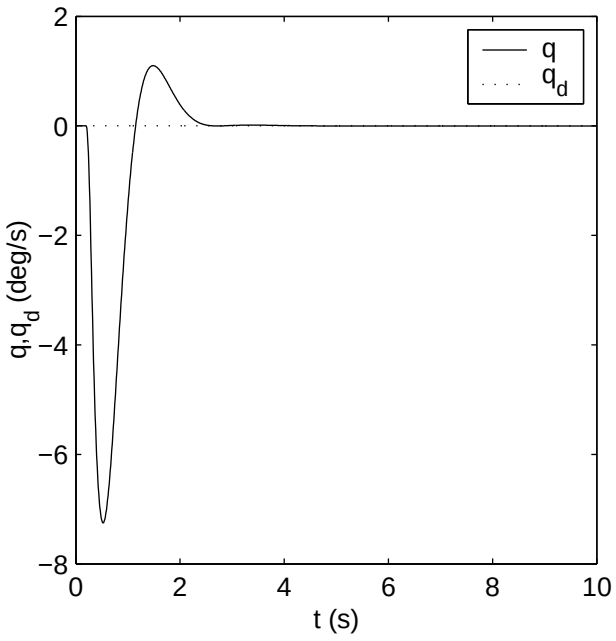

Fig. X.1. Transient response of linearized F-15 under AC to 10 degree stab failure

these responses, several factors will be considered. The first is the magnitude of error that is encountered at the time of the failure. It is clear that the responses in figures X.2 and X.3 experience nearly the same magnitude of error upon encountering a failure. These responses

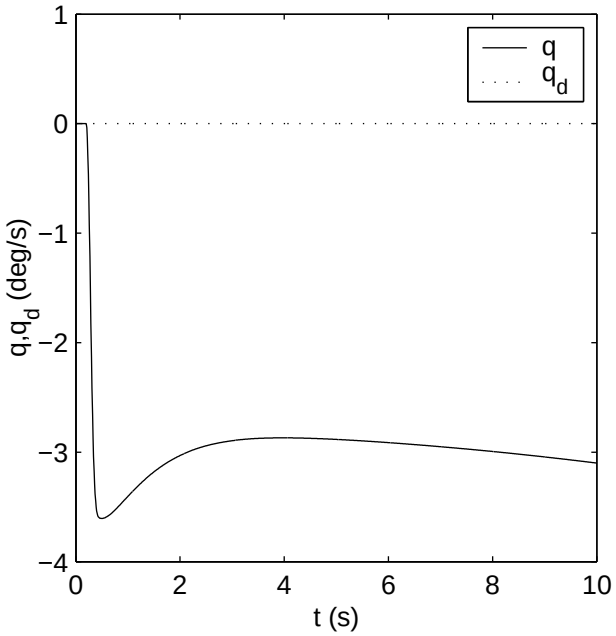

Fig. X.2. Transient response of linearized F-15 under SMC to 10 degree stab failure

correspond to the sliding mode and adaptive robust control methods. The adaptive control method has a much larger transient associated with the failure.

Additionally, we can examine the trend in error magnitude as a function of the failure magnitude for each of the control methods. Figures X.4, X.5, and X.6 show the maximum amplitudes of the error plotted as a function of the failure amplitude for adaptive control, sliding mode control, and adaptive robust control respectively. These figures note a few important things. First, we see that ARC and SMC allow the smallest transient magnitude. The magnitudes allowed for ARC and SMC are very similar to one another. This is what we expect to see since it is the goal of ARC to assimilate the transient performance of SMC into adaptive control. The trends for each methodology are linear with respect to the failure amplitude. This is because for the SISO case, the plant as well as the dynamic inversion control law are linear. The stuck actuator appears as a constant disturbance. Because of the choice of regressor as well as the use of a saturation function in place of a signum for the

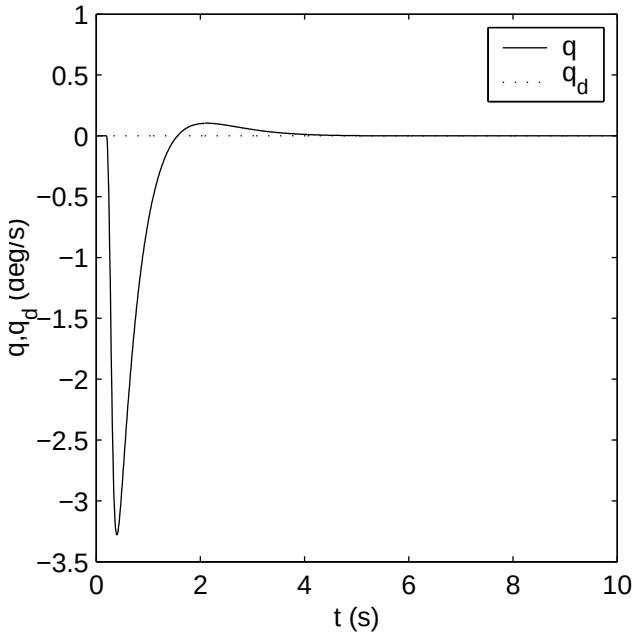

Fig. X.3. Transient response of linearized F-15 under ARC to 10 degree stab failure

SMC, the transfer function from the disturbance to the output is linear in a large band.

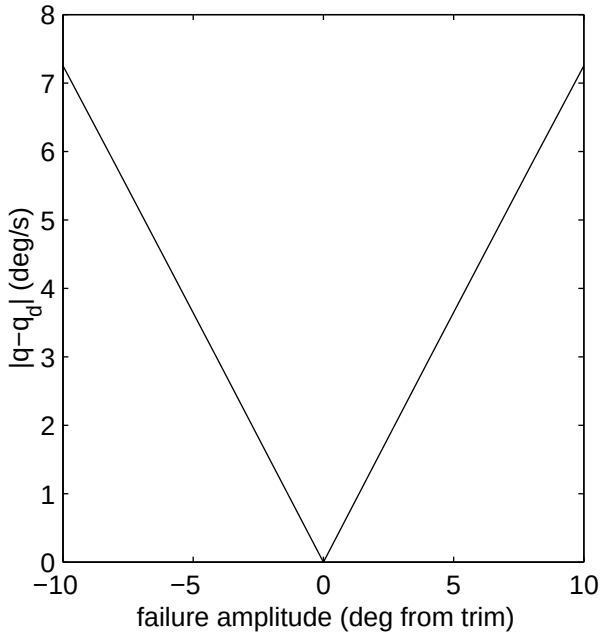

Fig. X.4. Maximum error magnitude as a function of failure amplitude for AC

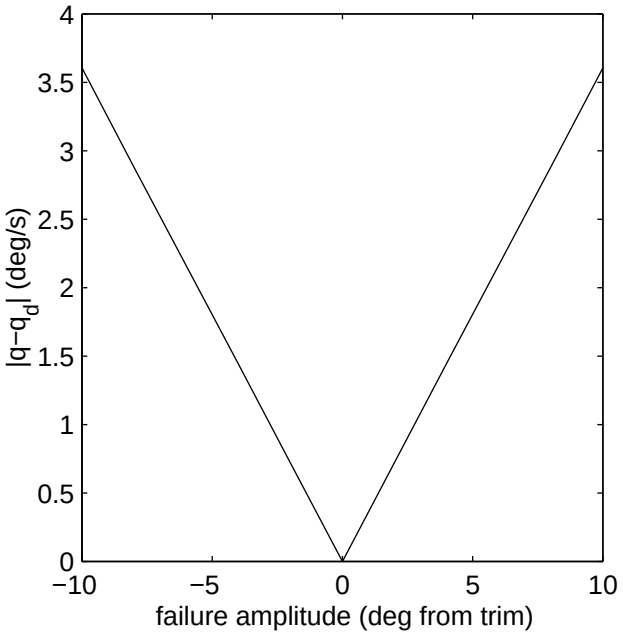

Fig. X.5. Maximum error magnitude as a function of failure amplitude for SMC

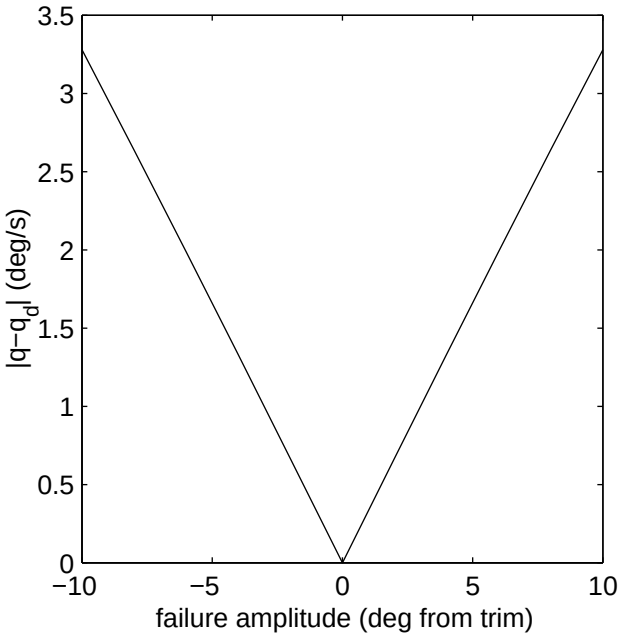

Fig. X.6. Maximum error magnitude as a function of failure amplitude for ARC

2. Full nonlinear F-15

The full nonlinear simulation of the F-15 IFCS aircraft provides a tougher control problem and also a better example of a practical system. As with the linearized system, the quality of each outer loop controller will be judged based on its transient response characteristics. Figures X.7, X.8, and X.9 show the transient response of the F-15 simulation to a stabilator failure to 8 degrees from trim at $t = 5$ seconds. As with the linear case, there are several important observations that must be made for these responses. Unlike the linear case, a failure in one axis results in disturbances in all three axes as demonstrated by the figures. The goal of the outer loop controllers is to minimize the effect of these disturbances.

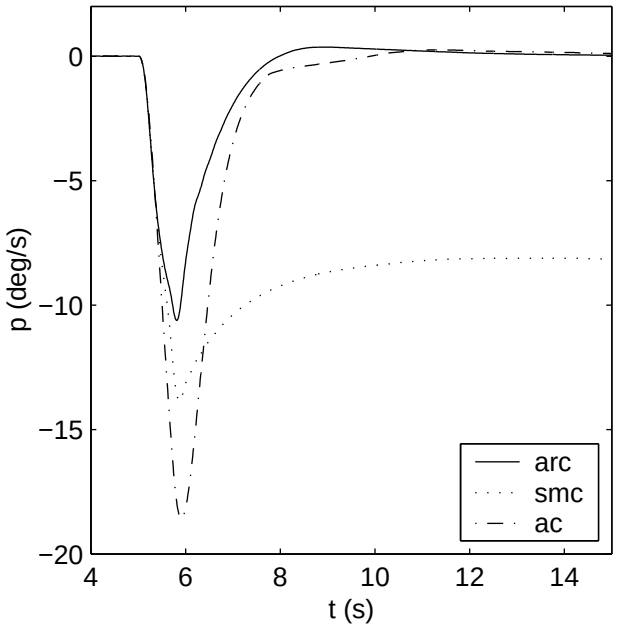

Fig. X.7. Roll axis transient response of nonlinear F-15 to 8 degree from trim stab failure

The figures provide a comparison of the ability of each control methodology to arrest the departure from the commanded body rates and to bring the aircraft back to its initial state. In the pitch axis, the ARC and SMC schemes are the most effective at quickly compensating for the failure. Examining figures X.7 and X.9 shows that this improvement

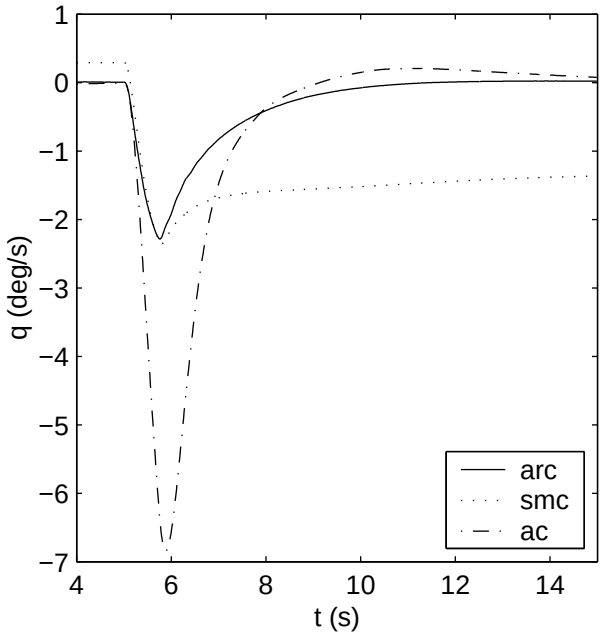

Fig. X.8. Pitch axis transient response of nonlinear F-15 to 8 degree from trim stab failure

in reponse does not come at the expense of the other axes. For the roll axis, the ARC scheme seems to work the best. Figures X.7, X.8, and X.9 are representative of the response for every failure position. The maximum error can be related to the failure amplitude as was done for the linear case. Figures X.10, X.11, and X.12 show the maximum transient error magnitude for each of the roll, pitch, and yaw axes respectively. In contrast to the linearized model, the maximum tracking error amplitude does not appear to be related linearly to the failure amplitude, although the shape of the curve is similar. The adaptive control technique clearly shows a much larger sensitivity to the failure amplitude. The SMC and ARC techniques provide the best response in terms of the maximum transient error. The pitch axis response (Figure X.11) exhibits some interesting behavior behavior for ARC and SMC. As the failure amplitude approaches -13 degrees from trim, the transient error amplitude begins to grow very quickly with failure position. This has to do with limitations in the stabilator surface position of the aircraft. As the failure amplitude gets large in the

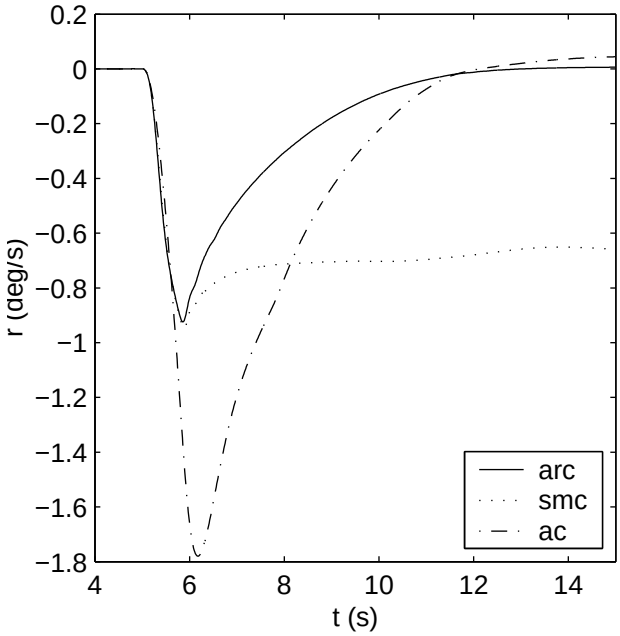

Fig. X.9. Yaw axis transient response of nonlinear F-15 to 8 degree from trim stab failure

negative direction, the required compensation in the positive direction begins to get close to the surface position limit. The pitch axis of the F-15 has only two control surfaces, left and right stabilator. When one of these becomes unresponsive (the right stabilator for our example), the aircraft has only one actuator to control the pitch direction. When this actuator becomes saturated, the maximum moment is achieved, limiting the speed of the response. This is the reason for the large increase in error for the pitch axis at around -13 degrees from trim.

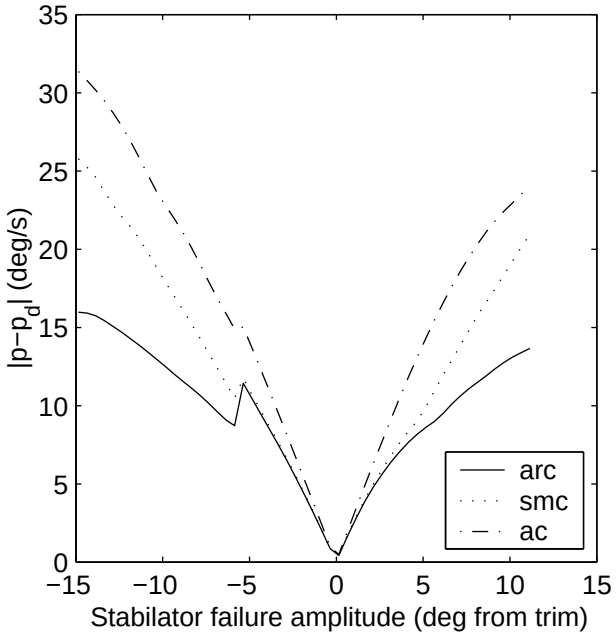

Fig. X.10. Maximum error magnitude as a function of failure amplitude for roll axis

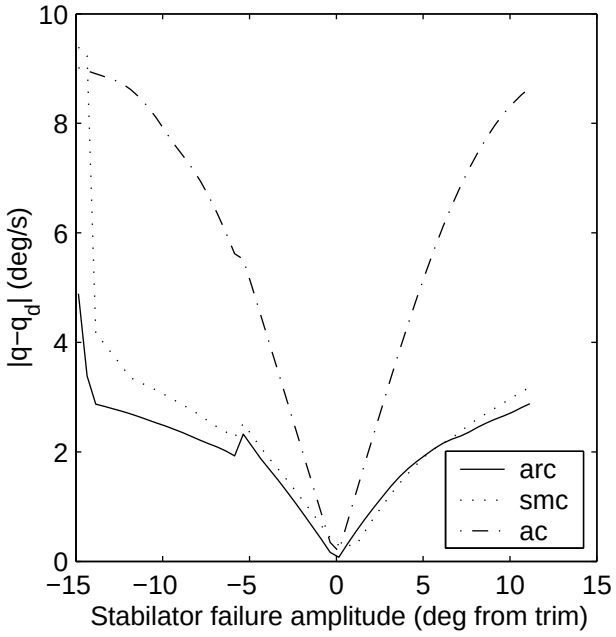

Fig. X.11. Maximum error magnitude as a function of failure amplitude for pitch axis

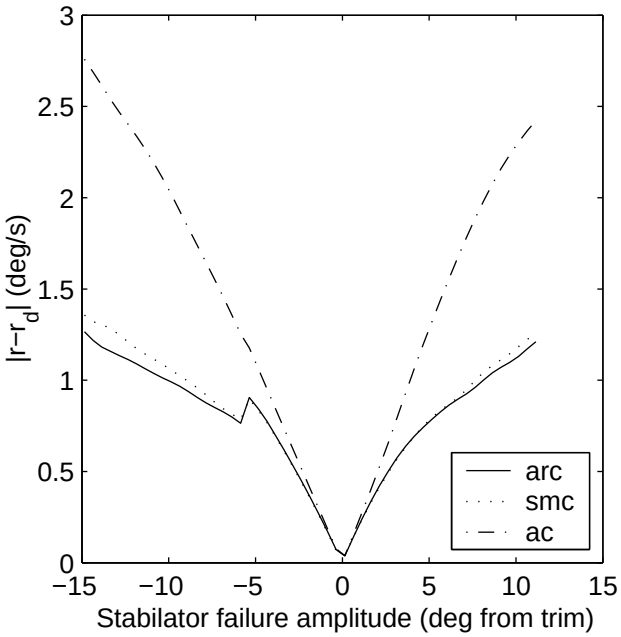

Fig. X.12. Maximum error magnitude as a function of failure amplitude for yaw axis

B. Tracking Response Analysis

Once an actuator fails, and the aircraft has been restored to straight and level flight, it is important that the plane still exhibit a maximum degree of maneuverablilty. If the plane were to recover, but then were to fly unpredictably afterward, this would be unacceptable. It is ideal to be able to recover to normal flight, and to be able to bring the plane home. Landing the plane would become extremely difficult if when the pilot commanded pitch, the plane rolled excessively. Not only must the aircraft respond predictably, it must also be sensitive enough to pilot to allow the pilot enough authority to bring the plane home or land. In this section, the three outer loop control methods are compared with respect to their ability to track a command or series of commands. The performance will be measured in terms of a frequency weighted performance measure as well as a command weighted measure.

1. Linearized F-15

We begin our analysis with the linearized F-15 model. For this model, only one type of command profile (as diplayed in Figure IX.2) will be considered. Because we are only looking to control one axis, there is no cross-coupling from other axes. Because of this, a single doublet input provides enough information to adequately compare each of the three outer loop control methodologies. The responses of the sliding mode control, adaptive control, and adaptive robust control methodologies to a doublet input for the linearized F-15 model are given in figures X.13, X.14, and X.15 respectively. These cases are for failures at trim. This removes the steady state error associated with the sliding mode control methodology.

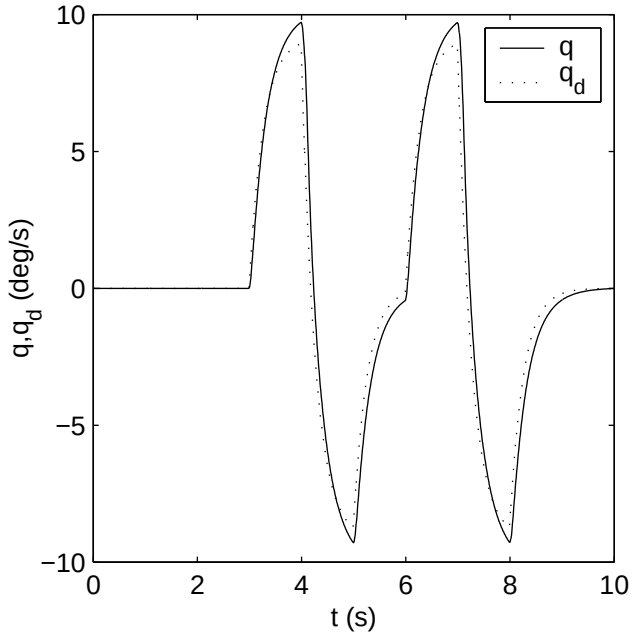

Fig. X.13. SMC doublet input response for linearized F-15 model

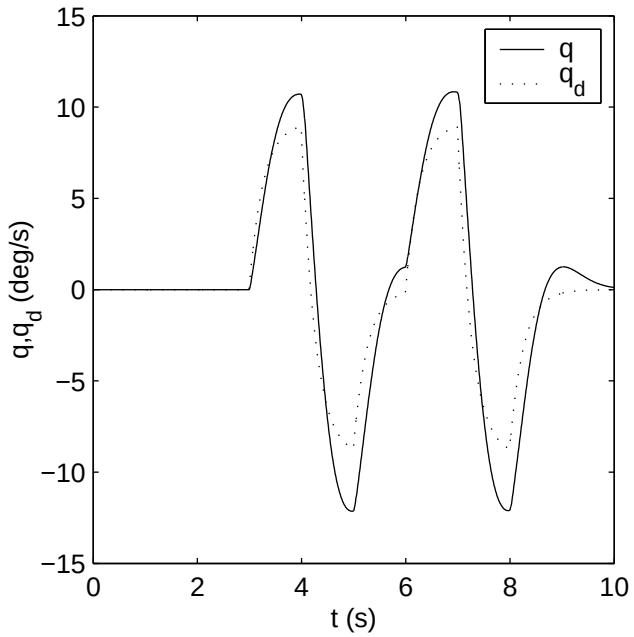

Fig. X.14. AC doublet input response for linearized F-15 model

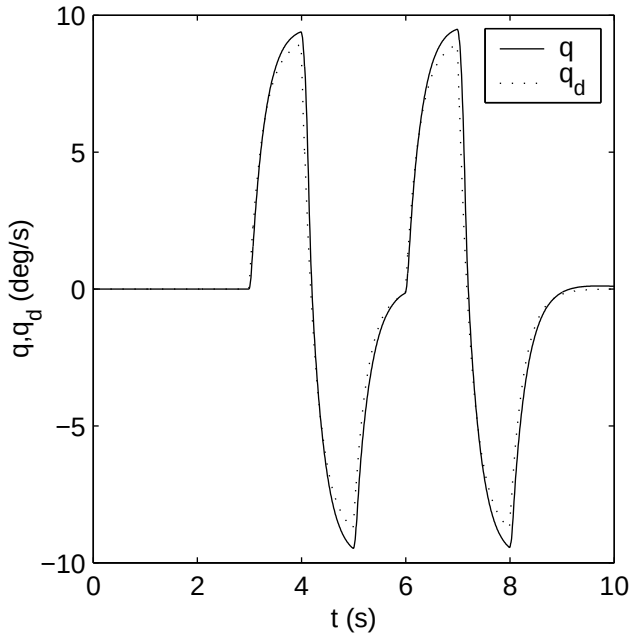

Fig. X.15. ARC doublet input response for linearized F-15 model

In aircraft applications it is always important to consider the control surface response when any state responses are considered. If the control responses are high frequency this is very unfavorable. The control surface responses provide a sanity check to ensure that the tracking response is acheived despate the limits imposed on the system and without the surfaces performing in odd ways. Figure X.16 shows the left stabilator response for the responses shown in figures X.13, X.14, and X.15 above. The right stabilator response is not show because it exhibits a constant amplitude response. To analyze the tracking ca-

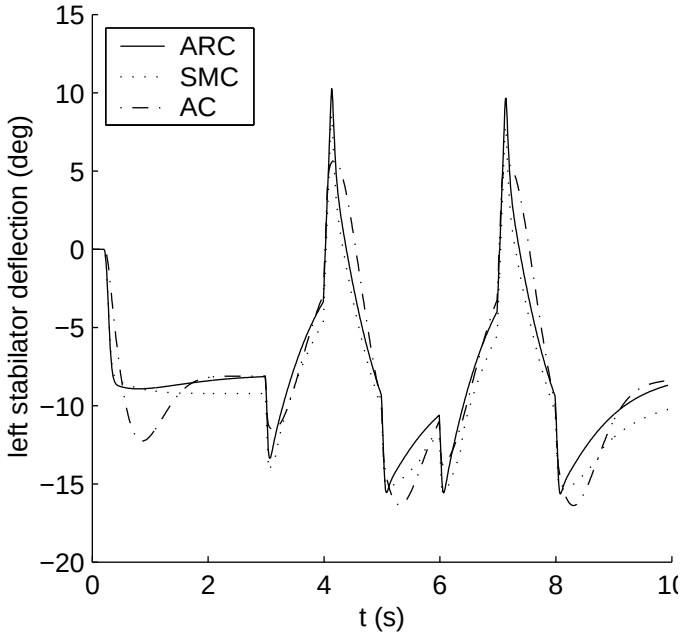

Fig. X.16. Left stabilator response of linearized F-15 for doublet inputs with a failure at trim

pabilities of each control methodology the measure discussed in section VIII is utilized. Because we are interested in tracking and not in the steady state errors, we will remove the average steady state error of each response before finding its measure value. If we examine the measure of each control loop for various failure amplitudes and command amplitudes, figures X.17, X.18, and X.19 are obtained. What is remarkable about these figures is the lack of change exhibited in the measure value due to a change in failure amplitude for

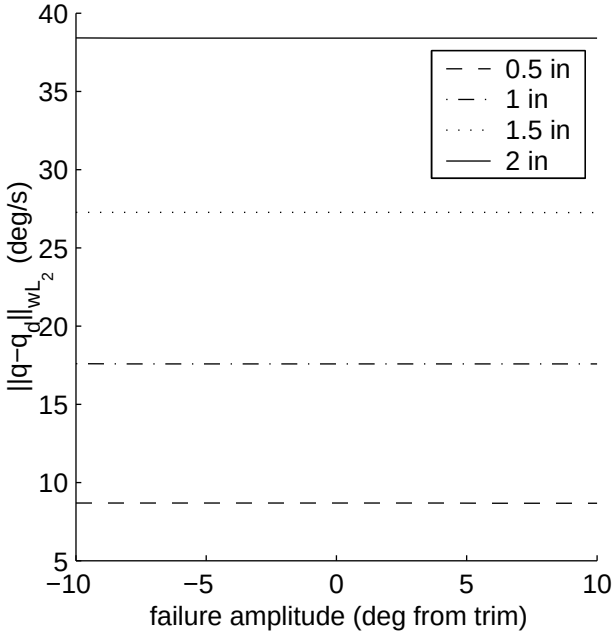

Fig. X.17. Weighted $\|q - q_d\|_{\mathcal{L}_{2\dot{u}}}$ of AC error response to failures for linearized F-15 model

figures X.17 and X.19. At first glance, this seems to be a mistake, but when the nature of the linear system under DI control is considered, it becomes clear that this is reasonable. A stuck actuator type of failure results in a constant disturbance acting on the system as well as a change in the state evolution (*A* and *B* matrices) under dynamic inversion control. The change in the *A* and *B* matrices is independent of the failure amplitude, however. Furthermore, the AC and ARC laws contain integral action (due to the adaptive portions of the control). This integral in the feedforward path of the system serves to eliminate constant steady state error. Therefore, as long as an actuator limit is not reached, the steady state error can be removed. Therefore, for these cases, the failure position does not affect the tracking accuracy. For the SMC case, this seems to be true because the steady state error has been removed (which an integral control would do if part of the control law). However, the measure value is not flat over the entire region of failures. In addition, as the command amplitude gets larger, the measure value tends to vary more with failure amplitude. This is

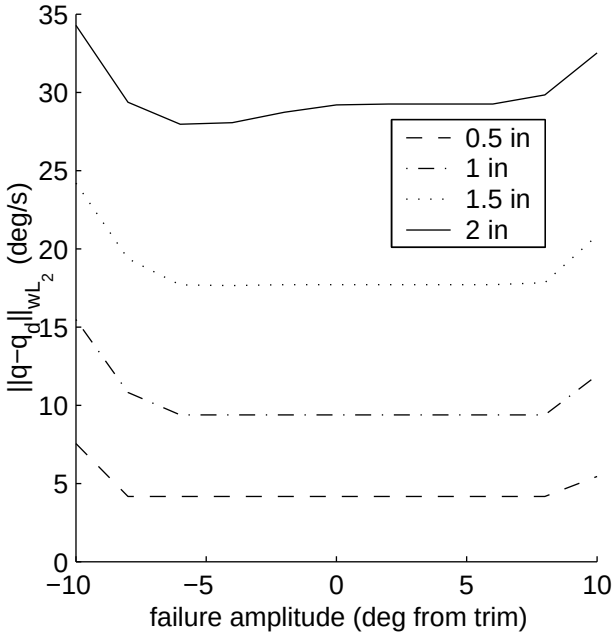

Fig. X.18. Weighted $\|q - q_d\|_{\mathcal{L}_{2\hat{u}}}$ of SMC error response to failures for linearized F-15 model

a result of the failure of SMC to eliminate steady state errors. A steady state error results in a non-zero steady-state *z* (the sliding surface value). The result is a saturation of the sliding mode portion of the control law during pilot commands, causing the control to become nonlinear. This does not occur in ARC due to the adaptive portion of the control forcing z to zero in steady state. The adaptive portion of the control allows the control to stay in the linear region more consistently and utilize the full range of the sliding mode controller. Figure X.20 shows some values for $h(t,x)\,\mathrm{sat}(z/\varepsilon)$ for the ARC and SMC laws. This figure is for a stick amplitude of 2in. and a failure amplitude of -8 degrees from trim. As the figure demonstrates, the SMC law is much closer to saturation in the negative direction. This results in a far smaller "gain" in the negative direction because the control has less room to deviate from equilibrium (although the control has more relative authority in the positive direction). Even with the sensitivity to failure amplitude exhibited by the SMC outer loop controller, the measure values obtained are still smaller than that of AC. This means that

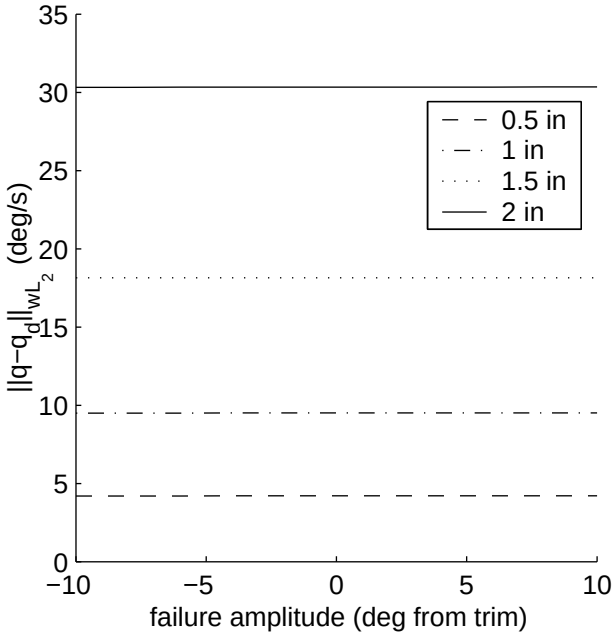

Fig. X.19. Weighted $\|q - q_d\|_{\mathcal{L}_{2\dot{u}}}$ of ARC error response to failures for linearized F-15 model

with steady state error not included, the tracking performance of SMC is better than that of AC. The measure values for ARC are equivalent to that of SMC, but without the sensitivity to failure amplitude (disturbance size).

2. Full nonlinear F-15

For the full nonlinear simulation of the F-15 aircraft, similar results are expected. With the addition of other control axes, the problem becomes more difficult. To capture the full extent of the problems caused by coupling three different maneuvers will be examined. These maneuvers were explained in Section IX and displayed in figures IX.3, IX.5, and IX.7.

Plain Doublets The first maneuver will be simliar to the one utilized in the linearized F-15 model. Each axis will be excited independently. This means that while one axis is tracking, the other two are regulating. This case will be the simplest one examined and

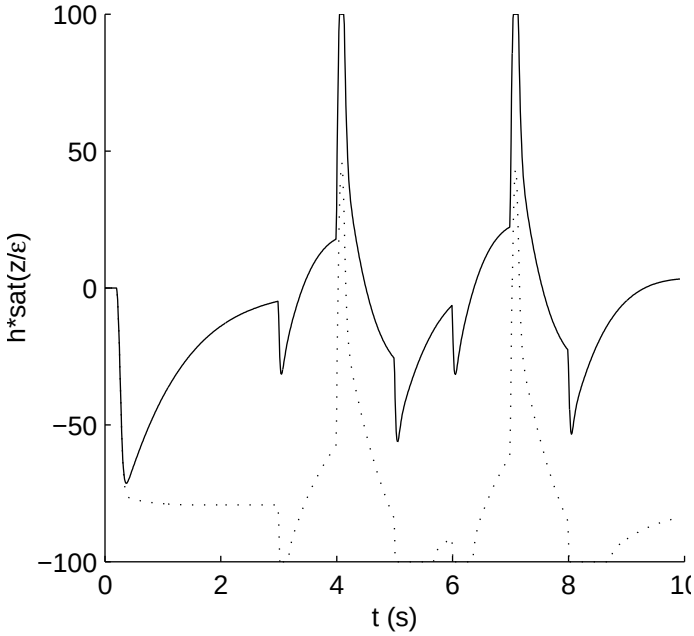

Fig. X.20. Time response of $h(t,x)\,\mathrm{sat}(z/\varepsilon)$ for ARC and SMC

will also exhibit the most accurate tracking results in terms of the performance measure denoted by $\|\cdot\|_{\mathcal{L}_{2\dot{u}}}$. Sample responses for each axes (roll, pitch, and yaw) given a 4 degree from trim stabilator failure are given in figures X.21, X.22, and X.23. These figures depict the response of the aircraft under each control methodology. As with the linearized case, the steady state error does not decay to zero for the SMC methodology. If the constant error is removed from the SMC control the control will track fairly accurately. This is the premise behind ARC. The responses in figures X.21 - X.23 also depict the cross coupling associated with the disturbances induced on each axis by DI mismatch in the other axes. This cross-coupling is not present when there is no failure. The figures demonstrate that while each of the control methodologies does stabilize the aircraft and track a reference command, each control methodology performs different tasks well. As mentioned for the linearized F-15, the control surface responses are important in ensuring that the response does not contain high frequencies. Figures X.24, X.25, and X.26 show the control surface

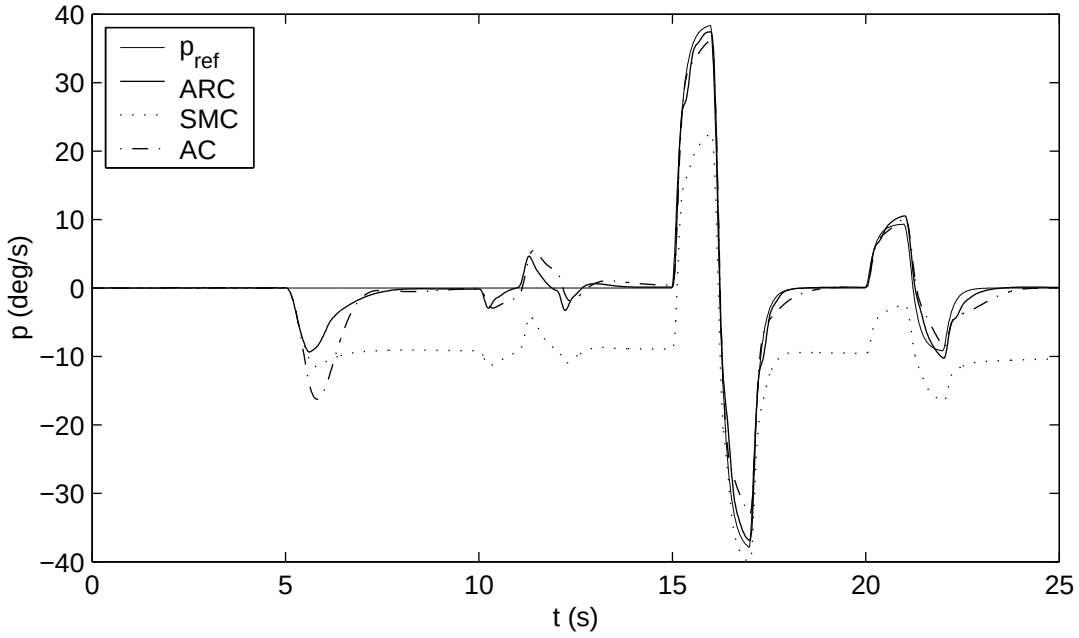

Fig. X.21. F-15 Roll axis response to PD input given a +5 degree from trim stabilator failure

responses of the F-15 to the PD input profile given a +5 degree from trim stabilator failure at $t = 5$ seconds. The right stabilator response is not shown because it is constant until the failure and then moves to +5 degrees from trim. The ailerons can only be commanded differentially and rudders symmetrically, so the differential and symmetric commands are shown. These commands show that there is no oscillation in the control surfaces that might lead to instability or PIO. They also clearly show how the other control surfaces must reconfigure in order to maintain control of the aircraft and eliminate steady state error. The control surface response for SMC clearly shows how the aircraft is not maintaining level flight due to steady state errors. This is why the surfaces do not settle down in steady state. The surface responses for the remainder of the thesis will be omitted to reduce redundancy. The responses are all fairly similar to those seen in these figures in terms of their frequency content.

To help judge the tracking abilities of each control technique, a version of the weighted

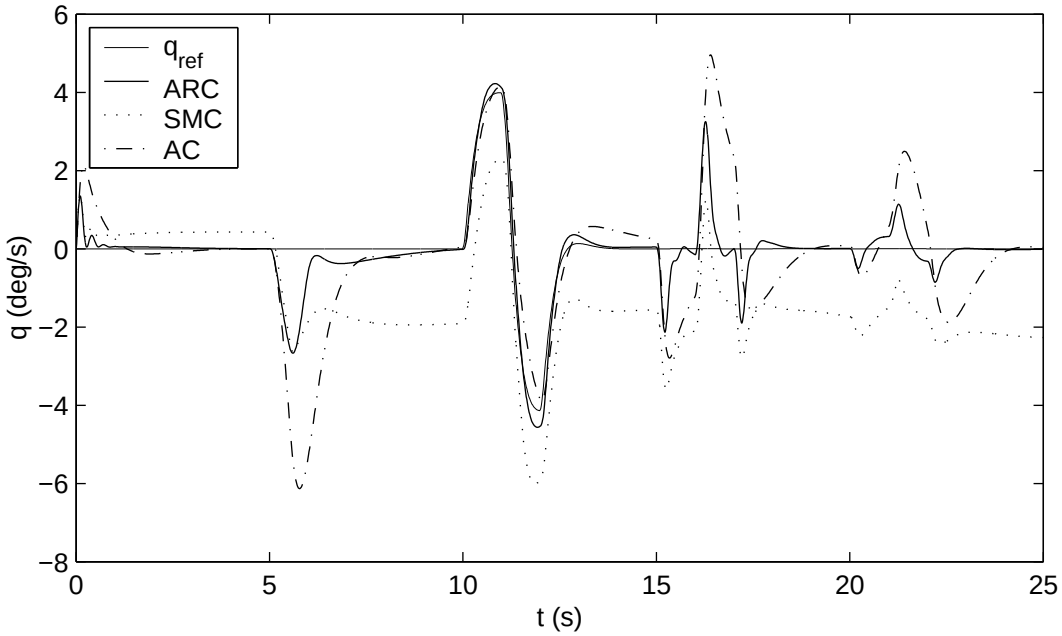

Fig. X.22. F-15 Pitch axis response to PD input given a +5 degree from trim stabilator failure

$\mathcal{L}_2$ norm described previously will be used. The specific performance measure utilized will be that defined by (VIII.5). More specifically, we will combine this measure with the weighting in the norm denoted by $\|\cdot\|_{\mathcal{L}_{2W}}$ so that we have a weighted version of the measure, which will be defined by $\|\cdot\|_{\mathcal{L}_{2Wcc}}$. The usage of the weighted measure allows the penalization of high frequency error. Utilizing a measure that takes into account cross coupling allows increased penalization of error that occurs for "easy" tracking tasks over error that occurs because of large, quick commands.

Figures X.27, X.28, and X.29 show the relationship between the measure value of the error signal, and the failure amplitude. Unlike the linear case, there is more sensitivity to the failure amplitude. However, there is no clear relationship to describe this dependence. As the failure amplitude gets large enough, the tracking ability of each control methodology begins to decline and the measure value increases in size rather rapidly. This is more pronounced for SMC because of the inability of method to trim. For the figures, the steady

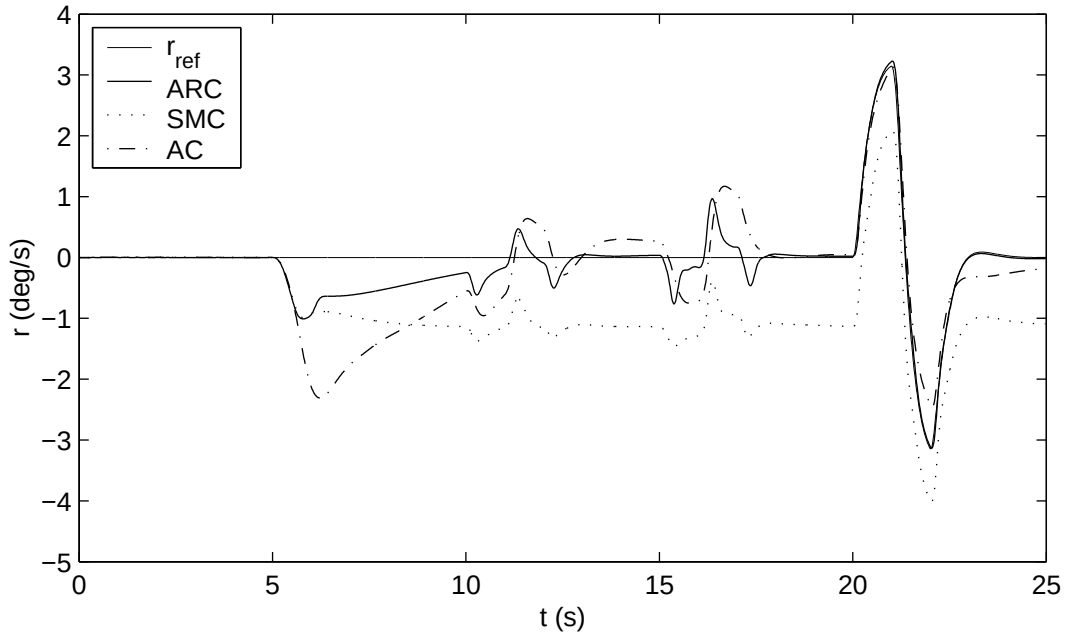

Fig. X.23. F-15 Yaw axis response to PD input given a +5 degree from trim stabilator failure

state error portion of SMC is removed to allow for a more fair comparison. The SMC results are more difficult to quantify because after a command in any axis, the aircraft will never return to its previous state. SMC displays more sensitivity to failure amplitude (especially as the failure amplitude becomes more negative) because of the saturation problem discussed in figure X.20. On the whole, these figures show that ARC and SMC do the best job of tracking. ARC exhibits better tracking qualities than SMC on the whole spectrum of failure amplitudes. The figures demonstrate that even when performing pilot commands in each axis separately, to maintain tracking properties and reduce cross coupling, ARC seems to be the best choice.

Figures X.27 - X.29 have been generated for stick and pedal inputs of 0.5”. Similar figures can be generated for larger command amplitudes, Figures X.30 - X.32 are generated for 1.5” stick and rudder inputs. These figures show that as the command amplitude increases, the errors (and hence the performance measure as a function of the errors) be-

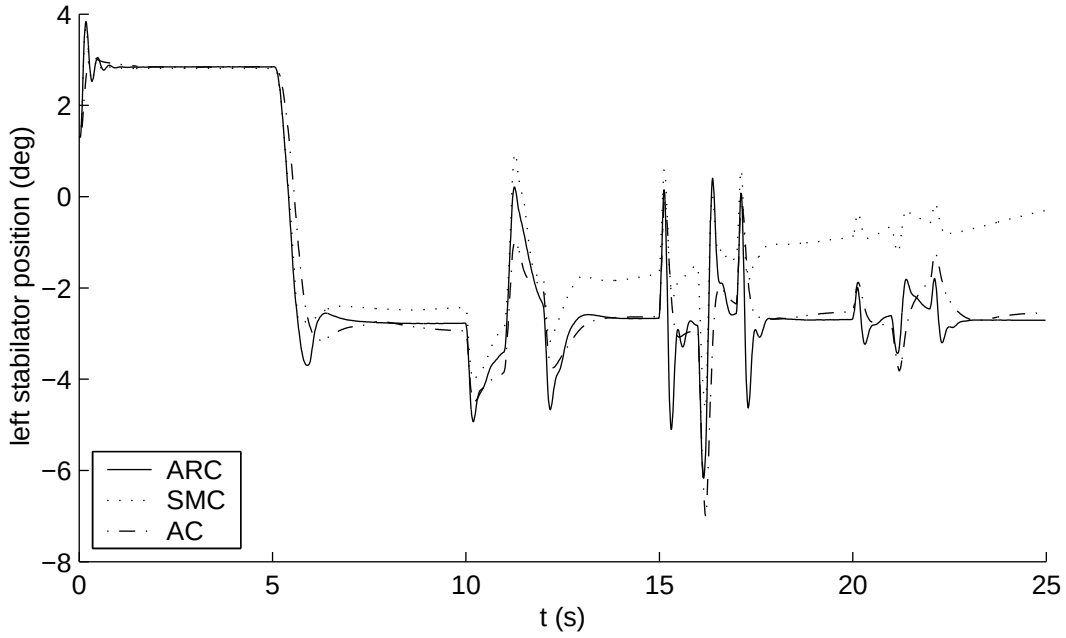

Fig. X.24. F-15 stabilator response to PD input given a +5 degree from trim stabilator failure

come larger. This increase in size of the tracking error is not proportional to the increase in command size because the cross-coupling measure helps to minimize this. The tracking error increase instead is caused by surface limits, coupling between axis, and control limitations. For sliding mode control, the control saturation problem becomes worse causing its ability to track to decline. All of the methodologies begin to suffer at higher command amplitudes when the failure position reaches -10 degrees from trim due to surface limitations. ARC varies less than the other methodologies with command amplitude.

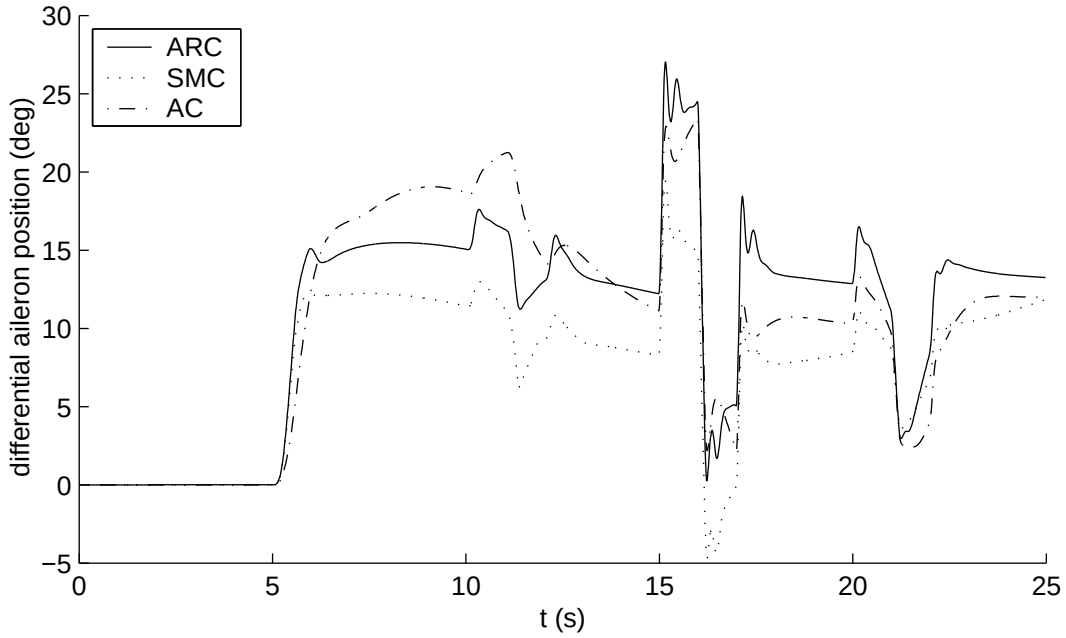

Fig. X.25. F-15 aileron response to PD input given a +5 degree from trim stabilator failure

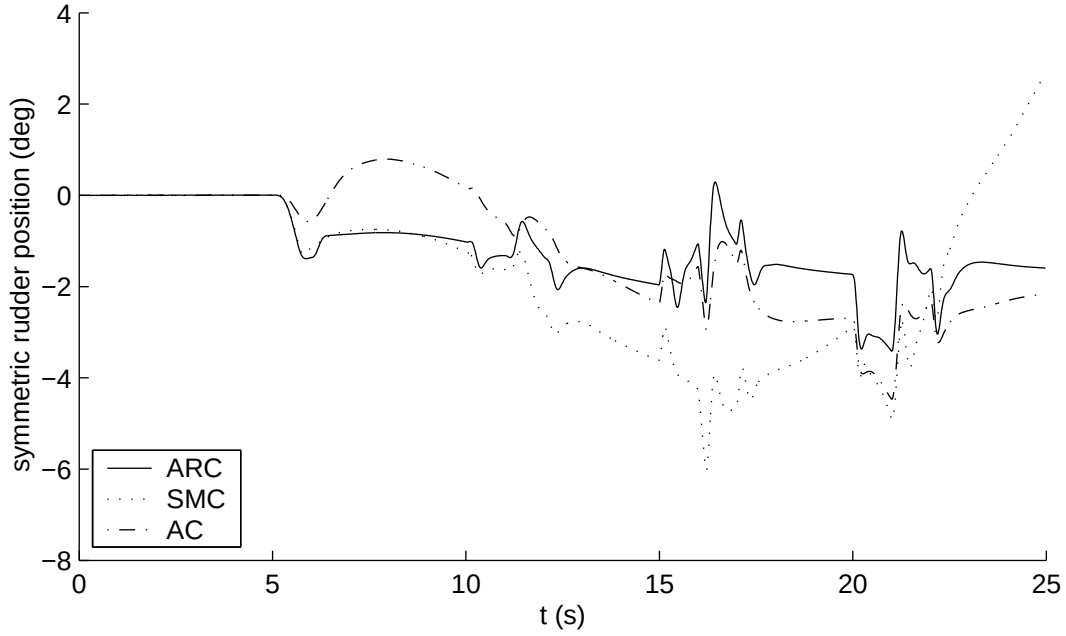

Fig. X.26. F-15 rudder response to PD input given a +5 degree from trim stabilator failure

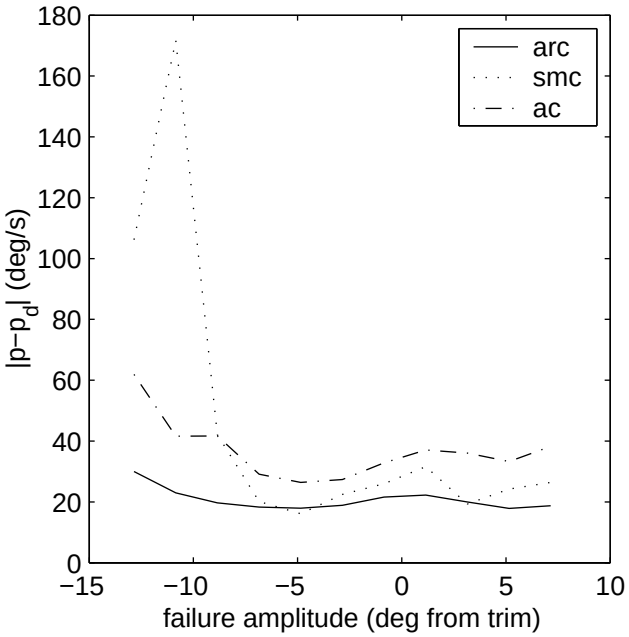

Fig. X.27. $\|p - p_{des}\|_{\mathcal{L}_{2Wcc}}$ as a function of failure amplitude for 0.5” PD input profile

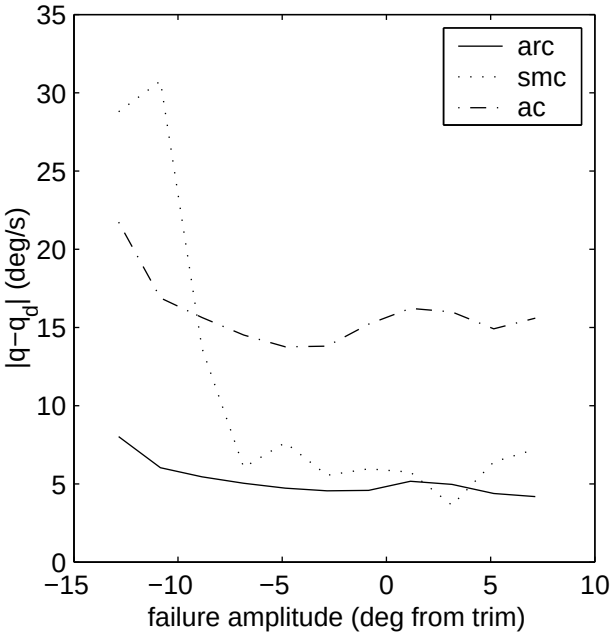

Fig. X.28. $\|q - q_{des}\|_{\mathcal{L}_{2Wcc}}$ as a function of failure amplitude for 0.5” PD input profile

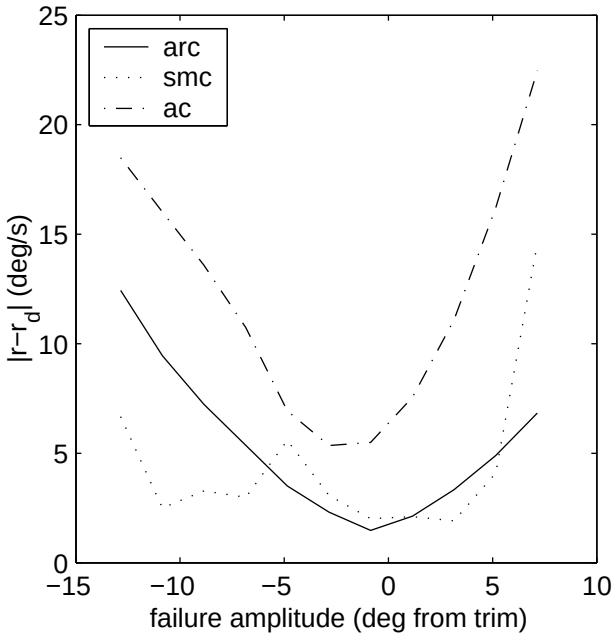

Fig. X.29. $\|r - r_{des}\|_{\mathcal{L}_{2Wcc}}$ as a function of failure amplitude for 0.5” PD input profile

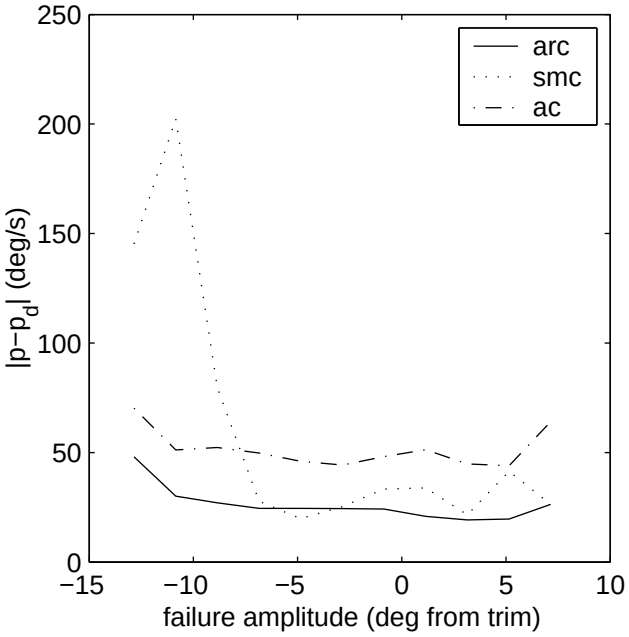

Fig. X.30. $\|p - p_{des}\|_{\mathcal{L}_{2Wcc}}$ as a function of failure amplitude for 1.5” PD input profile

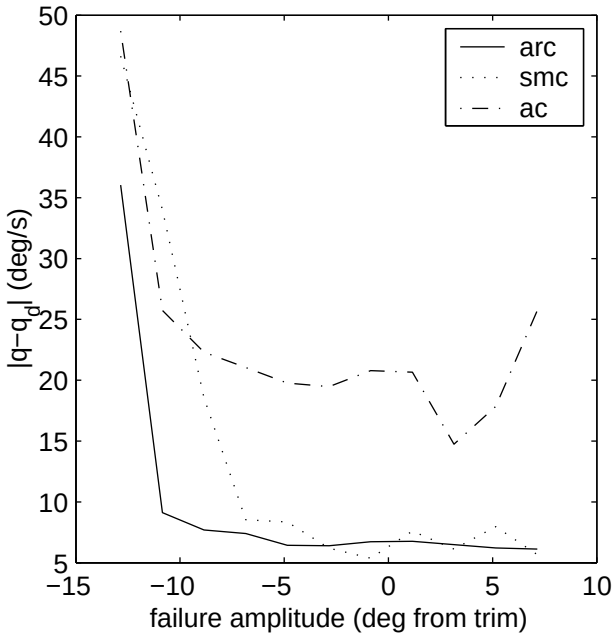

Fig. X.31. $\|q - q_{des}\|_{\mathcal{L}_{2Wcc}}$ as a function of failure amplitude for 1.5” PD input profile

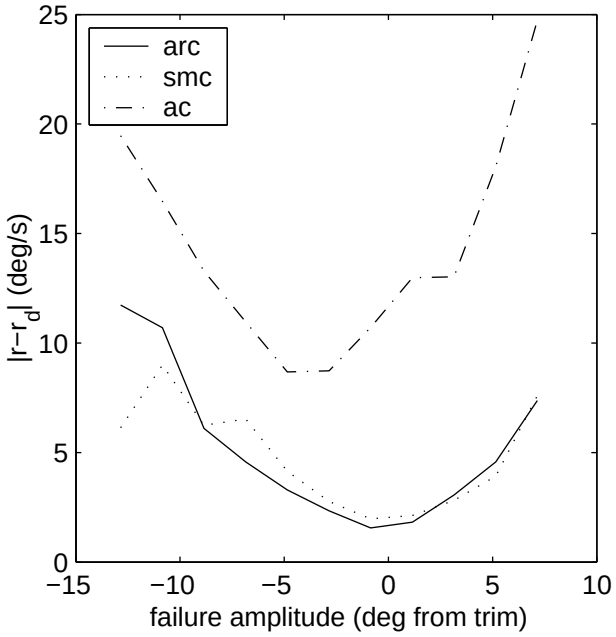

Fig. X.32. $\|r - r_{des}\|_{\mathcal{L}_{2Wcc}}$ as a function of failure amplitude for 1.5” PD input profile

Coupled Doublets The PD input profile provided a baseline for how the outer loop controllers are expected to perform. The input profile serves as a best case scenario. It is the easiest on the surfaces because it does not combine axes. This is particularly important in the pitch axis because the stabilators that control pitch are also allocated to control roll as well. If one stabilator fails, then only one actuator is available for the pitch axis, but this actuator is also being utilized to control the roll axis as well. When the pilot only commands one axis at a time, this problem is not that important. When the pilot attempts to track commands in multiple axis, the problem is realized. Thus, the CD input profile is designed to test the ability of the control methodologies to deal with this cross coupling in isolated cases. Figures X.33, X.34, and X.35 show the aircraft response in each axis to 1" stick and rudder inputs for the CD input profile in the presence of a -5 degree from trim stabilator failure. This input profile excites two axes at a time with a doublet. The

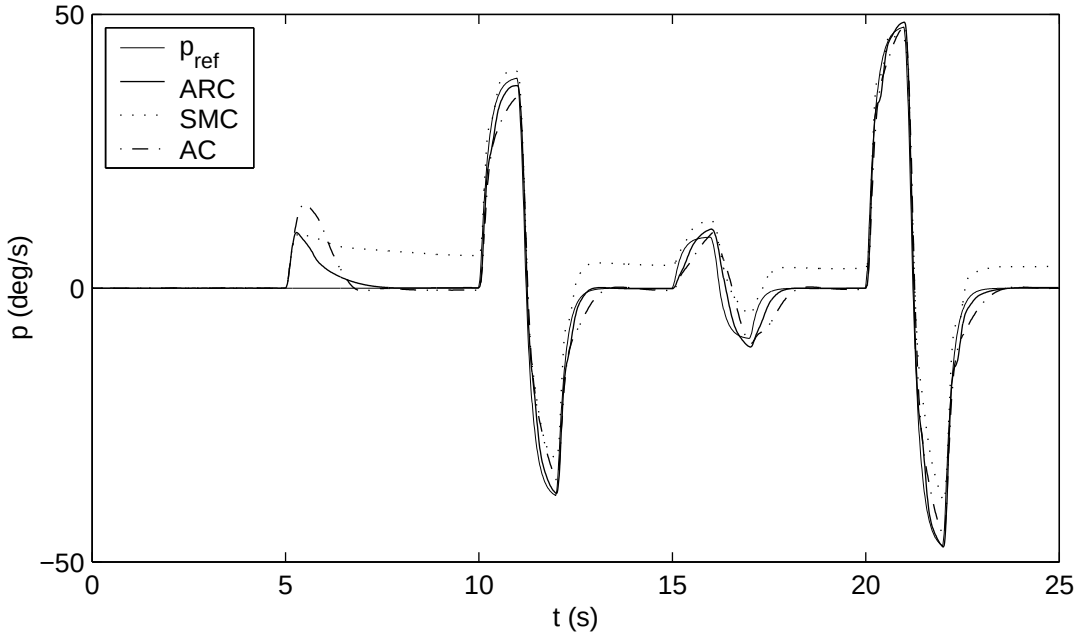

Fig. X.33. F-15 Roll axis response to CD input given a -5 degree from trim stabilator failure

first doublet is performed in the roll and pitch axes, the second in pitch and yaw axes, and

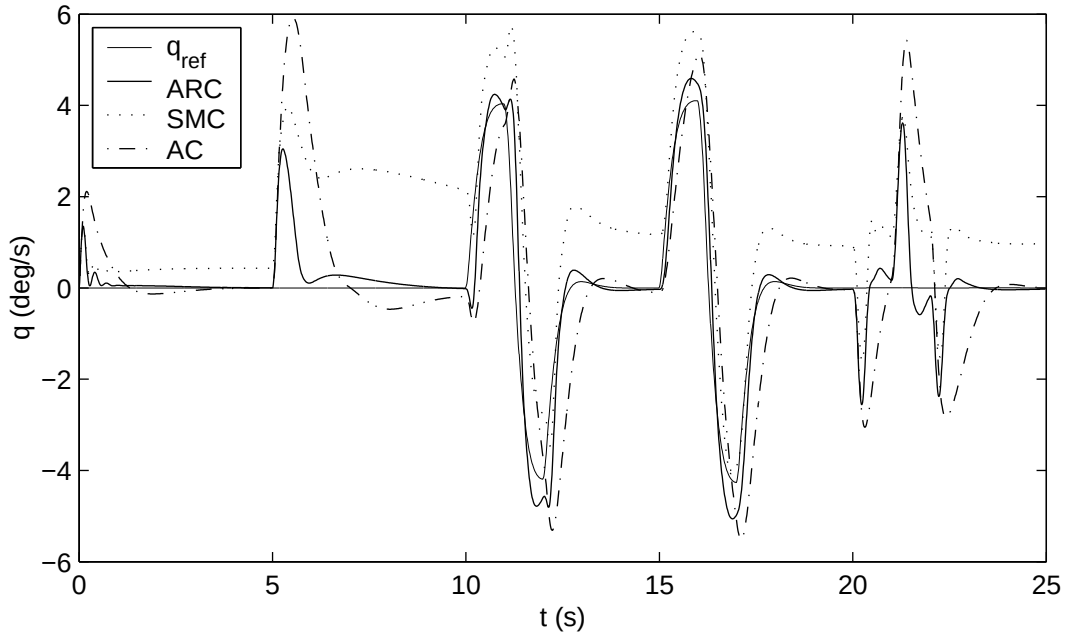

Fig. X.34. F-15 Pitch axis response to CD input given a -5 degree from trim stabilator failure

the third in the roll and yaw axes. The roll and yaw axes exhibit similar characteristics to those in figures X.21 and X.23. In the pitch axis the coupling begins to play a role in the pitch/roll axis doublet set ($t = 10s$). When the simultaneous pitch and roll doublets begin, the pitch response first moves in the wrong direction due to the failure and the added cross coupling. The AC outer loop technique exhibits this behavior more drastically than the other two methods. We also see that the tracking accuracy seems to degrade for each of the three methods and more specifically for the AC method. As with the PD input profile, we can examine the measure values of each error response versus the stabilator failure amplitude. Figures X.36, X.37, and X.38 display these measure values for 0.5" stick and pedal inputs. The measure values for the CD input profile are slightly larger than those for the PD inputs, but the change is not extremely large due to the cross-coupling normalization. The comparison of figures X.27, X.28, and X.29 with figures X.36, X.37, and X.38 shows that the measure values are fairly similar. This means that the measure defined as $\|\cdot\|_{\mathcal{L}_{2Wcc}}$

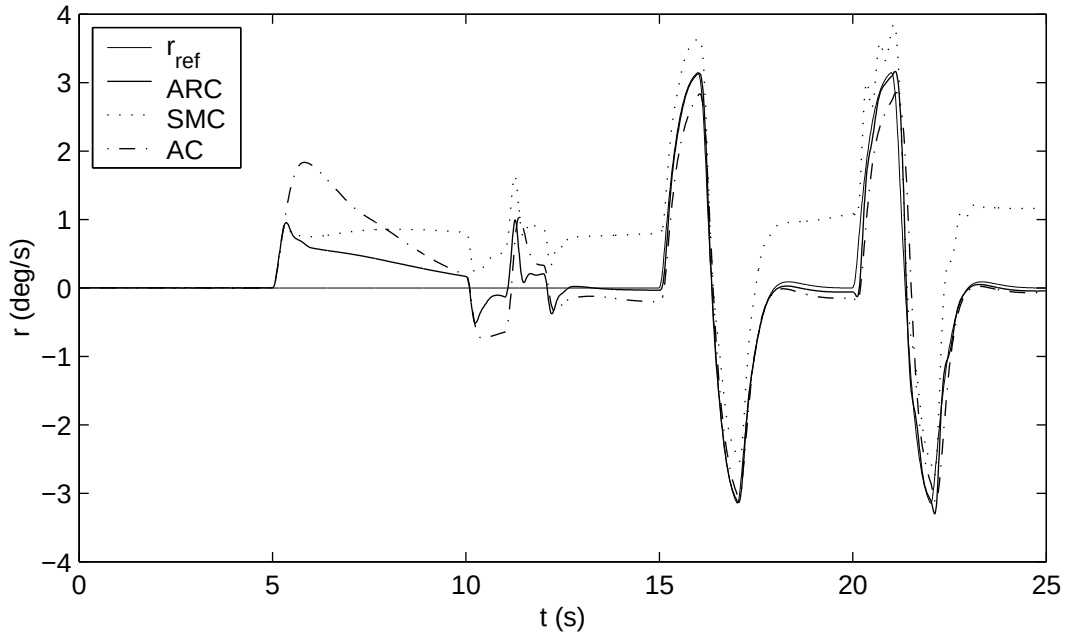

Fig. X.35. F-15 Yaw axis response to CD input given a -5 degree from trim stabilator failure

can be used to compare a wide range of maneuvers regardless of the aggressiveness of the input (at least in terms of tracking response - overall response will be compared later). The figures again demonstrate that ARC outperforms both SMC and AC in tracking of a more aggressive maneuver. The tracking accuracy again remains fairly constant for ARC regardless of the failure amplitude for the p and q axes. Because of the aggressiveness of the maneuver, as the failure amplitude gets larger the tracking accuracy declines at a rapid rate. This is again true especially in the negative direction. The AC and SMC techniques begin to suffer from this even for the 0.5” stick inputs. Figures X.39, X.40, and X.41 show the relationship between failure amplitude and the $\|\cdot\|_{\mathcal{L}_{2Wcc}}$ value of the error for each of the three control axes for 1” stick and pedal inputs. The values increase with command amplitude because the aggressiveness of the maneuver keeps the aircraft from physically being able to track with the current control allocation. At this point, surfaces are coming close to hitting rate limits during the maneuver. Again, because there is only one actuator controlling the

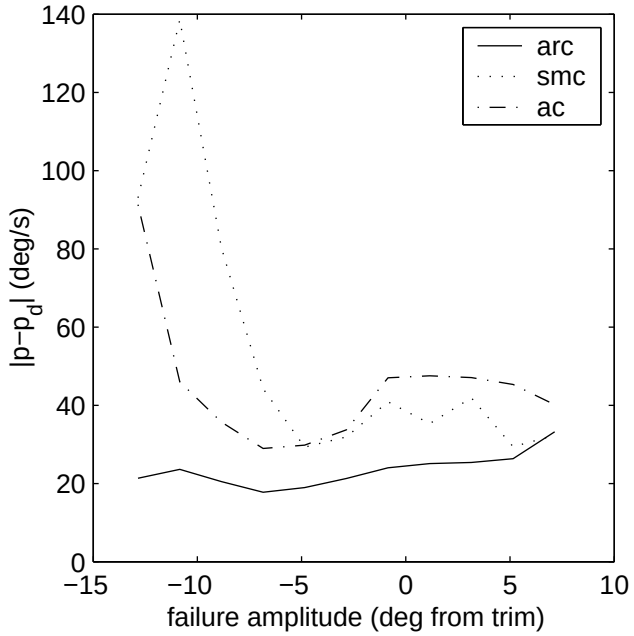

Fig. X.36. $\|p - p_{des}\|_{\mathcal{L}_{2Wcc}}$ as a function of failure amplitude for 0.5” CD input profile

pitch axis, there has to be a trade-off between tracking quality in the axes when multiple axes are excited. This is why the measure values of the error responses of each axis go up as the command amplitude increases. On the whole, the figures demonstrate that ARC performs simple as well as fairly aggressive tracking maneuvers much better than SMC and AC alone.

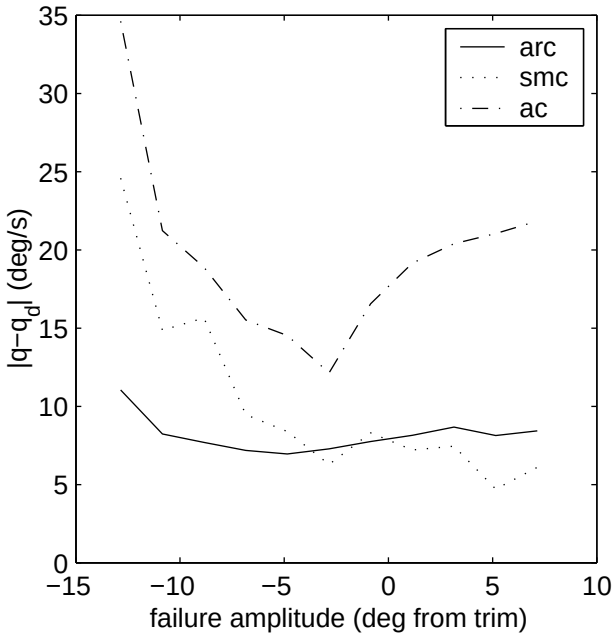

Fig. X.37. $\|q - q_{des}\|_{\mathcal{L}_{2Wcc}}$ as a function of failure amplitude for 0.5” CD input profile

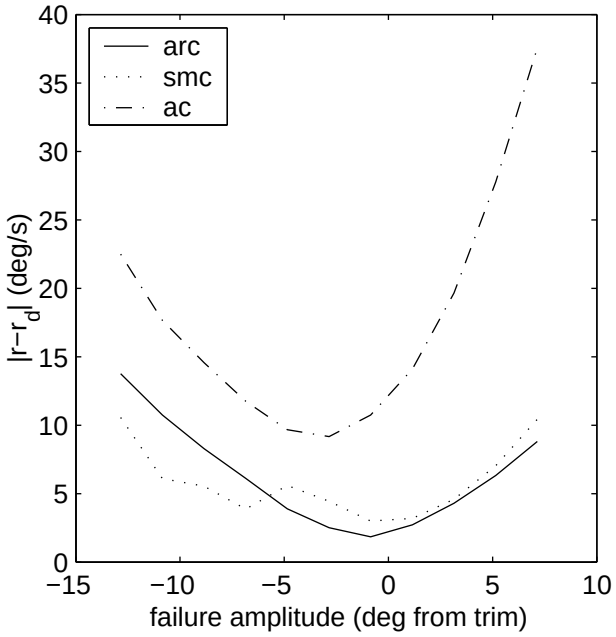

Fig. X.38. $\|r - r_{des}\|_{\mathcal{L}_{2Wcc}}$ as a function of failure amplitude for 0.5” CD input profile

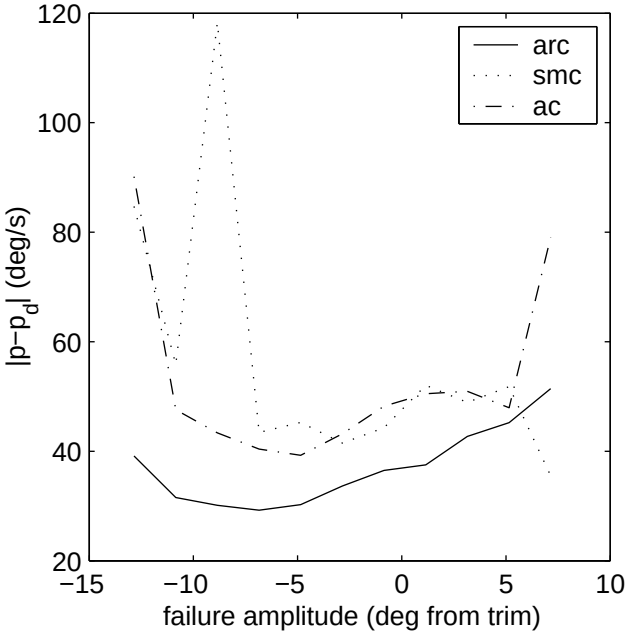

Fig. X.39. $\|p - p_{des}\|_{\mathcal{L}_{2Wcc}}$ as a function of failure amplitude for 1.0” CD input profile

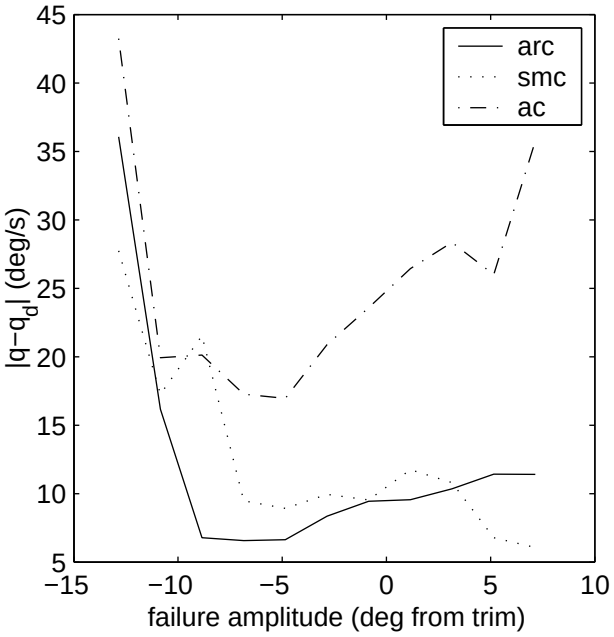

Fig. X.40. $\|q - q_{des}\|_{\mathcal{L}_{2Wcc}}$ as a function of failure amplitude for 1.0” CD input profile

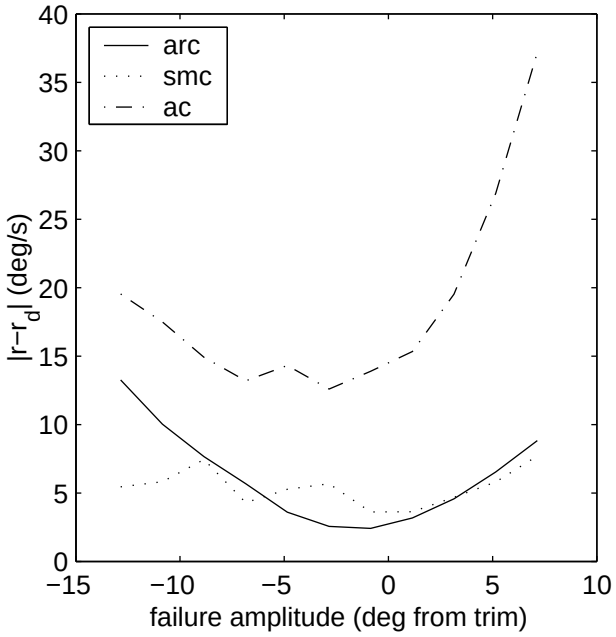

Fig. X.41. $\|r - r_{des}\|_{\mathcal{L}_{2Wcc}}$ as a function of failure amplitude for 1.0” CD input profile

Aggressive Doublets The PD input profile provided a fairly baseline maneuver to test the tracking ability of each control methodology. The CD input profile was a bit more rigorous and tested the ability of each control methodology to track a command input in a more aggressive maneuver. It also tested the ability of the cross-coupling measure to rate controllers independently of the input. Now, the AD input profile will be examined. This set of inputs will be the most aggressive and will rigorously test the ability of each to control methodology to retain tracking accuracy and stability in the face of difficult maneuvers. Figure IX.7 shows the stick and pedal inputs used for this manuever and figure IX.8 shows the reference commands generated as a result. Figures X.42, X.43, and X.44 show the response of the aircraft to a 0.5” AD input profile with a -3 degree from trim stabilator failure. The responses show the tracking abilities of each control methodology to a

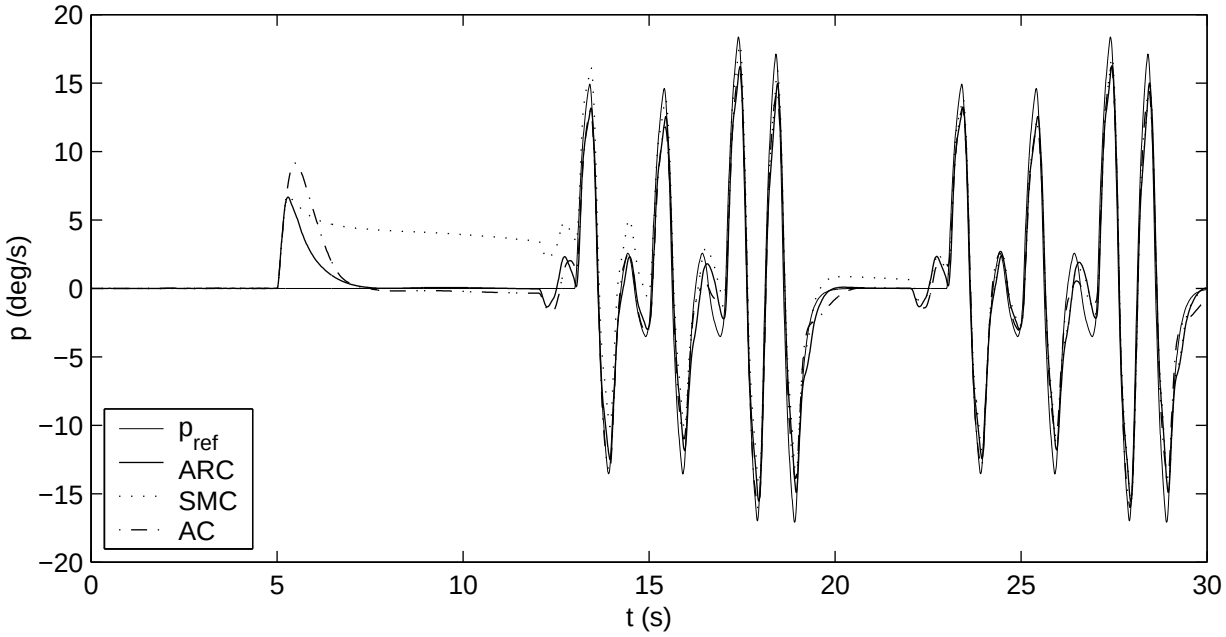

Fig. X.42. F-15 Roll axis response to AD input given a -3 degree from trim stabilator failure

more aggressive input profile in the presence of a failure. This input profile induces large amounts of cross-coupling disturbances that each control methodology must handle. This

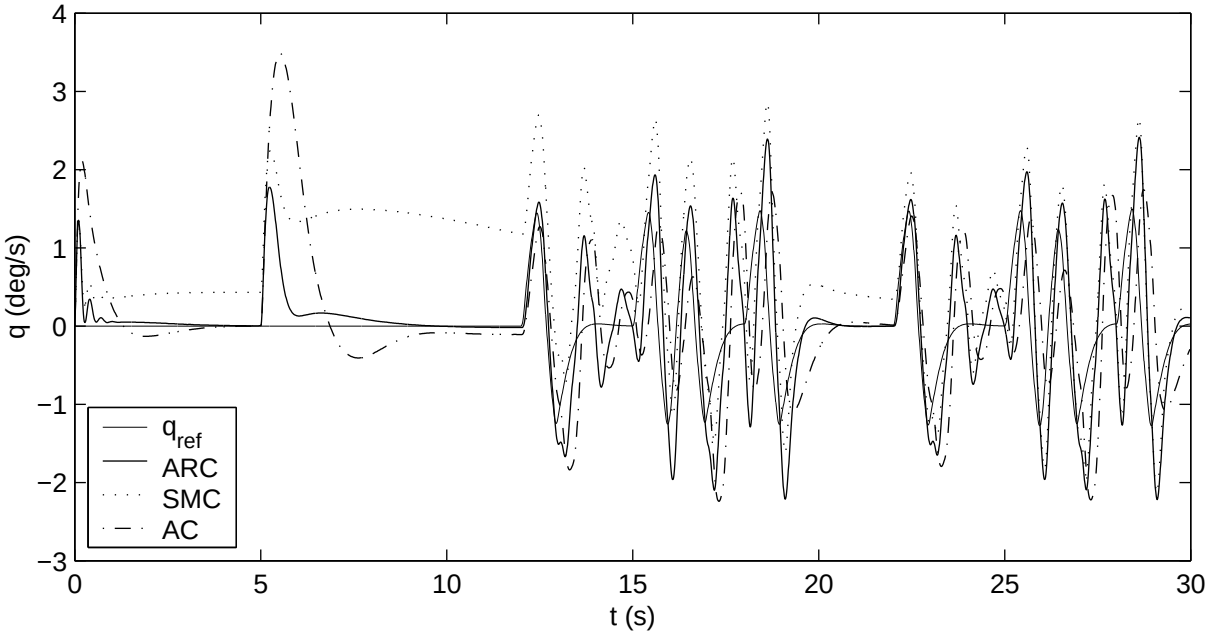

Fig. X.43. F-15 Pitch axis response to AD input given a -3 degree from trim stabilator failure

coupling makes pitch tracking very difficult. The roll and yaw responses exhibit very good command tracking, but the tracking quality of the pitch axis response is declining. More specifically, a lag-like behavior begins to appear in the pitch axis. This is a result of rate limiting in the actuators. Figures X.45, X.46, and X.47 display the relationship between the failure amplitude and the value of the cross coupling measure. As has been done all throughout the tracking results, the steady state portion of the error has been subtracted from the sliding mode portion of the control. The measure values for this input profile are again similar in magnitude to those of the other input profiles. The results are similar to those of the previous input profiles for the pitch axis. In the yaw axis, some differences begin to materialize. For the positive failure amplitudes the ARC and AC methodologies begin to have the same measure value. This did not occur for the less aggressive maneuvers. For the roll axis, the measure value of the error response actually becomes larger for the ARC scheme than for the AC and SMC schemes. While tracking performance of the ARC

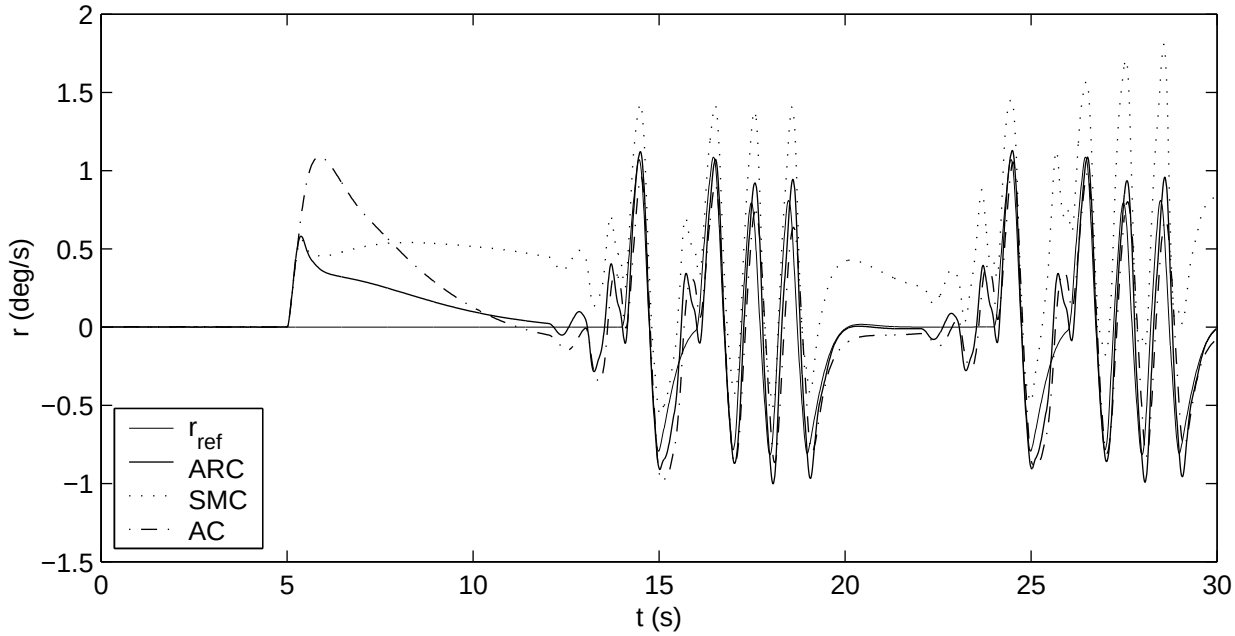

Fig. X.44. F-15 Yaw axis response to AD input given a -3 degree from trim stabilator failure

and SMC schemes should be fairly equivalent, it is not expected that AC should outperform ARC in tracking performance. The reason for this becomes even more clear upon examining figures X.48, X.49, and X.50. These figures show that as the command amplitude increases for the AD input profile, the performance of the ARC in the pitch axis remains about the same while the performance of the other control methodologies becomes much worse. The pitch axis performance gains in ARC over the other methodologies comes at the expense of the roll axis and to a lesser extent the yaw axis performance as shown in figures X.48 and X.50. Examining roll and pitch axis responses for AC clearly demonstrates this phenomenon. As the failure amplitude increases on amplitude in the positive direction, the roll axis performance of AC actually improves while the pitch axis performance grows steadily worse. For ARC, the pitch axis performance is maintained while the roll axis performance grows worse. This trade-off is necessary because we are hitting the limits of what the aircraft is capable of accomplishing without control reconfiguration.

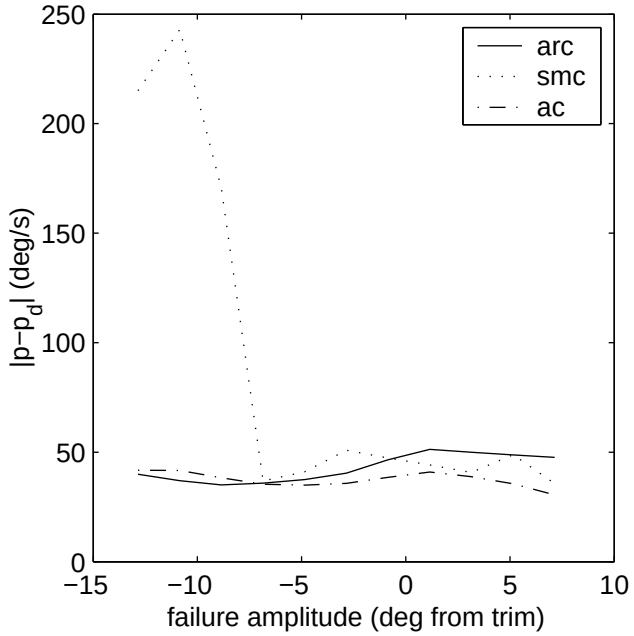

Fig. X.45. $\|p - p_{des}\|_{\mathcal{L}_{2Wcc}}$ as a function of failure amplitude for 0.25” AD input profile

This trade-off can be adjusted by changing the relative gains in both control methods. It is important to realize, however, that up until the most aggressive maneuvers, the tracking performance of the ARC methodology has been far superior to the other methods in each axis. This relationship between the aggressiveness of a maneuver and the tracking ability of each axis is important when trying to design a control law that can cover the entire range of a flight envelope.

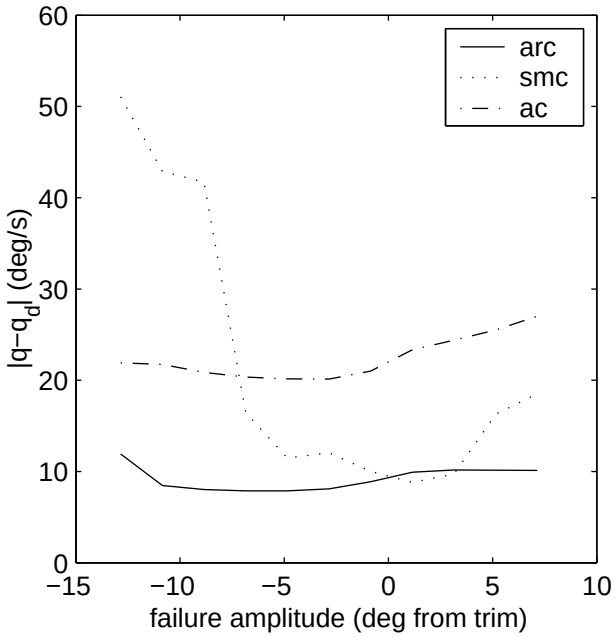

Fig. X.46. $\|q - q_{des}\|_{\mathcal{L}_{2Wcc}}$ as a function of failure amplitude for 0.25” AD input profile

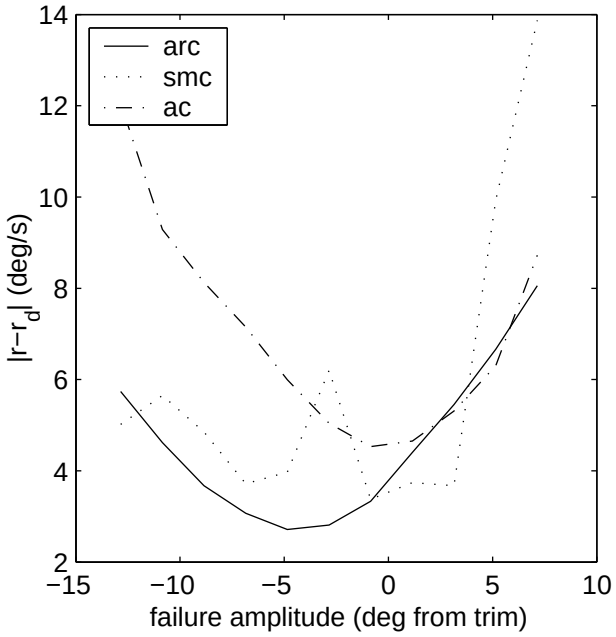

Fig. X.47. $\|r - r_{des}\|_{\mathcal{L}_{2Wcc}}$ as a function of failure amplitude for 0.25” AD input profile

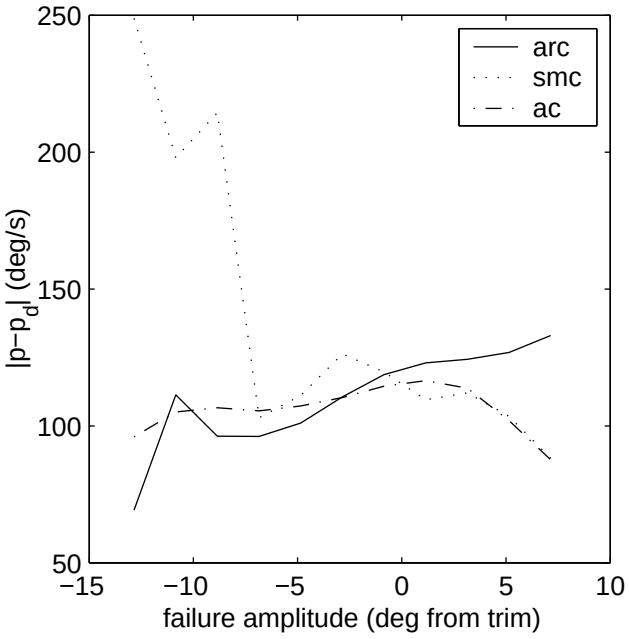

Fig. X.48. $\|p - p_{des}\|_{\mathcal{L}_{2Wcc}}$ as a function of failure amplitude for 0.75” AD input profile

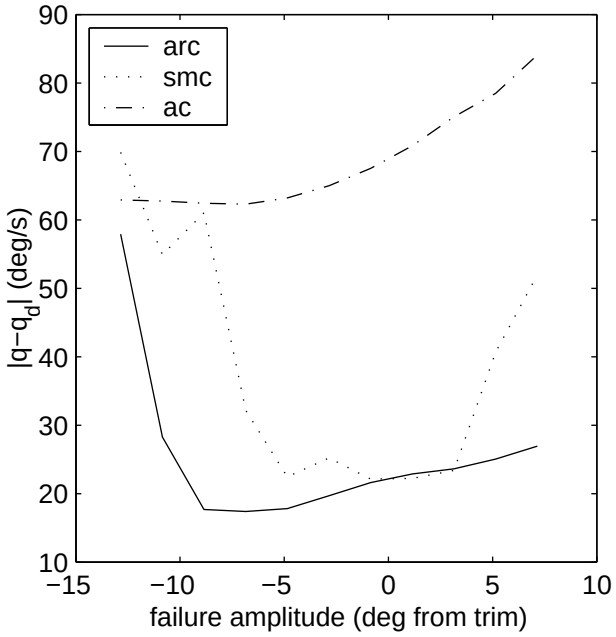

Fig. X.49. $\|q - q_{des}\|_{\mathcal{L}_{2Wcc}}$ as a function of failure amplitude for 0.75” AD input profile

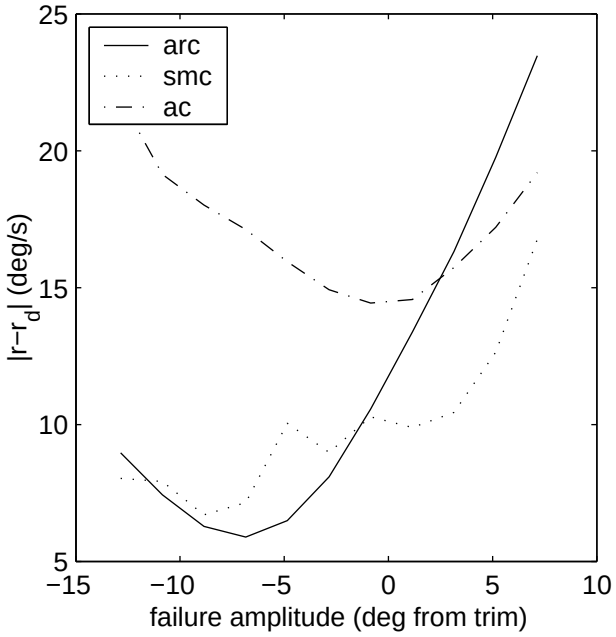

Fig. X.50. $\|r - r_{des}\|_{\mathcal{L}_{2Wcc}}$ as a function of failure amplitude for 0.75” AD input profile

C. Steady State Response Analysis

In this section, the steady state response of the aircraft to a failure while under the control of each of the outer loop control laws will be examined. The analysis of this is very straightforward and does not require any special tools. The steady state response will be examined with respect to failure amplitude.

1. Linearized F-15

As demonstrated by figures X.1 and X.3, the steady state error given a hard-over failure for the adaptive and adaptive robust control methodologies goes to zero. As a result, it is not necessary to show figures for this. The sliding mode control methodology does not force steady state error to zero (a method of changing this will be discussed later). This error is dependent on the failure amplitude. Figure X.51 shows the steady state error as a function of the failure amplitude. The error is nearly linearly dependent on the failure amplitude. The change occurs when failure amplitude gets large and control saturation begins to play a role. Figure X.51 demonstrates the failure of SMC to deal with steady state error. The steady state error can be reduced by making the boundary region of the sliding mode controller smaller (reducing the ε parameter in (V.18)); however, the error will not be forced to zero in the presence of a nonzero uncertainty.

2. Full nonlinear F-15

This same result will hold true for the nonlinear simulation of the F-15 as well. Figures X.7, X.8, and X.9 show the response of the system in the presence of a failure for the roll, pitch, and yaw axes respectively. Again, we note that for AC and ARC, the tracking error decays to zero as expected. These figures also show that the tracking error for the SMC case does not in fact decay to zero, but converges to some constant value.

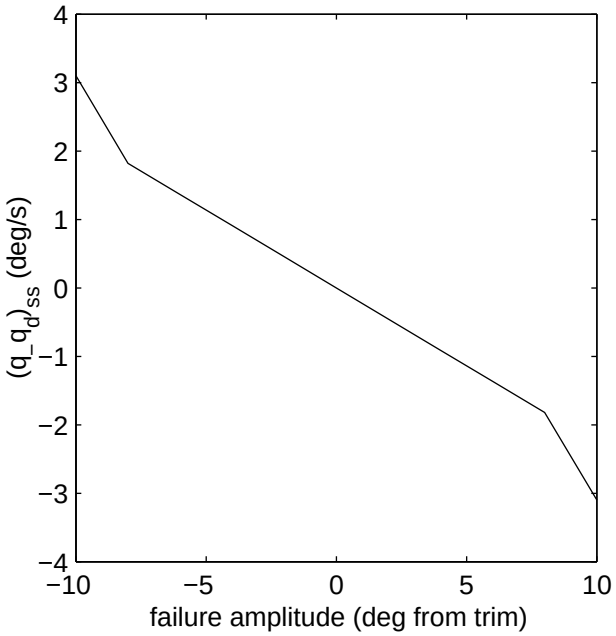

Fig. X.51. Steady state error response of SMC as a function of failure position

Figures X.52, X.53, and X.54 show the steady state tracking error of SMC with respect to the failure amplitude for the roll, pitch, and yaw axes respectively. While for the linearized case we observed a very smooth fairly linear curve, we see that this is not as true for the nonlinear case. In the pitch axis, we see a very sharp incline in the steady state error value as the failure amplitude increases in the negative direction. This results in a small improvement in the roll axis for these failure amplitudes. On the whole, the steady state error still remains fairly linear with respect to failure amplitude for the SMC controller. These figures confirm what was already known. The ARC and AC control methodologies have the best steady state error properties, while SMC retains undesirable steady state error.

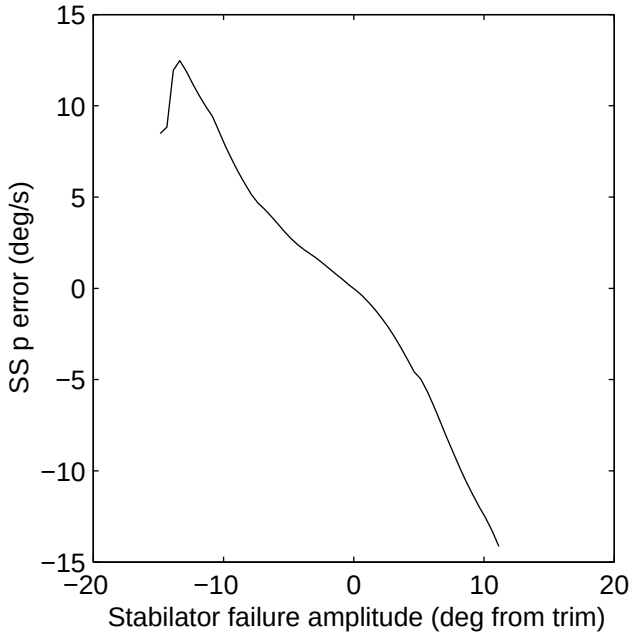

Fig. X.52. Steady state roll axis error response of SMC as a function of failure position

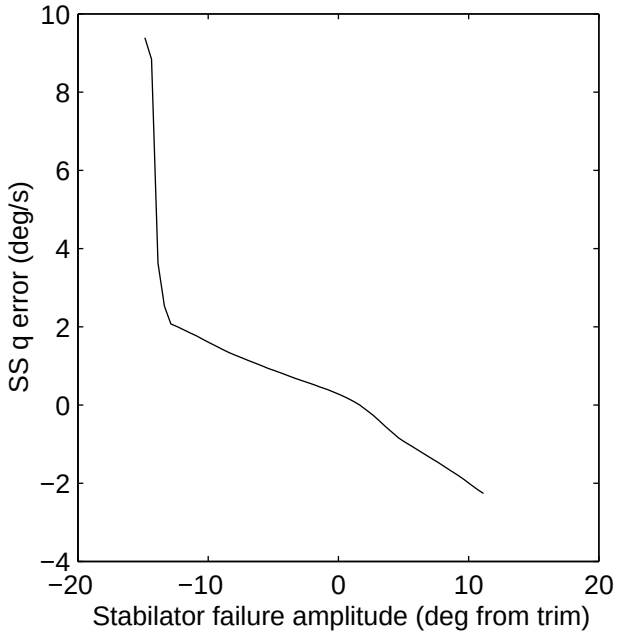

Fig. X.53. Steady state pitch axis error response of SMC as a function of failure position

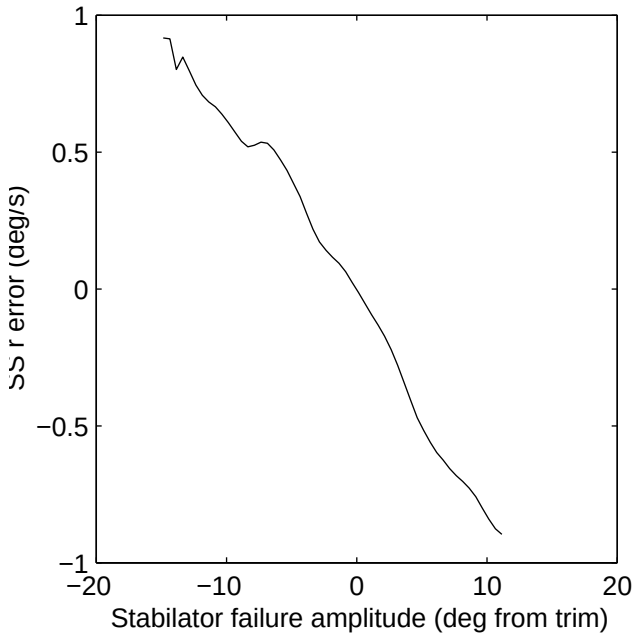

Fig. X.54. Steady state yaw axis error response of SMC as a function of failure position

D. Overall Response Analysis

Previously, the tracking response, transient response, and steady state response of each outer loop controller to pilot inputs were considered independently. It is at this point natural to assess the overall response of each controller to the various maneuvers while taking into account each of the three response characteristics examined previously. This will be accomplished by once again modifying the weighted $\mathcal{L}_2$ norm that has been utilized throughout the analysis. The measure defined in (VIII.5), denoted by $\|\cdot\|_{\mathcal{L}_{2cc}}$, will be used. For the linear case, it has already been mentioned that this measure simplifies down to the measure defined in (VIII.3), denoted as $\|\cdot\|_{\mathcal{L}_{2\dot{u}}}$. These measures will serve to penalize errors that are not induced by pilot commands. These measures will also be frequency weighted to penalize high frequency error responses. The frequency weighted versions of the measures $\|\cdot\|_{\mathcal{L}_{2\dot{u}}}$ and $\|\cdot\|_{\mathcal{L}_{2cc}}$ will be denoted $\|\cdot\|_{\mathcal{L}_{2W\dot{u}}}$ and $\|\cdot\|_{\mathcal{L}_{2Wcc}}$.

1. Linearized F-15

The transient analysis of the linearized F-15 model showed that SMC and ARC dealt most effectively with the transient errors that occur when the aircraft experiences a failure. The adaptive control method, while eventually removing the failure, arrests the failure after the aircraft has departed significantly from its target trajectory. The tracking results were very similar to the transient results. The ARC and SMC methodologies provided the best command tracking performance in general. The SMC method began to have problems when the failure amplitude grew too large. Finally, the steady state analysis showed that while ARC and AC remove constant steady state errors that occur from a hard-over failure, SMC could not remove this error. For larger failure amplitudes, this error may be beyond the trim range of the aircraft. To try to make a more broad assessment of the performance of each control methodology, all of these response characteristics are included

in the $\|\cdot\|_{\mathcal{L}_{2W\dot{u}}}$ measure and the error response of the aircraft to hard-over failures is again analyzed. Figures X.55, X.56, and X.57 show the measure values of the error response

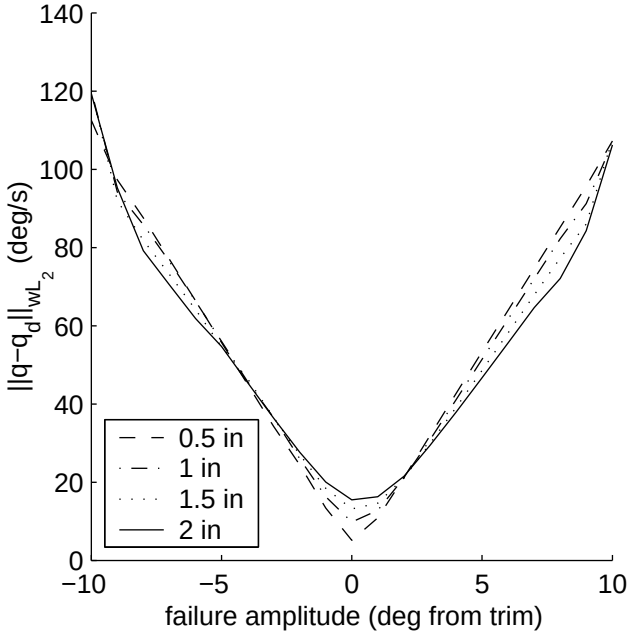

Fig. X.55. $\|q - q_d\|_{\mathcal{L}_{2W\dot{u}}}$ versus failure position for linearized F-15 with SMC method

of each control methodology to failure amplitudes between -10 and +10 degrees from trim. The frequency and input weighted measure is taken for the error response of the linearized aircraft to a sequence of commands. Examples of the types of responses used to generate these figures are shown in figures X.13, X.14, and X.15. These figures show sample responses for a failure at trim inserted at approximately $t = 0.25s$. For off-trim failures, a departure from steady state would be observed, the aircraft would be restored, and then the maneuver would begin. Figures X.55, X.56, and X.57 include information about the performance of the aircraft under different failure and command amplitudes. The figures mesh together in one performance measure value the errors associated with the transient behavior at the onset of a failure, the tracking behavior, and the steady state error. The ARC outer loop controller performs best overall. This is what was expected given the performance of

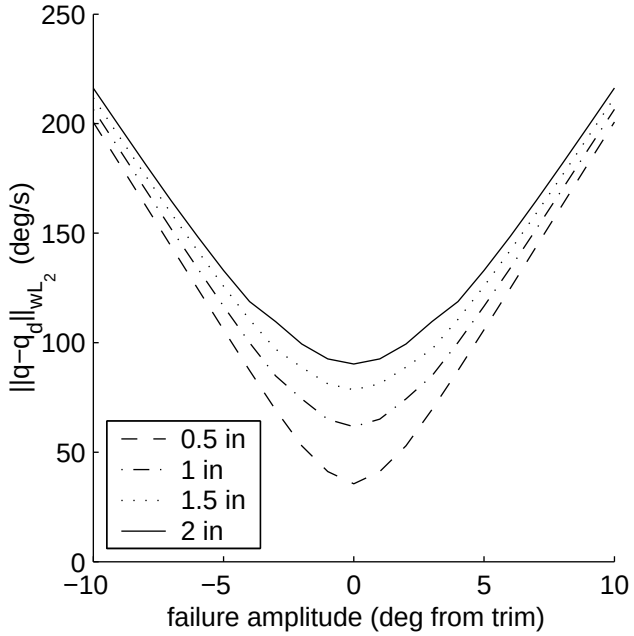

Fig. X.56. $\|q - q_d\|_{\mathcal{L}_{2W\dot{u}}}$ versus failure position for linearized F-15 with AC method

ARC in each of the three main areas discussed previously (transient, tracking, and steady state performance). As expected, the measure value increases with failure amplitude as it becomes more difficult to track rapidly changing commands. This is true for each methodology except SMC. For SMC, as failure amplitude gets large, the measure values reverse temporarily and then return to the expected order. This is because the steady state error is not removed as they were in the analysis of the tracking cases. Because the measure weights based on command amplitude, the steady state error is proportionally smaller for higher command amplitudes than for lower command amplitudes. This is because it is more acceptable to have some error for rapid, large amplitude commands than for slower, smaller amplitude commands. Overall, SMC and ARC are the least affected by command amplitude in terms of the change in their measure values.

Unlike the measure of the pure tracking response for each methodology, the measures of the overall responses are more affected by failure amplitude for this linear case. This is

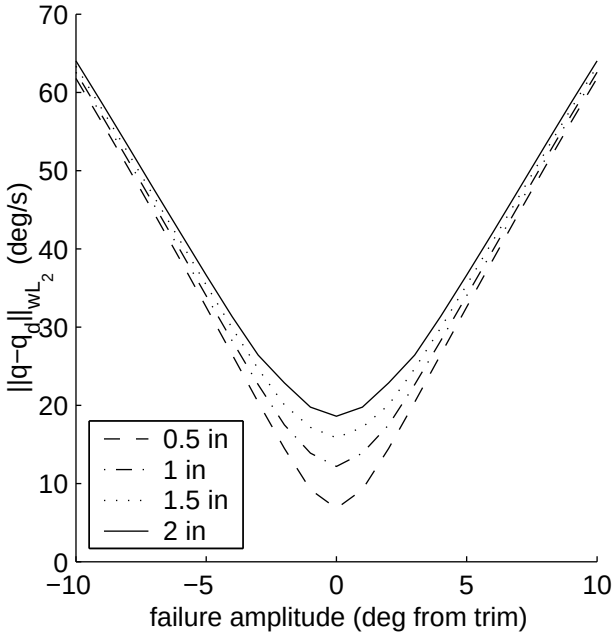

Fig. X.57. $\|q - q_d\|_{\mathcal{L}_{2W\dot{u}}}$ versus failure position for linearized F-15 with ARC method

mainly due to the transient response that occurs at the time of the failure. Figure X.58 the measures of the error response for each control methodology for a command amplitude of 2”. The figure shows that ARC outperforms the other methodologies over the range of failure amplitudes. The responses of ARC and SMC are the closest because steady state error is penalized less than tracking error due to the weighted measure used for measurement.

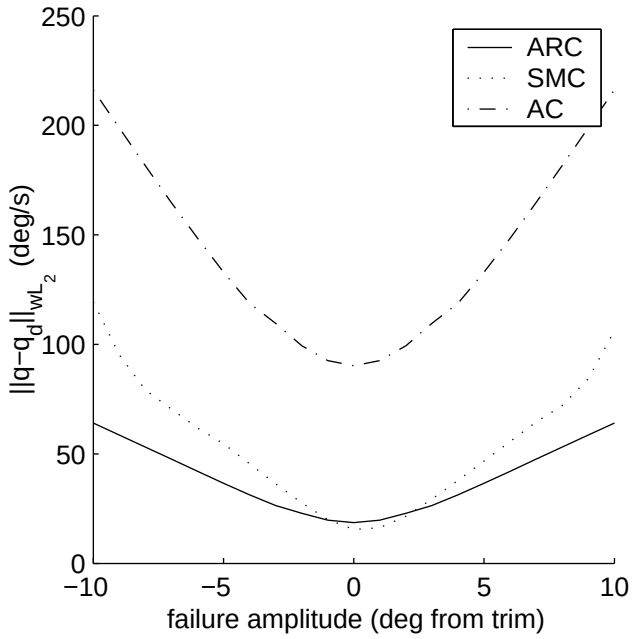

Fig. X.58. $\|q - q_d\|_{\mathcal{L}_{2W\dot{u}}}$ versus failure position for 2” stick inputs

2. Full nonlinear F-15

For the nonlinear F-15 model, analysis is slightly more complicated than for the linearized model. This is because there are multiple axes. When comparing the previous three performance areas separately, it was observed that ARC and SMC displayed the best performance for transient response. When analyzing tracking, several different maneuvers were utilized to examine the performance level of each control method. This allows for analysis of each control method based on the aggressiveness of the maneuver. This is important because the aircraft is being asked to perform in multiple axes that have no "knowledge" of each other. As was done for the tracking response analysis, each control methodology will be analyzed using its response to the three maneuvers.

Plain Doublets The analysis of the overall response of the nonlinear aircraft simulation will be judged based on the cross coupling measure of the aircraft response. The error signal will be taken from the aircraft respnose to the PD input profile. The responses are similar to those found in figures X.21, X.22, and X.23. Figures X.59, X.60, and X.61 display the measure response of the error signal of each axis under control of each of the outer loop methodologies. The measure values of the error responses are larger than those for the tracking responses alone because the responses include the transient error behavior. For the sliding mode control, the steady state error associated with the failure is not removed, increasing its measure value as well. This is why there is a larger sensitivity of the measure value of the error response of the system to the failure amplitude when the aircraft is under SMC control. For large failure amplitudes the value of the measure is quite large for SMC. The figures show that when tracking, transient error, and steady state error are all considered, ARC seems to be the most effective at maintaining adequate control of the aircraft and minimizing the tracking error induced by a hard-over failure. The figures also show that ARC maintains this performance better than the other methods over the

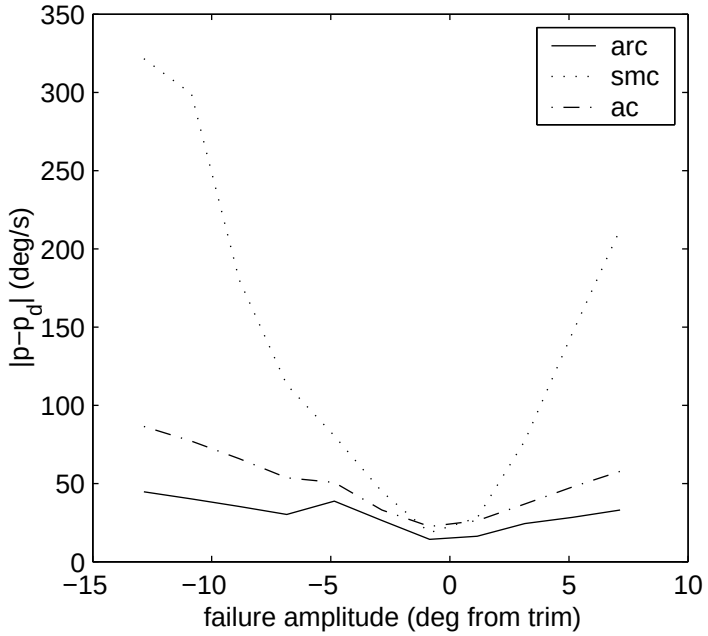

Fig. X.59. $\|p - p_{des}\|_{\mathcal{L}_{2Wcc}}$ as a function of failure amplitude for 0.5" PD input profile

range of failures. Unlike the linear case, the AC performs better on the whole than the SMC. This is also different from the tracking case. This is in large part due to the steady state error with the SMC. Because the maneuver takes place over a longer time for the nonlinear case, the steady state error becomes a larger factor than for the linear case. While this is a side-effect of using an $\mathcal{L}_2$ type measure, it is useful because the effect of a steady state error in the body axis rates affects integrated states such as θ and ϕ over time in the same manner. This is why for low failure amplitudes the SMC methodology outperforms AC, but for higher amplitudes this is not the case. Figures X.62, X.63, and X.64 show the response to different failure amplitudes for 1.5" stick and rudder inputs. The measure values in general are greater for the higher command amplitude because it becomes more difficult for the aircraft to track in multiple axes. In general the aircraft response under ARC control again has the lowest measure value for all axes and all failure amplitudes. In the roll axis, we begin to see the performance suffer at higher failure amplitudes. This will

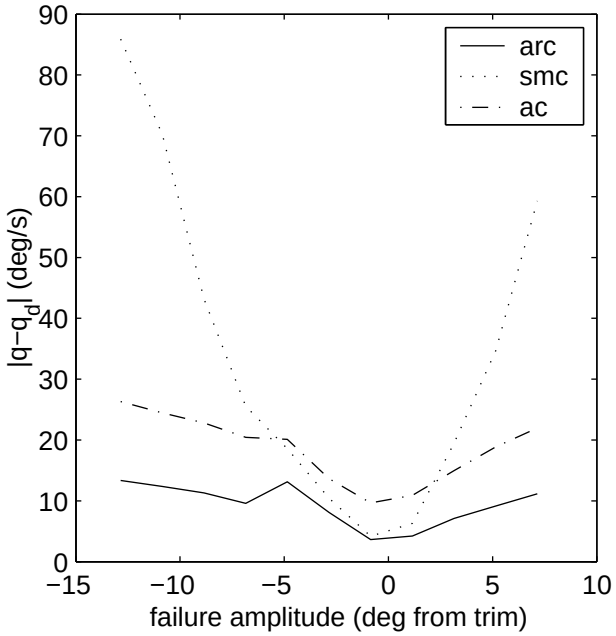

Fig. X.60. $\|q - q_{des}\|_{\mathcal{L}_{2Wcc}}$ as a function of failure amplitude for 0.5” PD input profile

become more apparent for more aggressive maneuvers. In general, the command amplitude does not affect the ordering of the measures for this maneuver. We do see that as command amplitude increases, the range over which SMC performs better than AC is widened.

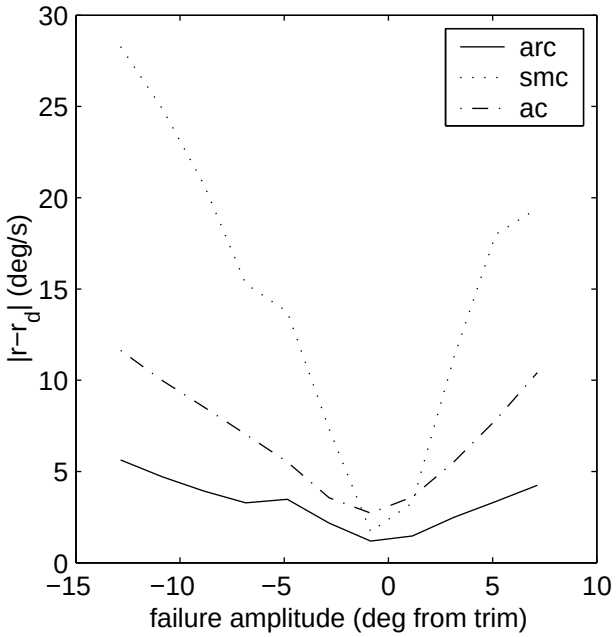

Fig. X.61. $\|r - r_{des}\|_{\mathcal{L}_{2Wcc}}$ as a function of failure amplitude for 0.5” PD input profile

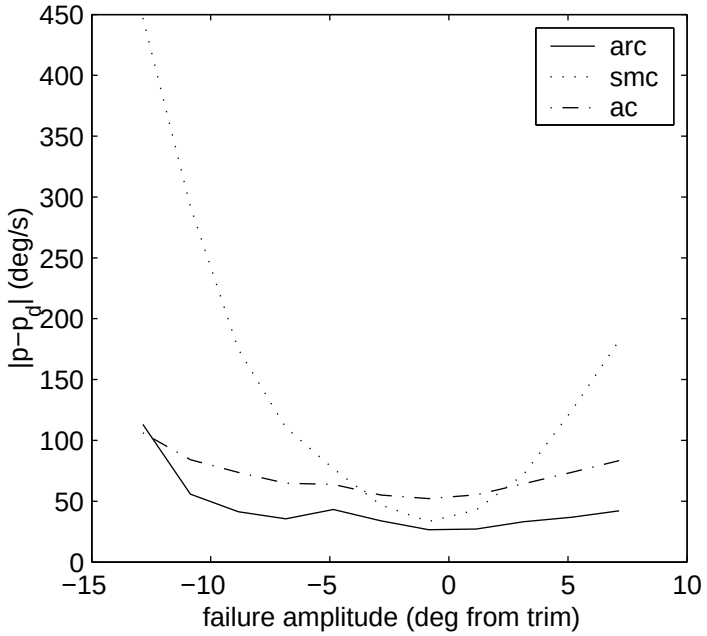

Fig. X.62. $\|p - p_{des}\|_{\mathcal{L}_{2Wcc}}$ as a function of failure amplitude for 1.5” PD input profile

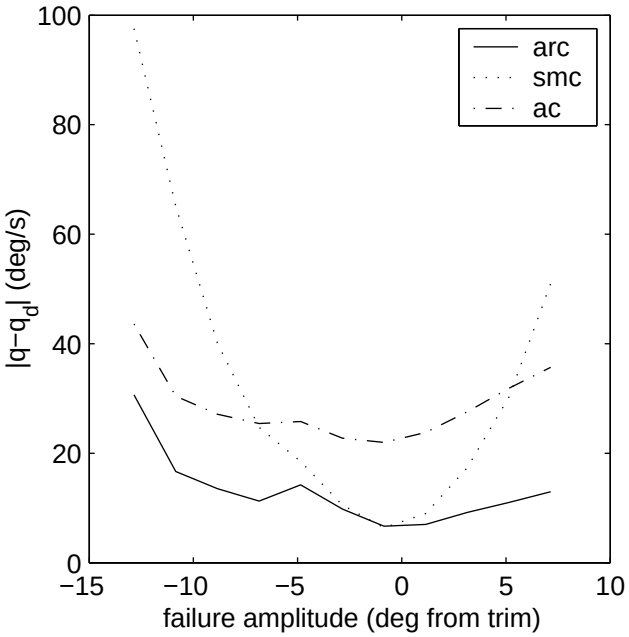

Fig. X.63. $\|q - q_{des}\|_{\mathcal{L}_{2Wcc}}$ as a function of failure amplitude for 1.5” PD input profile

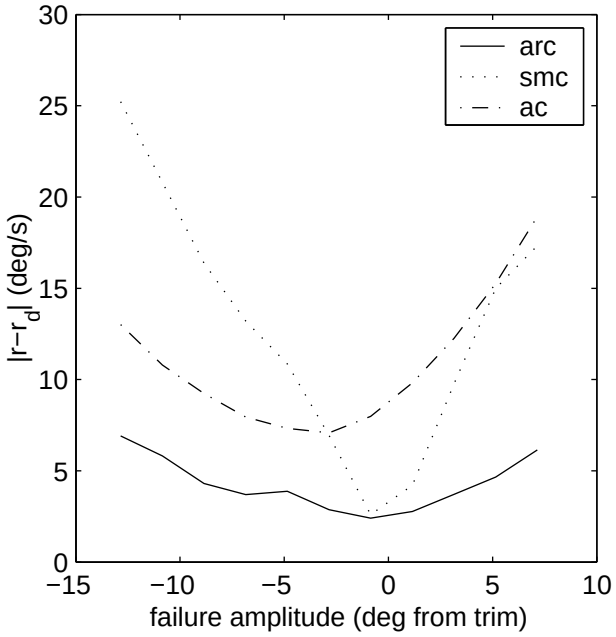

Fig. X.64. $\|r - r_{des}\|_{\mathcal{L}_{2Wcc}}$ as a function of failure amplitude for 1.5” PD input profile

Coupled Doublets As with the tracking analysis, a more aggressive maneuver is analyzed to see how each of the control methods perform. Sample responses for each of these axes to the CD input profile are given in figures X.33, X.34, and X.35. The error response over the entire maneuver is used for the cross coupling measure and used to analyze each maneuver as was done for the PD input profile. The measure values of the error responses of the

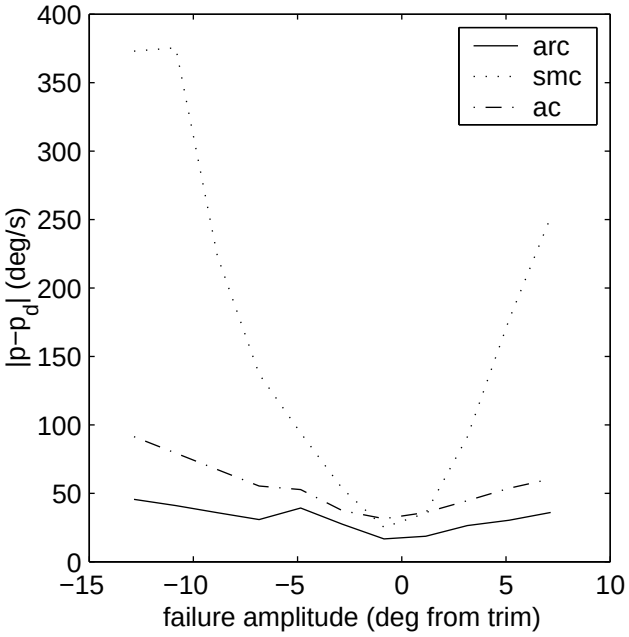

Fig. X.65. $\|p - p_{des}\|_{\mathcal{L}_{2Wcc}}$ as a function of failure amplitude for 0.5” CD input profile

aircraft to hard-over failures over a range of amplitudes for each control method are given in figures X.65, X.66, and X.67. These figures show the results of simulation with 0.5” stick and rudder inputs. As for the PD case, the ARC control law provides the lowest measure value over the range of failure amplitudes for each axis. Also as the figures for the PD input profile showed, the steady state error associated with SMC results in a large increase in the measure value as the failure amplitude increases. Even with a more aggressive maneuver, ARC provides the best overall response in terms of the $\mathcal{L}_{2Wcc}$ measure. For small failure amplitudes, SMC performs better than AC because the steady state error is small, meaning

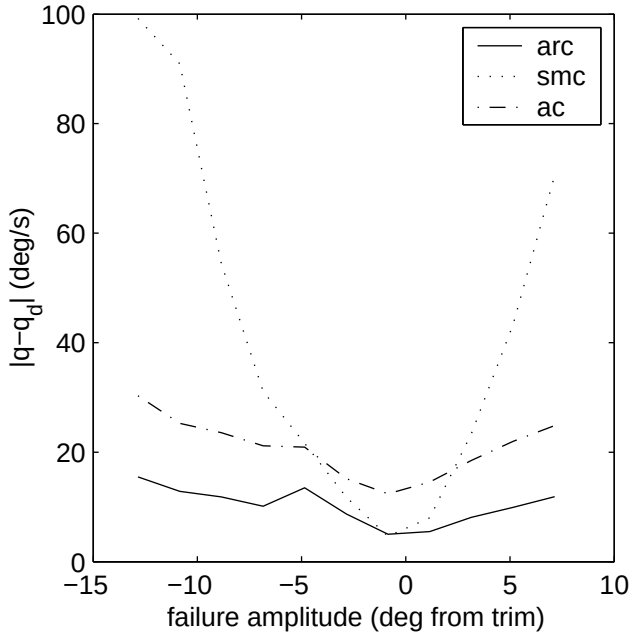

Fig. X.66. $\|q - q_{des}\|_{\mathcal{L}_{2Wcc}}$ as a function of failure amplitude for 0.5” CD input profile

a pilot would be able to trim the aircraft. This is reflected in the measure values as well. For larger failure amplitudes, AC performs better than SMC largely because of the steady state errors associated with the control and because of the saturation of the sliding mode control. Figures X.68, X.69, and X.70 show the effect of the failure amplitude on the system measure for a larger command amplitude. As for the PD case, we see that on the whole the measure values for the ARC methodology remain at about the same value, but those for AC increase. The measure values for SMC decrease somewhat because of the weighting used in the measure. For the more aggressive maneuver, we begin to see that to maintain performance in the pitch axis, roll axis performance begins to be sacrificed. This is evident at the higher failure amplitudes. In the pitch axis, the measure values for ARC are significantly lower than those for adaptive control for each failure amplitude. As the failure amplitude becomes larger, it is observed that in the roll axis, the measure of the error response for ARC approaches the same values as those for AC. Overall, the ARC response

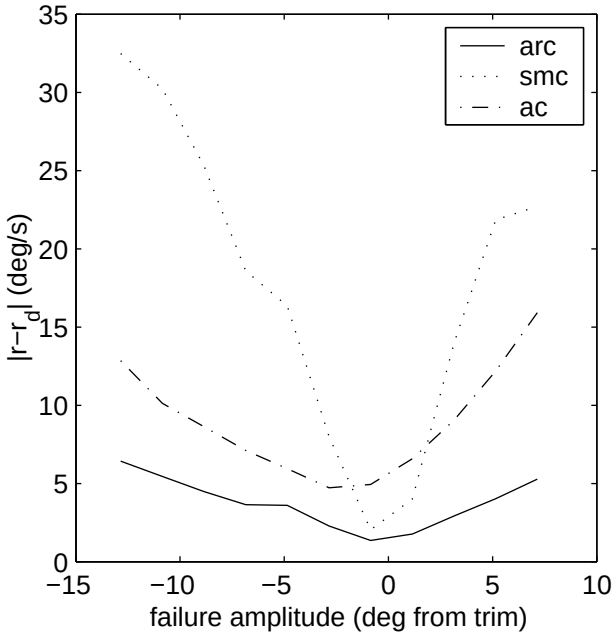

Fig. X.67. $\|r - r_{des}\|_{\mathcal{L}_{2Wcc}}$ as a function of failure amplitude for 0.5” CD input profile has the lowest measure values and clearly outperforms the other control methodologies.

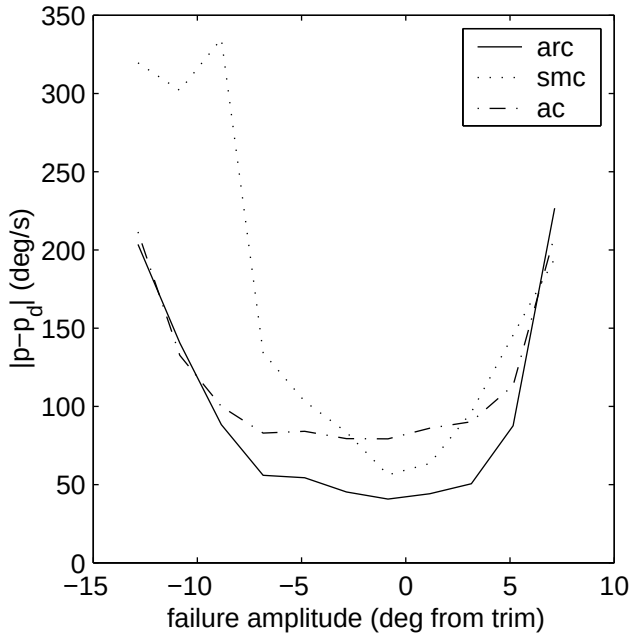

Fig. X.68. $\|p - p_{des}\|_{\mathcal{L}_{2Wcc}}$ as a function of failure amplitude for 1.5” CD input profile

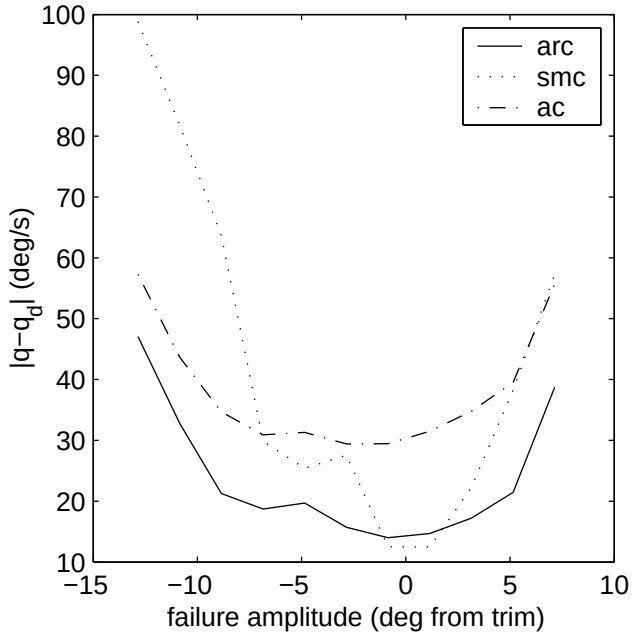

Fig. X.69. $\|q - q_{des}\|_{\mathcal{L}_{2Wcc}}$ as a function of failure amplitude for 1.5” CD input profile

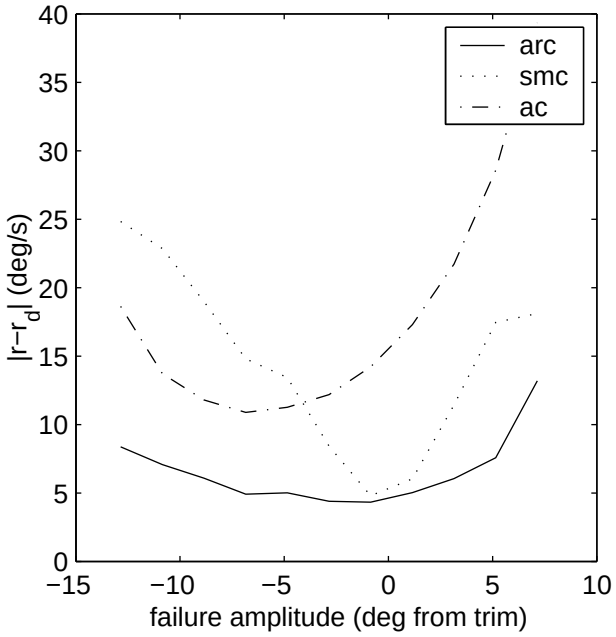

Fig. X.70. $\|r - r_{des}\|_{\mathcal{L}_{2Wcc}}$ as a function of failure amplitude for 1.5” CD input profile

Aggressive Doublets The aggressive doublets maneuver is the most aggressive maneuver in terms of command rate and excitation of multiple axes. As before, a measure similar to that used for the tracking analysis will be used to analyze the response of the aircraft from the initial transient at the onset of a failure until the end of the maneuver. The values used for analysis are the weighted measures of the error response of each axis to the AD input profile. Sample responses were shown earlier in figures X.42, X.43, and X.44. The rela-

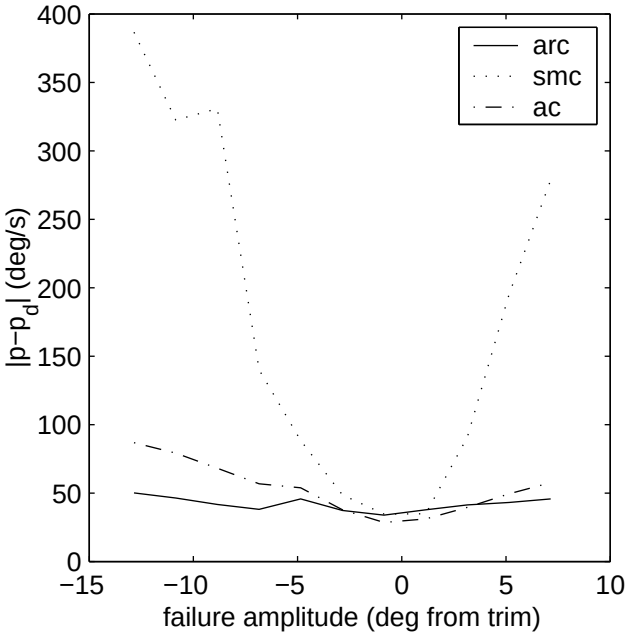

Fig. X.71. $\|p - p_{des}\|_{\mathcal{L}_{2Wcc}}$ as a function of failure amplitude for 0.25" AD input profile

tionship between the measure value of the error response and the failure amplitude is shown in figures X.71, X.72, and X.73. Again, for a small command amplitude ARC outperforms the other methodologies. For the roll axis, there is a small set of failure amplitudes around 0 degrees from trim where ARC is outperformed by the adaptive control methodology. As was discussed before, this is because maintaining pitch performance results in the sacrifice of peformance in other axes. If we compare the figures for each of the maneuvers, we see that as we increase the aggressiveness of the maneuver we begin to reach the limit of what

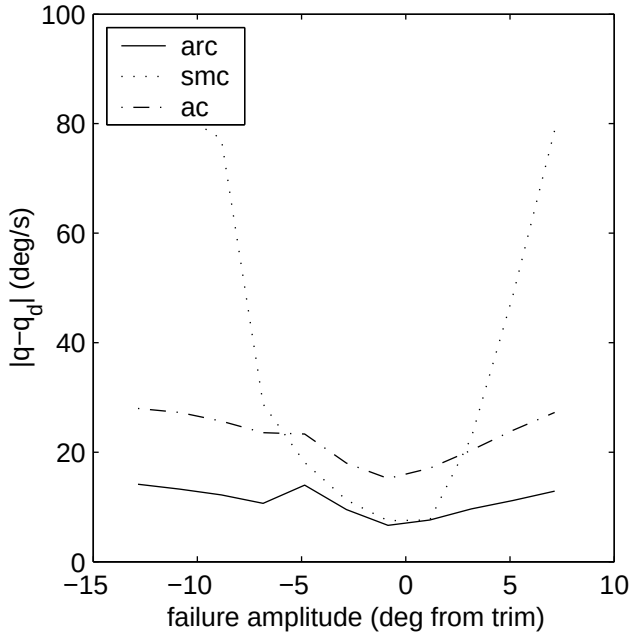

Fig. X.72. $\|q - q_{des}\|_{\mathcal{L}_{2Wcc}}$ as a function of failure amplitude for 0.25” AD input profile

can be accomplished without reconfiguration of the control. As was observed for the previous two sets of maneuvers, figures X.74, X.75, and X.76 display the loss of performance that occurs when increasing the command amplitude. When the command amplitude is increased by a factor of three, the pitch performance for the ARC method does not suffer, but the performance for AC does. For the roll axis, the performance of ARC at positive failure amplitudes begins to degrade to help insure pitch axis performance. For larger failure amplitudes, AC begins to outperform ARC. This shows again that the limit of what is possible without control reconfiguration is being reached. On the whole for smaller command amplitudes ARC performs better than the methodologies it combines. The combination of adaptive and sliding mode control yields more accurate tracking and better performance.

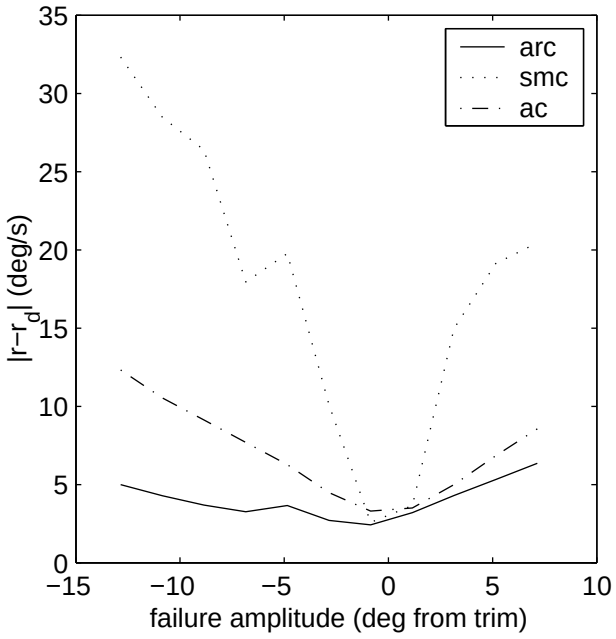

Fig. X.73. $\|r - r_{des}\|_{\mathcal{L}_{2Wcc}}$ as a function of failure amplitude for 0.25” AD input profile

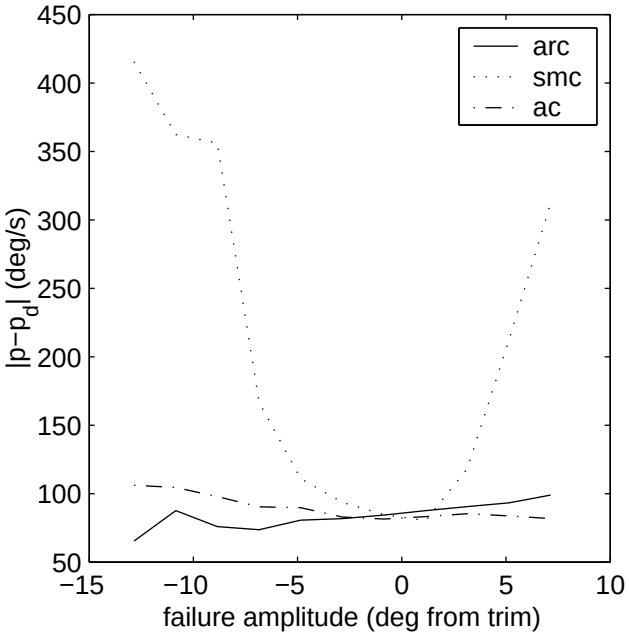

Fig. X.74. $\|p - p_{des}\|_{\mathcal{L}_{2Wcc}}$ as a function of failure amplitude for 0.75” AD input profile

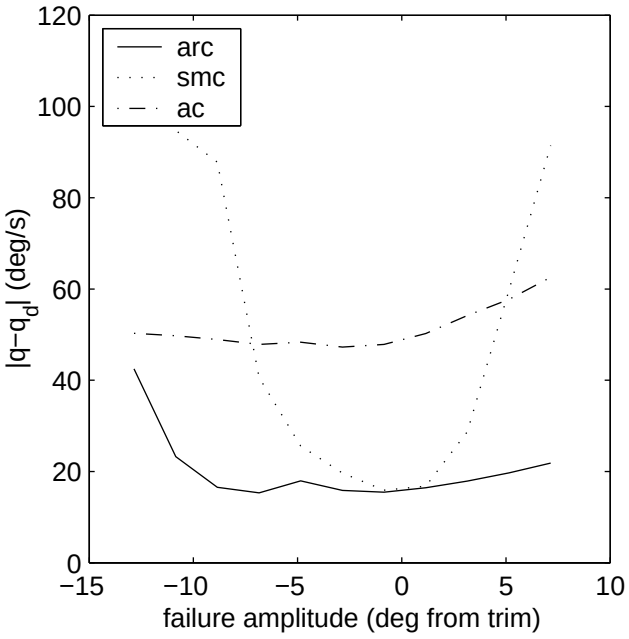

Fig. X.75. $\|q - q_{des}\|_{\mathcal{L}_{2Wcc}}$ as a function of failure amplitude for 0.75” AD input profile

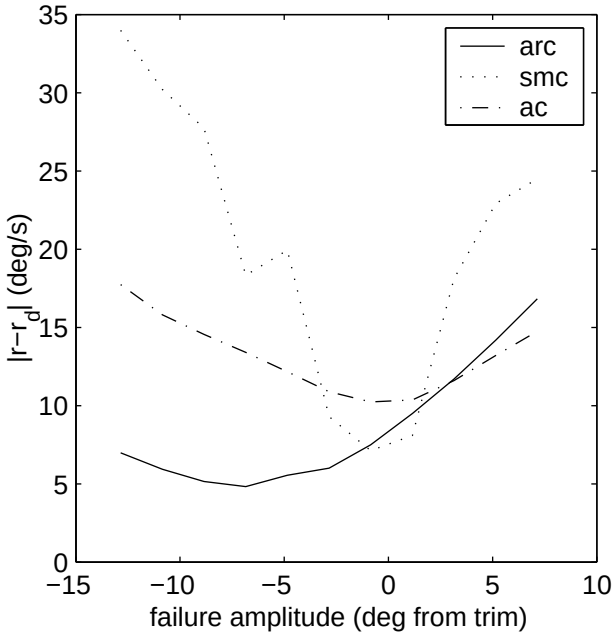

Fig. X.76. $\|r - r_{des}\|_{\mathcal{L}_{2Wcc}}$ as a function of failure amplitude for 0.75” AD input profile

CHAPTER XI

OTHER FAILURE CONDITIONS

Most of the research thus far has been geared toward hard-over failures, which was the original motivation of the work. There are several other failure modes that warrant discussion as well. These types of failures are fundamentally different from hard-over failures in that they create different types of disturbances on the system. Loss of surface failures result in a mismatch in the control effectiveness matrix in the dynamic inversion controller, but do not create an external disturbance on the system. A floating actuator type failure results in a mismatch in the control effectiveness matrix as well as an α dependent disturbance on the system. These two types of failures will be simulated for the linearized F-15 model and for an F-5A aircraft under dynamic inversion control. The input profile used for the F-5A for these failures will be the PD maneuver.

A. Loss of Surface Failure

A loss of surface failure occurs when part of a control surface is lost or when the surface loses its effectiveness. In these instances, a mismatch in the dynamic inversion can result because the moments provided by the surface have lessened. If the damage is asymmetric, this can result in different trim positions for the surfaces. For example, if a left stabilator loses 50% of its effectiveness for pitch command, a symmetric stab command will result in a roll. Since the DI control can only command the actuators along directions allowed by the control allocation (for the F-5, this means only symmetric surface commands for stabilators and rudders and differential commands for ailerons), the ailerons will be required to assume non-zero trim positions to account for the mismatch in this case. This type of failure is much less demanding than hard-over failures because some control is still retained and the change in the system dynamics is less drastic. Again, the linear case is considered and then

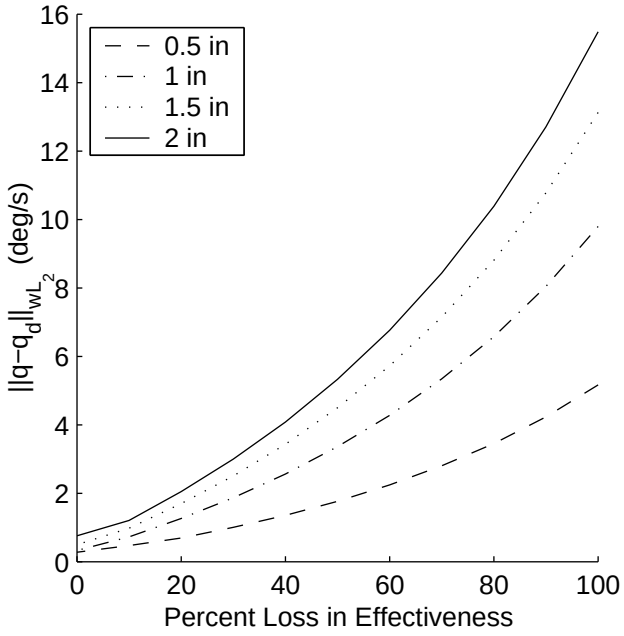

Fig. XI.1. $\|q - q_d\|_{\mathcal{L}_{2W\dot{u}}}$ for linearized F-15 response to loss of surface effectiveness for SMC

the nonlinear.

1. Linearized F-15

For the linear case, loss of surface effectiveness only requires alteration of the control authority needed to track reference commands accurately. The case is a simple case for the linear system because there is no cross-coupling between axes, and the control surface failure does not result in any disturbances. The lack of disturbance means that the trim point remains constant, thus no steady state error results. As a result, SMC does not have the steady state error woes that result from a hard-over failure. Figures XI.1, XI.2, and XI.3 show the measure values of the error response of the linearized F-15 model to a loss of surface effectiveness of the left stabilator. As expected, as the percentage loss of effectiveness increases, so does the measure value of the error. The measure values resulting from this type of failure are fairly small when compared with the measure values for hard

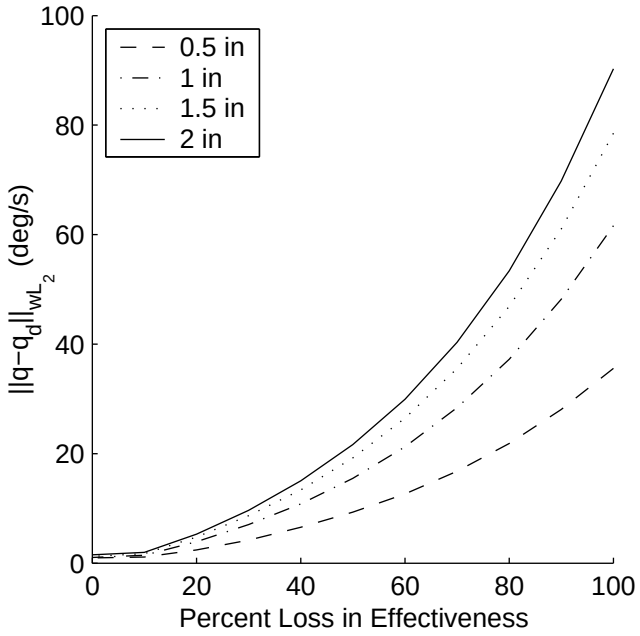

Fig. XI.2. $\|q - q_d\|_{\mathcal{L}_{2W\dot{u}}}$ for linearized F-15 response to loss of surface effectiveness for AC

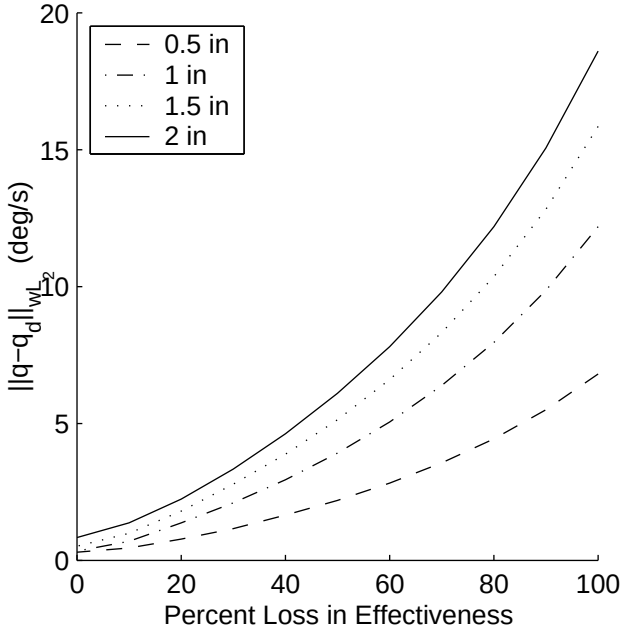

Fig. XI.3. $\|q - q_d\|_{\mathcal{L}_{2W\dot{u}}}$ for linearized F-15 response to loss of surface effectiveness for ARC

over failures (see figures X.55, X.56, and X.57). A complete loss of a surface results in a measure value only a little higher than that of a surface lock at trim. Of the three control methodologies, SMC handles this failure type the best, though the measure values of the error response are only a minimal improvement over ARC. This is largely due to the lack of steady state error. The simulation of the linearized case is a bit unrealistic because in actuality a new trim position would be found for the nonlinear aircraft and new linearized equations of motion developed. This is not carried out for this simple illustration, but it is a technicality that should be mentioned for completeness. If the same trim point were assumed at the start and new linearized equations used at the time of the failure, the SMC control would not perform as well because a steady state error would result.

2. Nonlinear F-5

The nonlinear simulation of the loss of effectiveness failure case will bring to light this difficulty. The simulation will be performed on the F-5 aircraft. While the actuator limits are much more stringent for this aircraft than for the F-15, it will serve as a good test case for this type of failure. As with the F-15 the impact of the stabilator failure will be analyzed for all three axes. For the F-5, the cross-coupling that results from a failure will be much smaller. There are several reasons for this. Differential stabilator has much less roll effect for the F-5 than for the F-15. This means the roll moments generated from the various stabilator surface failures will be much smaller than those of the F-15. This is one of the reasons that the F-5 was not used in the hard-over failure discussion (the surface limitations also played a factor in this decision - more discussion is available in the limitations section). In addition, the differential stabilators are not used to control roll. This is because of the smaller moments that they generate. This also serves to reduce the cross-coupling in the aircraft under failure because the remaining effective stabilator is not required to perform commands that control both the roll and pitch axes.

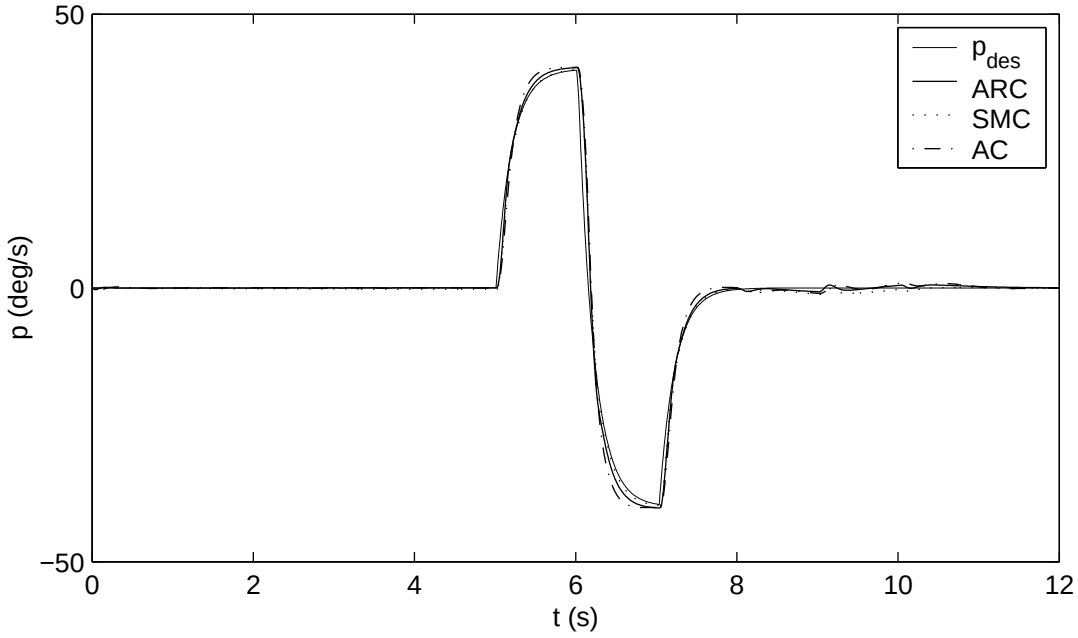

Fig. XI.4. Roll axis response to 80% loss of left stabilator effectiveness for 1” PD input

The response of the F-5 to loss of surface failure will be analyzed in terms of the cross-coupling measure that has been used multiple times in this thesis. Only the PD maneuver will be tested for this failure case. The responses of the F-5 under each control methodology to 1” stick and rudder PD inputs for an 80% loss of stabilator effectivess are given in figures XI.4, XI.5, and XI.6. The failure is introduced at $t = 0.25s$. There is not a large transient associated with this type of failure because there is no sudden disturbance introduced at the time of failure. There is a change in trim position due to the change in moment applied by the collective and differential stabilators. This change is very small for straight and level flight, however, meaning there is not a large transient. Because the changes in trim are small, the steady state error from SMC is also small. There is still some steady state error associated with the SMC control (this can be seen by examining figure XI.6 although this is partially associated with an improper trim), but the disturbance is small. Figures XI.7, XI.8, and XI.9 show the measure responses of each control method-

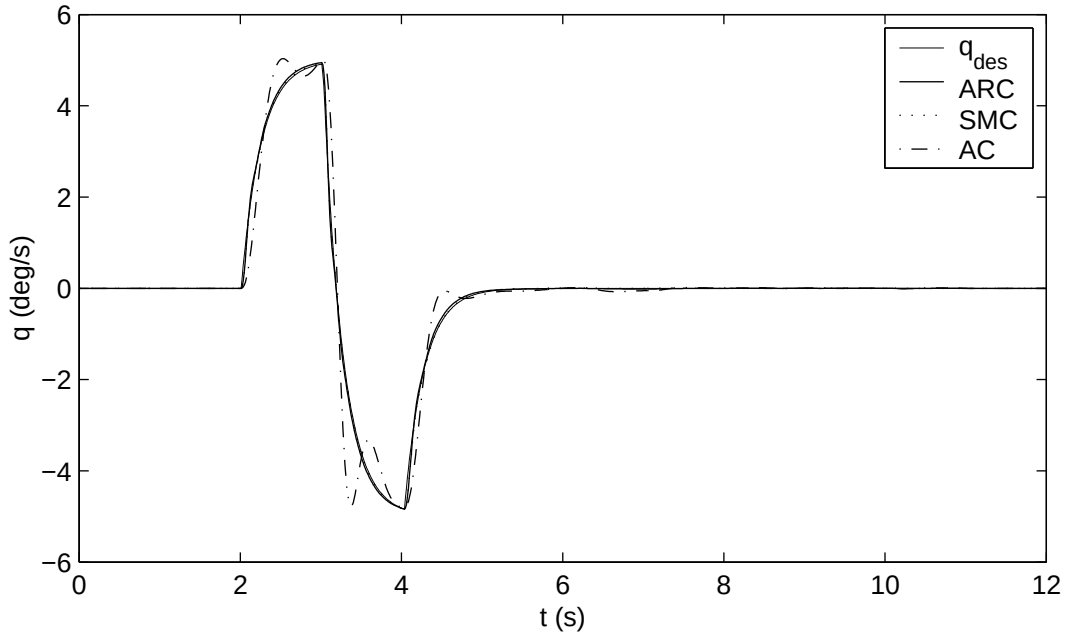

Fig. XI.5. Pitch axis response to 80% loss of left stabilator effectiveness for 1” PD input

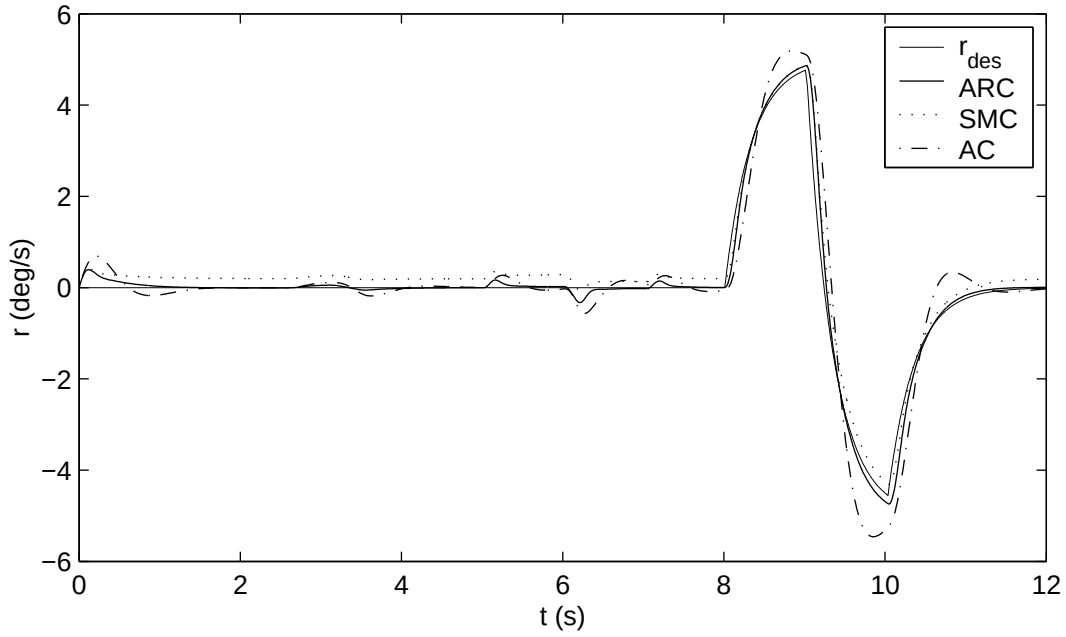

Fig. XI.6. Yaw axis response to 80% loss of left stabilator effectiveness for 1” PD input

ology to a range of left stabilator surface effectiveness losses. The roll and pitch axes error responses show that as more effectiveness is lost, the measure of the error response increases. For SMC and ARC, the sensitivity of the measure in the pitch axis to increase in loss of effectiveness is much smaller than for AC. For the roll axis, the value of the measure increase is nearly the same for AC and ARC, but the the increase is larger for SMC. Of particular interest is the fact that the performance measure response in figure XI.7 is not monotonically increasing. This has to do with the fidelity of the F-5 model. The table look up functions used to model the dynamics of the aircraft are not as fine as for the F-15 IFCS model. The result is that for certain failure amplitudes, a different area of the table is used. This results in the jumps demonstrated by the figure. For the yaw axis, the change is very small. This is because changes in the stabilators have little effect on the yaw axis. In general, the measure values for AC are higher than those of ARC and SMC. The gains of the AC portion of the control would be too high if used for AC alone, but when coupled with SMC (to form ARC), they work quite well. On the whole, we discover that though the advantage of ARC over SMC for tracking commands is small for this type of failure, ARC nevertheless performs better than the other methodologies with similar gains.

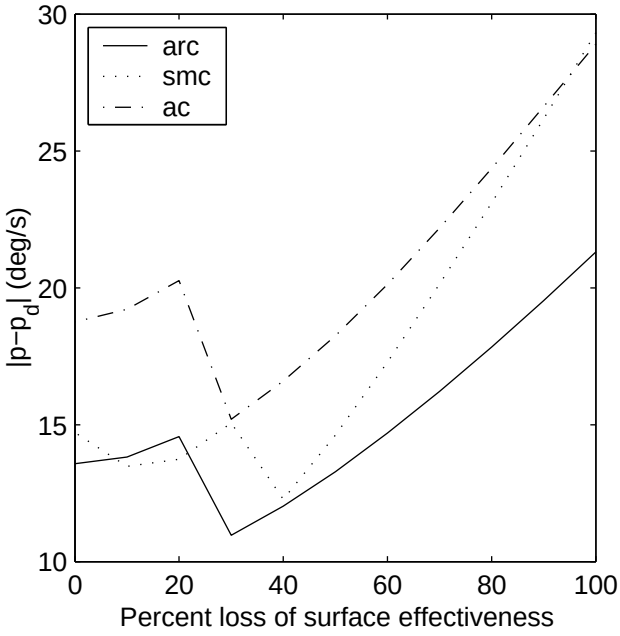

Fig. XI.7. $\|p - p_d\|_{\mathcal{L}_{2W\dot{u}}}$ of F-5 error response to loss of surface effectiveness for 1” PD input

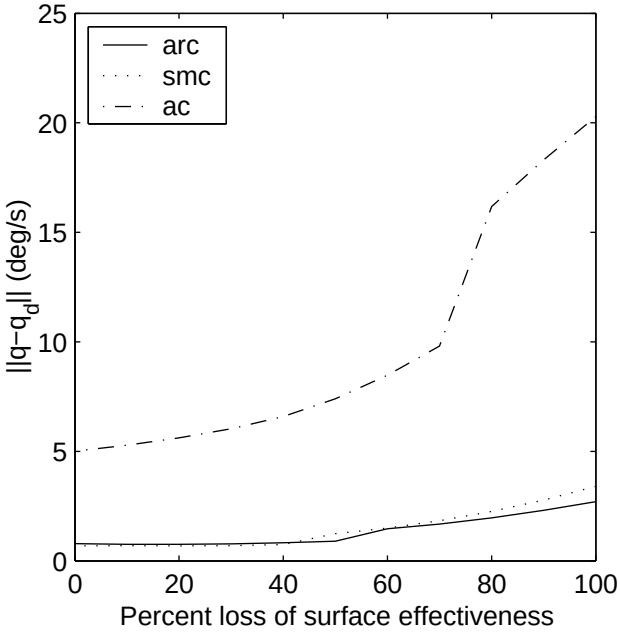

Fig. XI.8. $\|q - q_d\|_{\mathcal{L}_{2W\dot{u}}}$ of F-5 error response to loss of surface effectiveness for 1” PD input

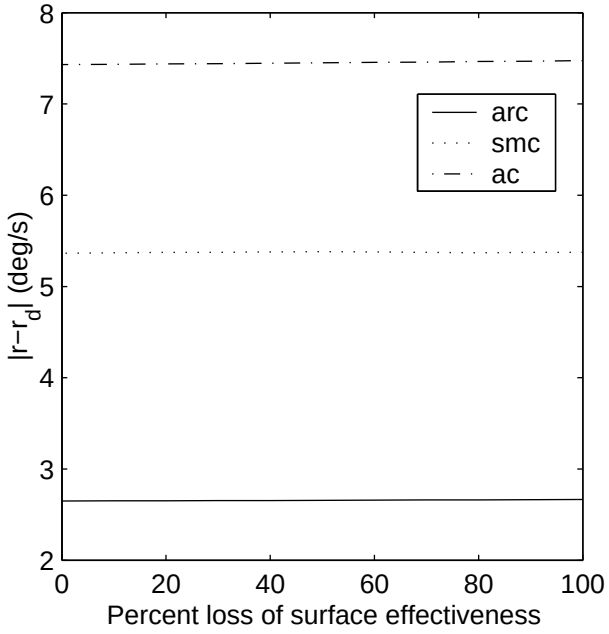

Fig. XI.9. $\|r - r_d\|_{\mathcal{L}_{2W\dot{u}}}$ of F-5 error response to loss of surface effectiveness for 1” PD input

B. Floating Actuator Failure

An additional failure mode that will be considered is the floating actuator failure. As mentioned previously, testing of this type of failure will involve loss of control of one of the stabilators at which time it will begin floating with α at the time of the failure. Of the three failure types considered, this type of failure is the most difficult for the control system to handle. This is because it not only involves a large change in the DI+plant dynamics, but a disturbance based on the angle of attack as well. The hard-over failure mode involved the same change in dynamics, but the locked surface resulted in a fairly constant disturbance (the change in disturbance is based on the change in the aerodynamic control derivatives associated with the surface). This failure type will be analyzed first for the linearized F-15 model and then for the nonlinear F-5 simulation.

1. Linearized F-15

For the linearized simulation model, at the time of the failure, the stabilator will change amplitude and become equal to the total angle-of-attack. This will result in a nonzero trimpoint for the system, so it can be expected that SMC control will have some problems dealing with the steady state error. Figure XI.10 shows the response of each control methodology to a floating stabilator failure for the linearized F-15 model. The figure shows the type of response we can expect from each control methodology. For the adaptive methodology, we begin to see some oscillitory behavior. This is because the AC technique has only assymptotic guarantees. The ARC and SMC techniques exhibit much better tracking behavior, but again the steady state error response under SMC is non-zero. The sensitivity of the tracking error response to the command amplitude is also considered. Figure XI.11 shows the weighted measure of the error responses for each control methodology for each command amplitude. It is surprising to see that the measure of the tracking error varies little with the

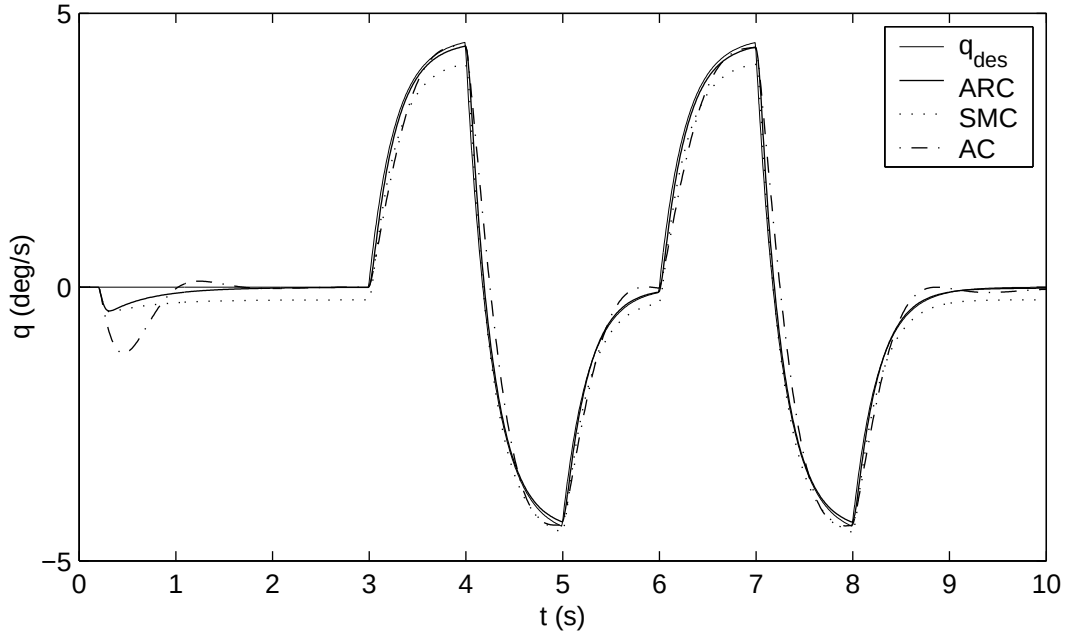

Fig. XI.10. Linearized F-15 response to 1” inputs under floating left stabilator failure

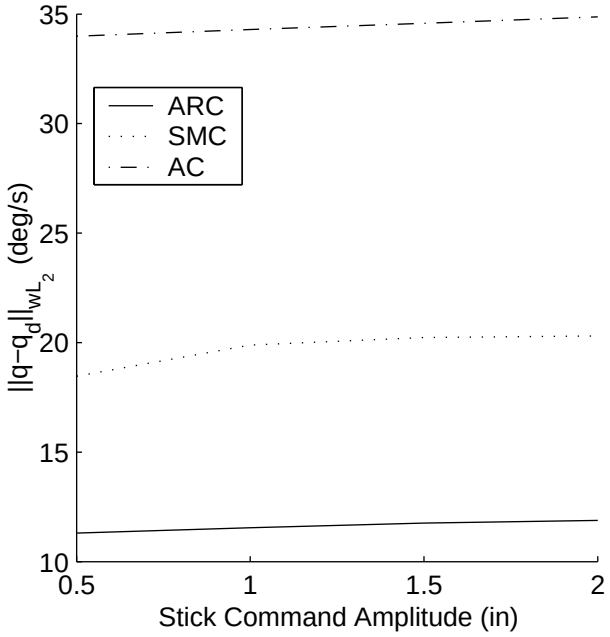

Fig. XI.11. $\|q - q_{des}\|_{\mathcal{L}_{2W\dot{u}}}$ versus command amplitude for linearized f-15 with floating stab

increase in command amplitude. If the error was not normalized by the derivative input into the DI, a linear behavior would be observed between the command amplitude and the measure of the error. Again, the lack of change in the measure value shows that the measure is in fact taking into account the aggressiveness of the command input and therefore has been designed correctly. The measure value changes little over the region because the disturbance varies with α, which depends on the commands through a largely integral relationship. What is observed is that the ARC methodology provides the lowest measure of the error response for the methods considered. The measure value for SMC is larger than ARC because of the steady state error due to the new trim point. Again, the AC technique has the highest measure value because of its poor tracking, but has some advantage in that it drives the steady state error to zero.

2. Nonlinear F-5

The nonlinear results will hightlight the effect of the floating actuator failure on the other axes of the aircraft and test the ability of the outer loop control to handle the disturbance in each axis. The cross coupling between axes will be smaller for the F-5 than for the F-15. Figures XI.12, XI.13, and XI.14 show the response of the F-5 under each control method to a 1” stick and rudder amplitude PD maneuver. The left stabilator begins to float at $t = 0.25s$. As expected, the SMC controller has some steady state error in each axis. The AC pitch axis response reveals that the adaptive controller has a difficult time tracking in the presence of the disturbance. Even with the angle of attack included as part of the regressor, the tracking performance is poor. Examining figure XI.13 reveals that the other controllers are in general unable to track pitch axis commands nearly as accurately as for hard-over failures as well. The SMC and ARC controllers exhibit much more accurate tracking performance, however. The decline in tracking accuracy is partially due to the low gains required for the F-5 because of the slower surfaces (the amount of

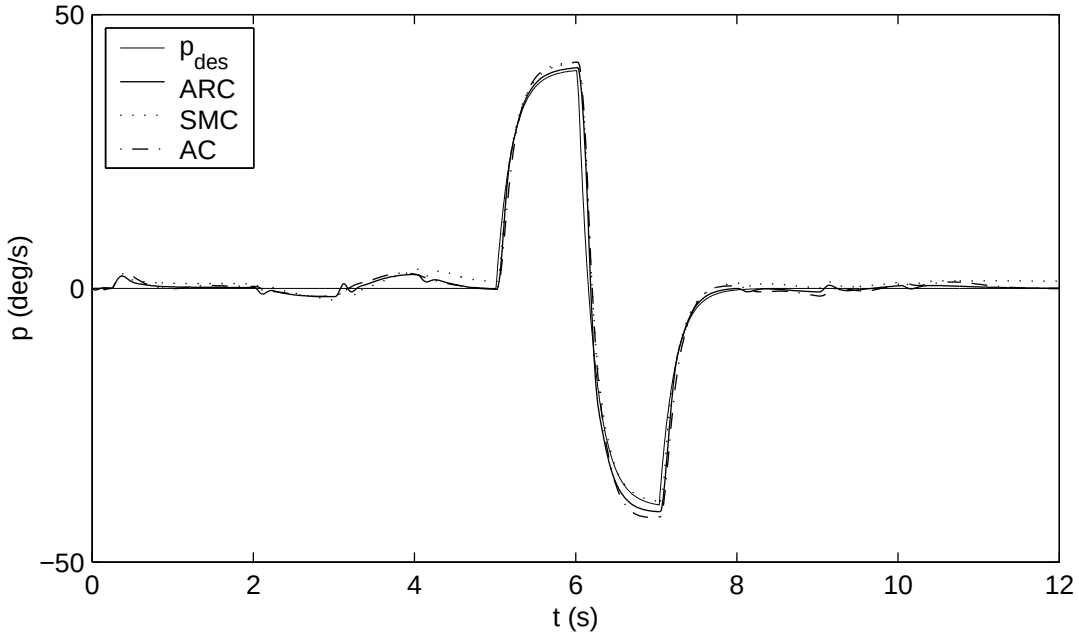

Fig. XI.12. F-5 roll axis response to 1” inputs under floating left stabilator failure

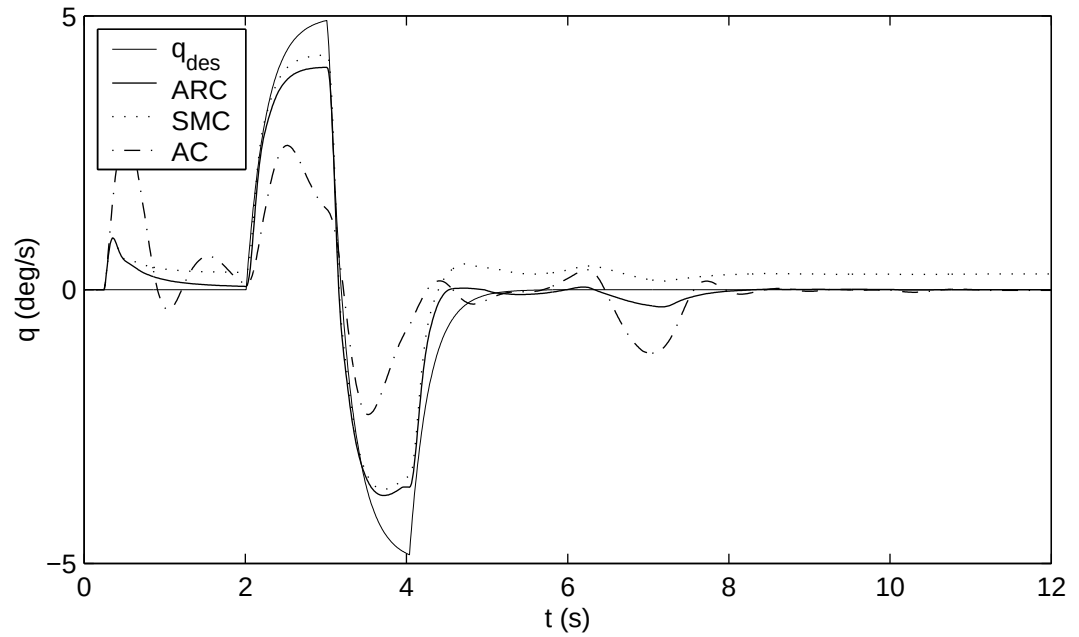

Fig. XI.13. F-5 pitch axis response to 1” inputs under floating left stabilator failure

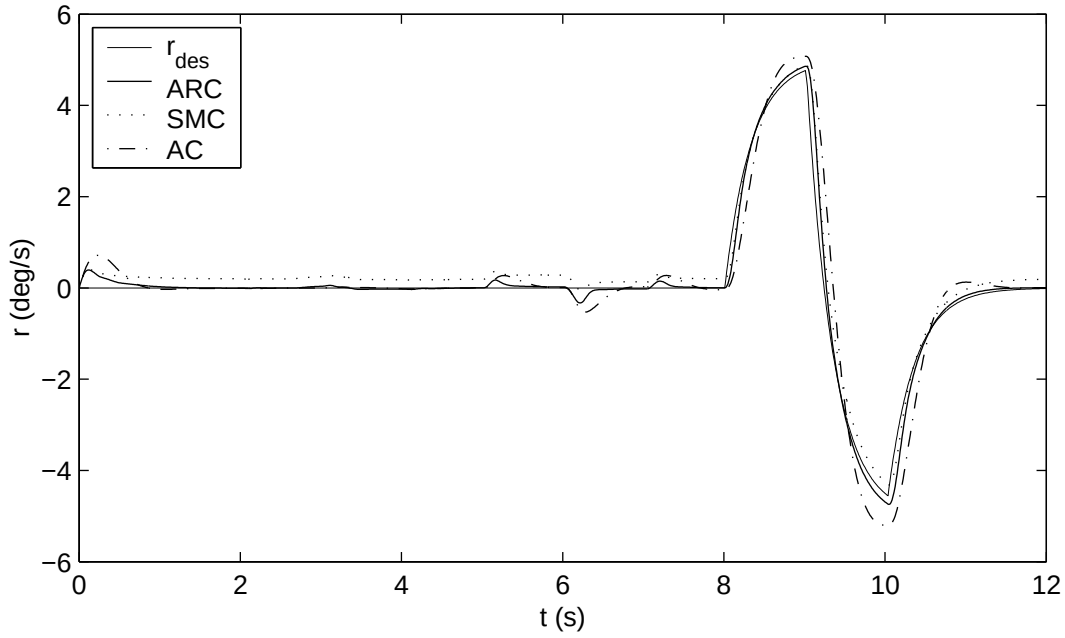

Fig. XI.14. F-5 yaw axis response to 1” inputs under floating left stabilator failure

actuator control authority (magnitude) available in the pitch axis is low as well). This will be discussed in more detail in section XIII. Figures XI.15, XI.16, and XI.17 show the measure values of the error responses of each control methodology as a function of the the command amplitude. There is a large difference in the behavior of each response from axis to axis. For adaptive gains equivalent to those in ARC, the AC controller is unable to track well in the pitch axis, so so the value of the measure is high. In general, the measure values are much larger for the AC methodology than for the other two methodologies. This is again because of the lack of transient guarantees. To speed the response, high “learning rates” are needed, which tend to cause a lag-like behavior when they interfere with surface rate and position limits. The addition of SMC to the adaptive law (ARC) allows the control to have the same gain, but still ensure stability. For high command amplitudes, the tracking accuracy of ARC begins to deteriorate because of surface position limit interference. The surface ranges on the F-5 aircraft are very narrow and hinder the

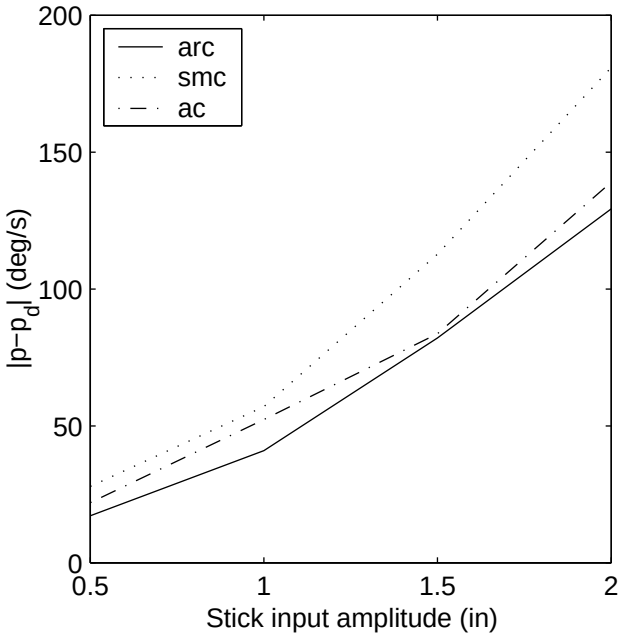

Fig. XI.15. F-5 $\|p - p_{des}\|_{\mathcal{L}_{2Wcc}}$ response to floating left stabilator failure

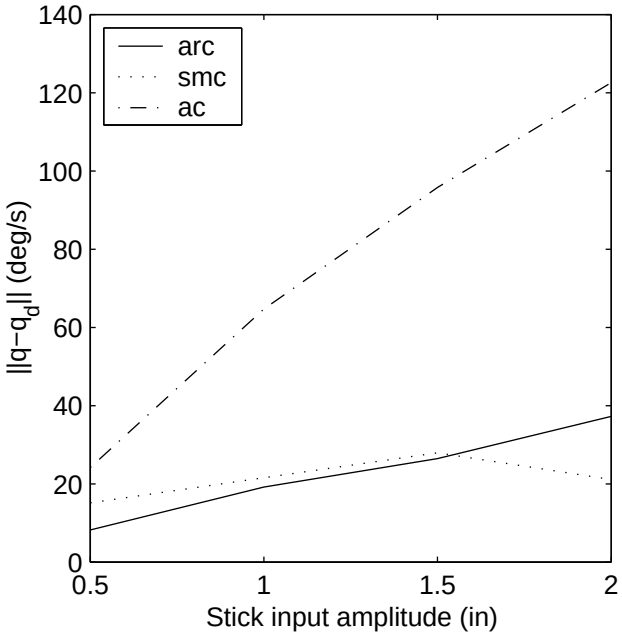

Fig. XI.16. F-5 $\|q - q_{des}\|_{\mathcal{L}_{2Wcc}}$ response to floating left stabilator failure

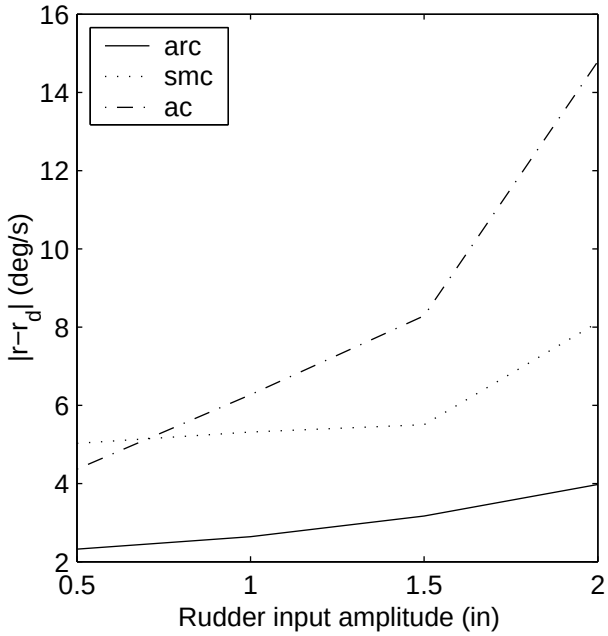

Fig. XI.17. F-5 $\|r - r_{des}\|_{\mathcal{L}_{2Wcc}}$ response to floating left stabilator failure

ability of the controller to perform (this is another reason why hard-over failures were tested for the F-15). For the pitch and yaw axes, the measure response stays fairly constant with command amplitude until surface position limits are reached for higher stick and rudder input amplitudes. For the pitch axis, there is a small increase in $\|q - q_{des}\|_{\mathcal{L}_{2Wcc}}$ as command amplitude increases. The measure of the roll axis response increases a larger amount with the command amplitude. The ARC methodology responds better as long as the system does not encounter a position limit, but the response decays rapidly when this occurs. Otherwise, the measures again show that the methodology outperforms SMC or AC alone.

CHAPTER XII

SMC WITH INTEGRATOR VERSUS ARC

In flight control applications of SMC it is common to include an integrator as part of the sliding surface [13, 14, 15, 16, 17, 18]. The objective of this inclusion is to deal with steady state errors (the purpose of the adaptive portion of the control for ARC). SMC regulates the filtered error response ($z \to 0$). The stability of the linear differential equation governing the sliding surface requires that every term that makes up the surface must decay to zero when $z = 0$. If an integrator is included as part of the surface and the SMC forces the system onto the sliding surface, the integral of the error must go to zero as $t \to \infty$. In essence, the control variable becomes the integral of the error instead of tracking error. On face, this does not sound out of the ordinary. However, if the dynamics of the system were to suddenly change resulting in a positive integral of the error, the system must undershoot by the same amount to allow the sliding surface to decay to zero. If a saturation function is used to replace the signum function in the SMC law as is common in practice, removing steady state error is accomplished by maintaining a steady-state z value.

Using a signum function, there is an obvious difference between ARC and SMC. With a saturation function, it might seem that these control laws would be equivalent to one another. This is not the case. As an example, consider the following dynamic system:

$$\begin{aligned} \dot{x} &= d(t) + \nu \\ |d(t)| &\leq D \end{aligned} \tag{XII.1}$$

The objective is to regulate the state, ($x \to 0$). The magnitude of the disturbance, $d(t)$, is bounded by D. This might be something that is encountered for an ideal inversion of the aircraft dynamics. The continous approximation of SMC with an integrator included as

part of the sliding surface has the following form:

$$\begin{aligned} \nu_1 &= -k_1 z_1 - D_1 \text{sat}(z_1/\varepsilon) \\ z_1 &= x(t) + \lambda \int_0^t x(t)dt \end{aligned} \tag{XII.2}$$

When the saturation operates in the linear region the above control law becomes:

$$\nu_1 = -(k_1 + D_1/\varepsilon)x - (k_1 + D_1/\varepsilon)\lambda \int_0^t x(t)dt \tag{XII.3}$$

When the saturation function reaches its upper limit the SMC law becomes the following:

$$\nu_1 = -k_1 x - k_1 \lambda \int_0^t x(t)dt - D_1 \tag{XII.4}$$

The ARC control law with continuous approximation is given by the following (d is modeled with a $\hat{\theta}$):

$$\begin{aligned} \nu_2 &= -k_2 z_2 - D_2 \text{sat}(z_2/\varepsilon) - \hat{\theta}_\pi \\ z_2 &= x(t) \\ \dot{\hat{\theta}} &= \gamma z_2 = \gamma x \end{aligned} \tag{XII.5}$$

When the saturation operates in the linear region, and $\hat{\theta}_\pi$ is not saturated:

$$\nu_2 = -(k_2 + D_2/\varepsilon)x - \gamma \int_0^t x(t)dt \tag{XII.6}$$

If the saturation function is at its upper limit, but $\hat{\theta}_\pi$ has not reached a limit:

$$\nu_2 = -k_2 x - \gamma \int_0^t x(t)dt - D_2 \tag{XII.7}$$

In both control laws, when operating in the linear region of the saturation function, the result is porportional-integral control. Using Equations (XII.3) and (XII.6) gains can be selected that make the control laws equivalent for this case. Upon reaching a saturation

limit, the gains that make the two control laws equivalent do not make Equations (XII.4) and (XII.7) equivalent. There are three major differences between ARC and SMC. First, the integral gain for ν_1 changes when $|z| > \varepsilon$, but does not change for ν_2. Second, $\hat{\theta}_\pi$ can be saturated meaning the integral portion of ν_2 becomes a constant maximum value. The integral portion of ν_1 may reduce gain but is otherwise unbounded. Third, if more is known about the model, these parameters can be included in the ARC law. This is not possible with SMC.

A second issue is the value of z, or that of the sliding surface itself. If signum functions are used to utilize a discontinuous SMC law, then z_1 will be forced to zero as $t \to \infty$. In practice, this is rarely used (particularly not in aircraft). Thus a saturation function might be used. As was mentioned previously, when using a saturation function with SMC alone, z does not approach zero. The result is the integral term in z (in the example above, $(k_1 + D_1/\varepsilon)\lambda \int_0^t x(t)dt$) absorbs the steady state error in z. The result is that $x(t) \to 0$. This creates a problem similar to what was observed in figure X.20 where the transient performance of the SMC controller begins to degrade as a result of z operating too close to saturation. To demonstrate this a comparison of the two methodologies with equivalent gains was simulated. Figure XII.1 shows this comparison. The test is run for the linearized F-15 model with 2 inch (the largest amplitude considered) stick and rudder inputs. Near trim, the figure shows that the two methods perform equivalently. This is because the sliding mode controller is not being saturated at trim. As the aircraft moves away from trim, the ARC controller continues to perform well, which the performance of the SMC controller begins to drift. This is the effect of the control operating near saturation. Figure XII.2 shows the $\text{sat}(z/\varepsilon)$ values of ARC and SMC for a simulation of the linearized F-15 with 2" stick inputs and a failure of 8 degrees from trim. The figure clearly shows that the SMC controller does not have the control authority in the positive z direction that ARC does as a result of z not decaying back to zero. This means that the controller becomes gain limited

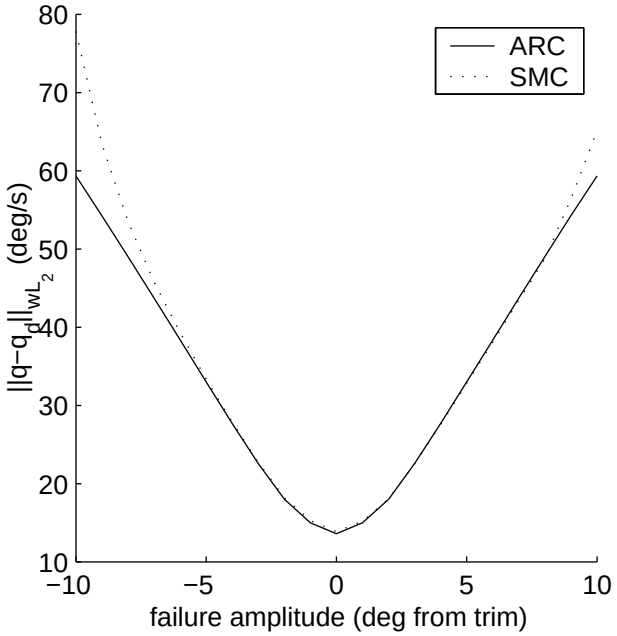

Fig. XII.1. Comparison of SMC with integral and ARC for linearized F-15 with 2” stick input

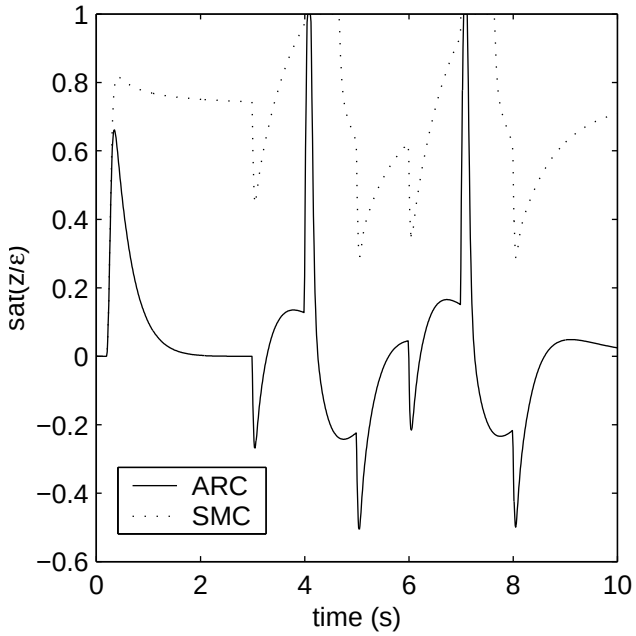

Fig. XII.2. $\mathrm{sat}(z/\varepsilon)$ for ARC and SMC control laws with 8 deg from trim failure

when $z/\varepsilon \rightarrow 1$, resulting in the decay in tracking seen in the measure value response in figure XII.1. ARC accounts for the the steady state errors and the slowly varying dynamics without the drawback of including an integral as a part of the sliding surface. This allows the system to achieve the sliding surface ($z \rightarrow 0$) even when using a saturation function in the SMC portion of the control law.

CHAPTER XIII

LIMITATIONS

In previous sections, discussion was presented concerning the ability of ARC to maintain aircraft stability and performance in the presence of actuator failures. Examples were presented for various types of failures, including loss of actuator authority, hard-over, and floating actuator failures. These highlighted the ability of ARC (as well as SMC and AC) to perform in the face of changing plant dynamics and large disturbances. If only these things were shown, it would seem that the ARC control methodology was a panacea for all control problems. However, there are many limitations involved when using ARC to obtain a solution to a control problem. These will be highlighted in this section.

A. Rate and Position Limitations

The aircraft control problem is made more difficult by the rate and position limits placed on the control surfaces. The rate limits effect the gain that a control can have, which in turn limits the ability of a control to reject disturbances and account for errors. For linear control, it is well known that to reject low frequency disturbances, a high gain is needed. Because sliding mode control is approximated linearly in the boundary layer region, the behavior of the controller will be similar to that of a linear controller while the error is in this region. Increasing the ε parameter, which adjusts the boundary layer thickness, lowers the "gain" of the SMC portion of the control, but also serves to widen the region. For the F-15, we observed that for the same gains for the sliding mode portion of the control, ARC had a large advantage. The allowable gains for the SMC law were limited because of rate limitations of the actuators on the F-15. This required a larger boundary layer region, which resulted in larger steady state error for SMC. While all the testing for the F-15 and F-5 show that ARC is on the whole superior to SMC and AC, there are some cases

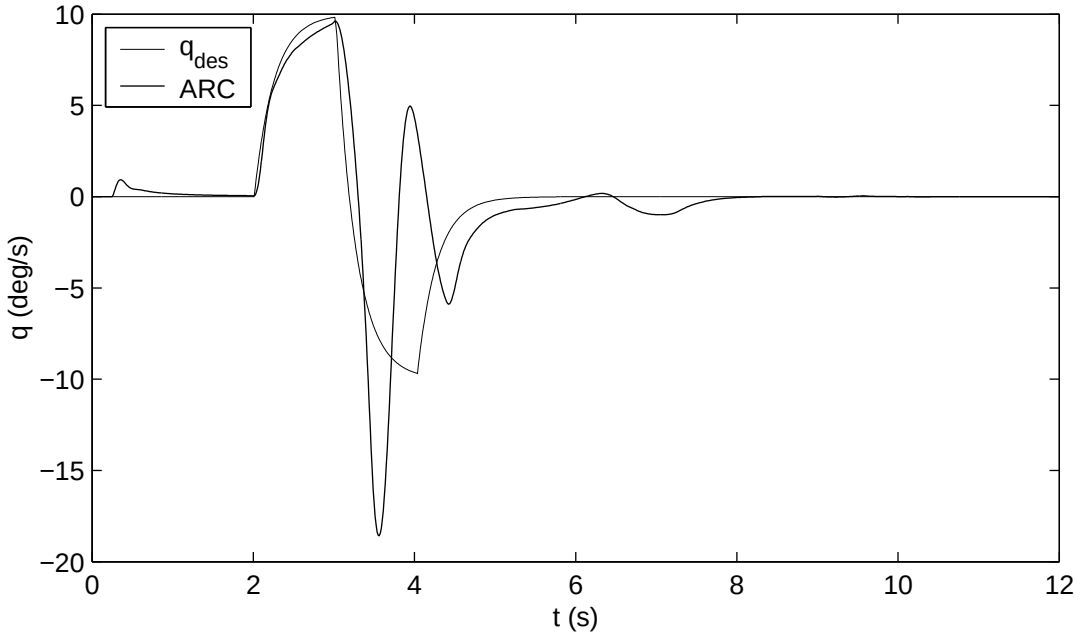

Fig. XIII.1. ARC pitch axis response for F-5 aircraft under stab float failure with 2” stick input

that show when things begin to break down. This is more apparent on the F-5. The F-5 has slower actuators, and a smaller range over which these actuators operate (particularly the stabilators). This places a limit on what can be accomplished via ARC. An example of this occurs for the F-5 aircraft when looking at larger command amplitudes during a floating actuator failure. Figure XIII.1 shows the pitch axis response for the F-5 when operating under a floating stabilator failure. The measure value of the error response for this case is $\|q - q_{des}\|_{\mathcal{L}_{2Wcc}} = 157.4$. Compared to the measure values of the response for other command amplitudes, this is fairly high (see figure XI.16). This oscillitory response is caused by the rate and position limits of the surfaces. Figure XIII.2 shows the right stabilator position over time for the response int figure XIII.1. At about $t = 4$ seconds, the stabilator reaches a position limit. This is because of the left stabilator position due to the failure. At this time, α is approximately zero, meaning that the left stabilator is off of trim by about -3 degrees. Therefore the right stabilator must compensate to keep the aircraft

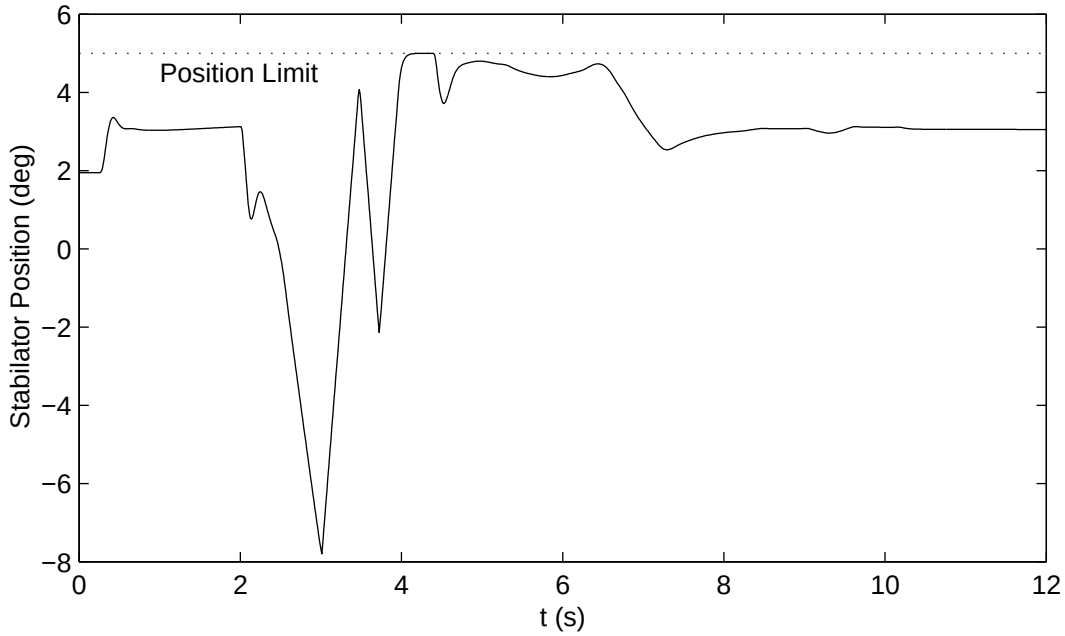

Fig. XIII.2. ARC right stabilator response for F-5 aircraft under stab float failure with 2” stick input

from pitching (which in turn induces a roll moment). However, the upper position limit is around 5 degrees, so it cannot compensate completely. This means that the limitations of the aircraft itself keep the control from being able to perform. For this particular problem, there is no control that can function unless more actuator authority is present (for example, if the ailerons are used for pitch as well). While the position limit being reached explains some of the error, it does not explain the largest portion of it. The larger tracking error results from rate limitations. Figure XIII.3 shows the stabilator rate response versus time for the same pitch rate command profile while the left stabilator is experiencing a failure. The stabilator hits a rate limit several times throughout the maneuver. These occur at times of the largest command rate and the largest change in amplitude. In particular, the actuators seem to hit their limits when the pilot input goes from its largest value to its smallest. These are the same times that we begin to see the largest discrepancies in tracking as well. The SMC control law does not exhibit this behavior to as large of an extent, but

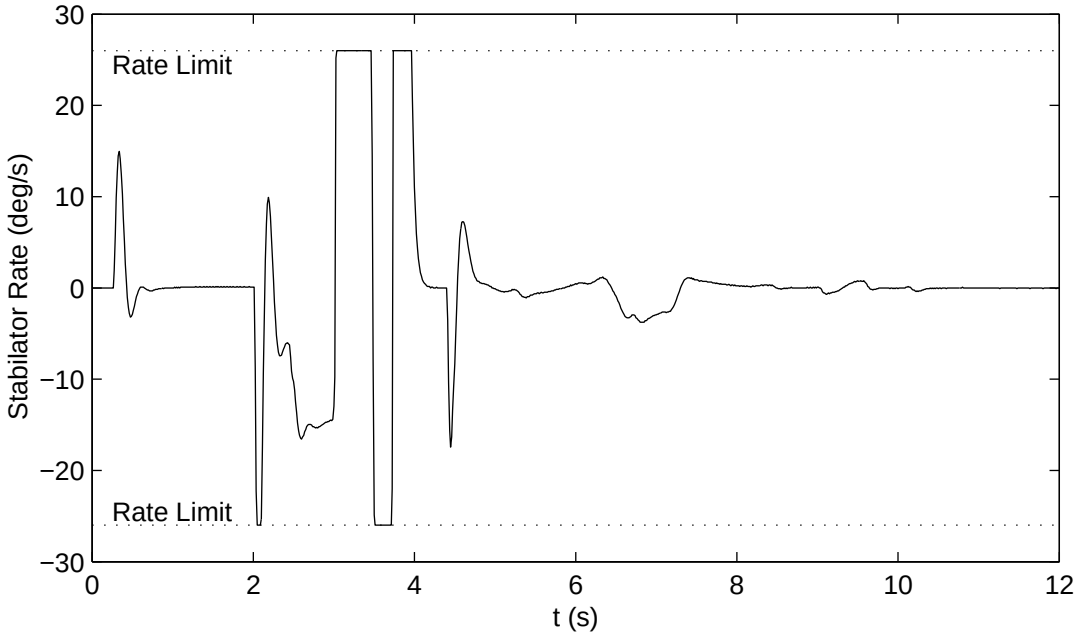

Fig. XIII.3. ARC right stabilator rate response for F-5 aircraft under stab float failure with 2” stick input

it is observed there as well. There are two reasons for this. The first is the “high” gains of system. The gains can be lowered to prevent this from happening, but this is at the expense of performance for failure cases with smaller command amplitude and for the hard-over failure cases. A second cause of the repetitive rate-limiting behavior lies in the adaptive portion of the control. The integral action in the adaptive law begins to “wind up” when a surface is saturated. The integral of the error increases, but increasing this value in the control law can do nothing because the control is saturated. This effect can be removed by changing the learning law to turn off when a surface is saturated and it learns in a direction that continues to saturate the control. While this will not alleviate the high gain problem itself, it helps to reduce some of the problems that occur when the control surfaces do hit rate limits. This is how ARC and AC are implemented for the results shown in section XI. The measure value of the error response for the command amplitude of 2” (shown in figure XI.16) is much smaller than the value of $\|q - q_{des}\|_{\mathcal{L}_{2W_{cc}}} = 157.4$ for

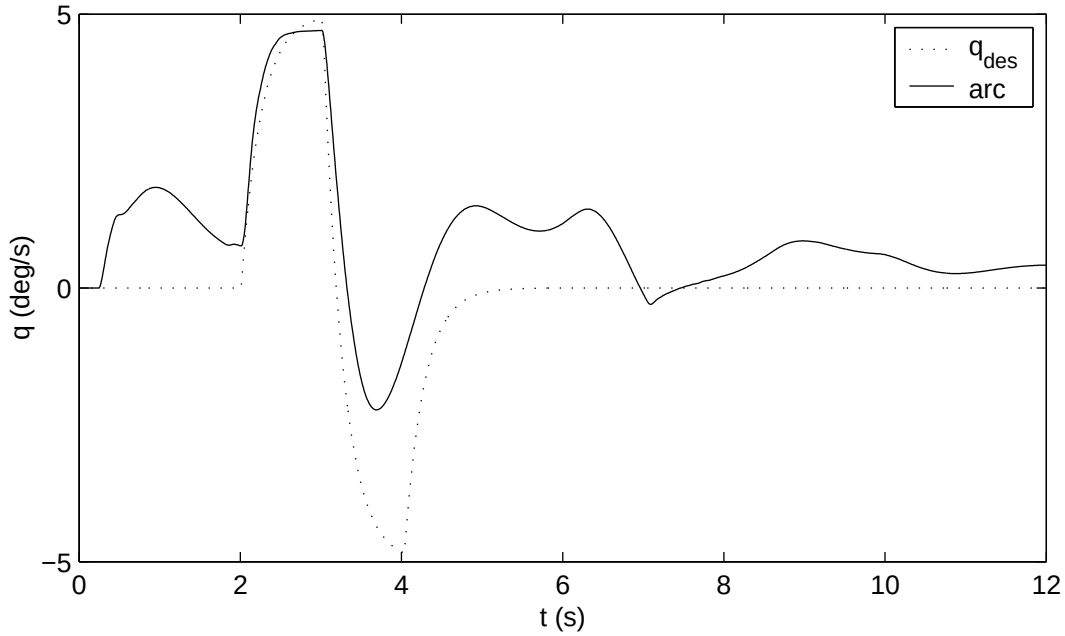

Fig. XIII.4. F-5 Pitch axis response for 1” stick inputs with -3 degree hard-over failure

the case shown in figure XIII.1. While this somewhat removes the negative effects of the adaptive control, the resulting control is more complicated, and there is still some rate and position limiting influence on the control.

While the floating actuator example dealt mainly with limitations that result from actuator rate saturation, another example can be formulated to show how the position limitations can result in poor performance. For this example, the effect of a hard-over failure on a maneuver will be considered for the F-5 aircraft. The F-5 stabilators have position limits of +5.5 and -17 degrees and rate limits of $\pm$26 degrees per second. For level flight the trim position of the stabilators is around 2 degrees, meaning that if a hard-over failure occurs around more than -3.5 degrees from trim, there is no possible way for the aircraft to level out at its current state (this is not entirely true because the control moment does not vary linearly with stabilator position). The response shown in figure XIII.4 illustrates this.

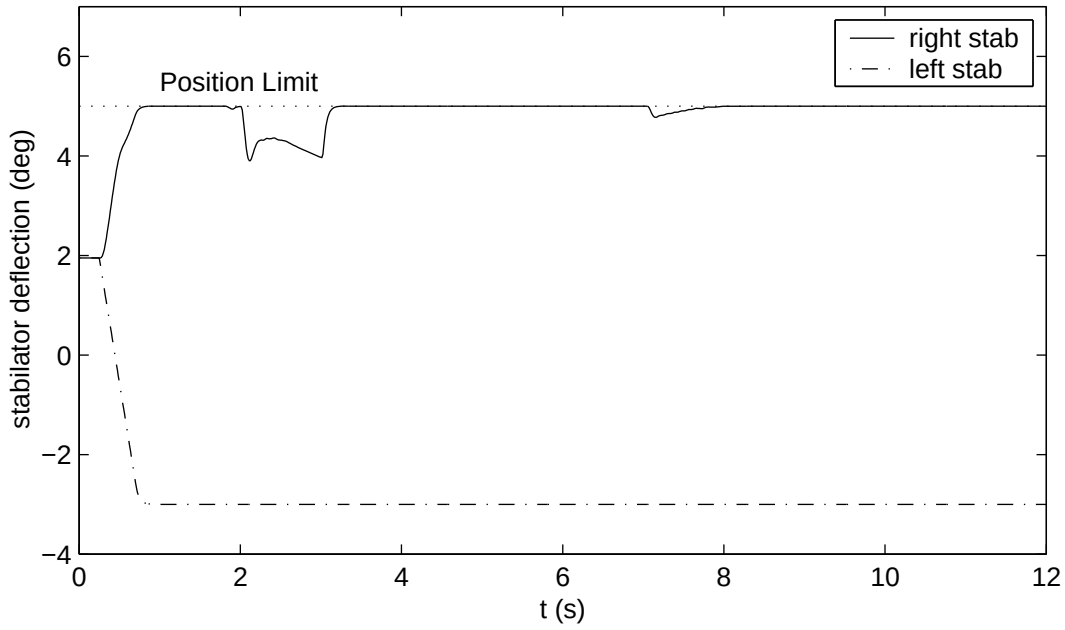

Fig. XIII.5. F-5 stabilator response for 1” stick inputs with -3 degree hard-over failure

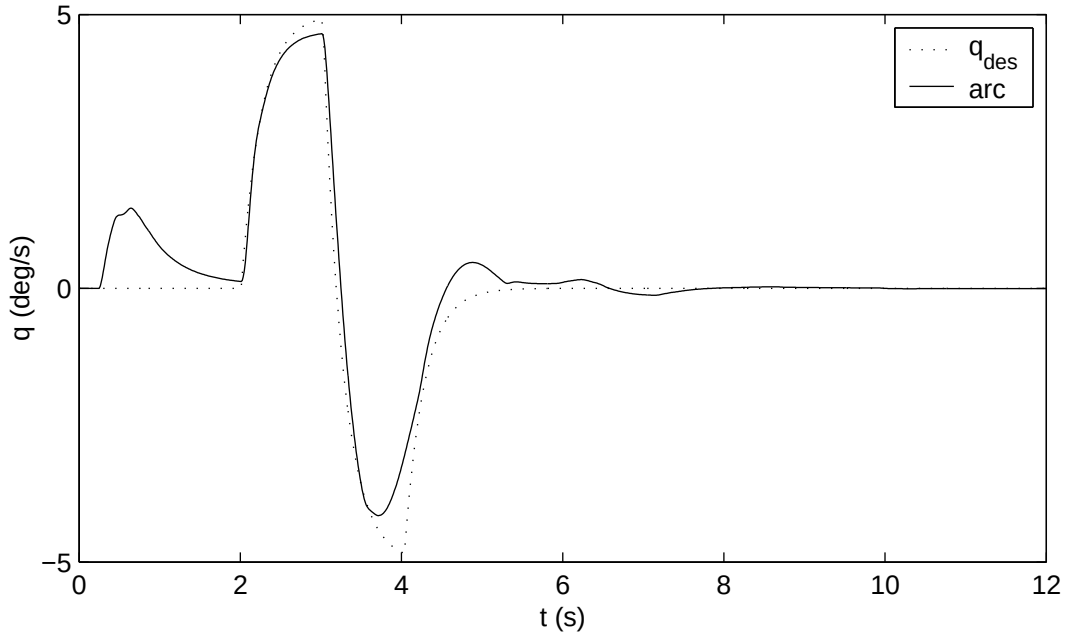

Fig. XIII.6. F-5 Pitch axis response for 1” stick inputs with -2 degree hard-over failure

Although the aircraft does not become completely uncontrollable, tracking accuracy is lost, and the aircraft is unable to level out. Figure XIII.5 shows the reason for this. The failed surface is locked at -3 degrees. To compensate for the resulting pitch moment, the right stabilator must induce an opposite pitch moment. However, the surface position limits of the aircraft prevent this from occuring. For this failure, the aircraft cannot be stabilized without the use of additional surfaces or the throttle (the pilot might reduce throttle to bring pitch rate down, for example). In general, once the limits of the aircraft are reached, improving the control cannot improve the response of the aircraft. As a sidenote, consider figures XIII.6 and XIII.7. These figures show the pitch response and stabilator positions for the same input profile, but with a failure amplitude of -2 degrees instead of -3 degrees. These figures show that the performance of the aircraft for this case has improved immensely over the case previously described. If the failure is in the opposite direction, the position limit does not have an impact, and the resulting error response is as good if not better than the nonlinear F-15 model respnoses. In this manner, the position limitations of the aircraft play a huge role in what can be accomplished through control.

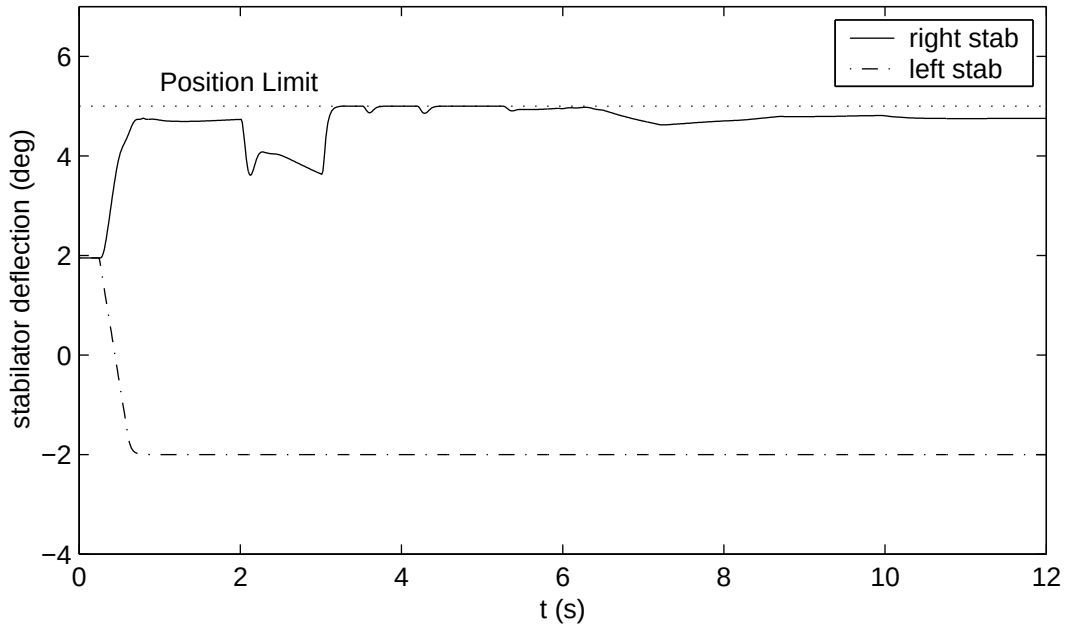

Fig. XIII.7. F-5 stabilator response for 1” stick inputs with -2 degree hard-over failure

B. Control Allocation

Not only do the properties of the aircraft limit the ability of the controller to perform, but the control allocation plays a large role as well. Throughout the simulations, there has been a constant control allocation for each model. For example, for the nonlinear F-15 simulation, the synthetic actuator command was allocated to be applied in full to the ailerons and 1/4 to each stabilator. For the F-5, each set of actuators were assigned a specific axis (ailerons for roll, stabilators for pitch, rudders for yaw). This control allocation is the same both before and after the failure. When a failure occurs, the actual control allocation changes, but the DI and outer loop controlers are unaware of this, so they compensate by high gain. This means not only must the control laws account for the disturbance that results from the failed actuator, but they must also overcome a complete and possibly instantaneous change in plant structure. This change in plant structure can also be modeled as an input related disturbance. With adaptive control, it is possible to estimate the plant in such a way that the new structure could be learned, but with the addition of SMC, this becomes more difficult. Without integrating the control allocation terms into the adaptive control, the change in control effectiveness must be overcome by the high gain SMC portion of the control. Coupled with the rate and position limitations, this hinders the performance that can be acheived.

As a simple example, consider the linearized F-15 model under ARC control. Figure XIII.8 shows the pitch rate response of the linearized F-15 model to a -10 degree hard-over failure for the ARC response with a constant control allocation as well as with a new control allocation. For the new control allocation, the control effectiveness was cut in half to account for the loss of the 2nd pitch actuator. With a change in control allocation, there is no model mismatch, and the only errors the control must overcome are small modeling errors (from using a more simplified linear system for the DI) as well as the disturbance

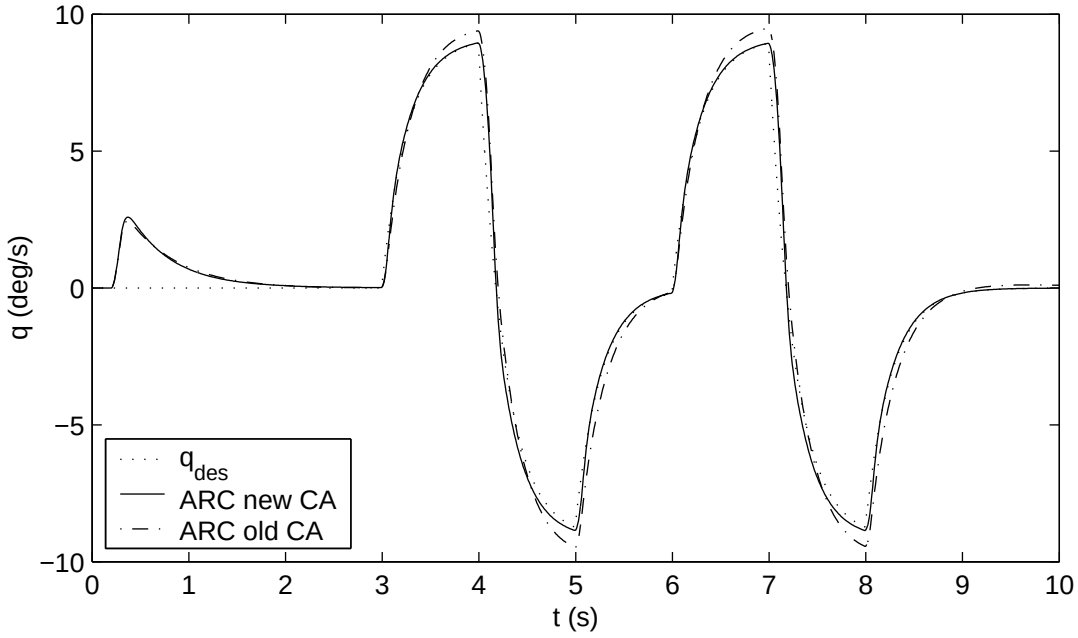

Fig. XIII.8. Linearized F-15 response to hard-over failure with and new and old control allocations

from the stuck control surface. For a full nonlinear case, the effect of a control allocation change is not quite as straighforward, but the results are similar. The simple result shown for the linear case in figure XIII.8 demonstrates the limitations of what can be accomplished via outer loop control. However, while altering the control allocation scheme can be an effective way to improve the performance of the control system, the difficulty lies in the selection of a scheme without knowledge that a failure has indeed occurred. Therefore, the results in figure XIII.8 are a “best case” scenario. While this problem is outside the scope of this research, exploration of online control reconfiguration would certainly aide in reducing the limitations of what can be acheived via outer-loop control.

CHAPTER XIV

CONCLUSION

The problem of maintaining performance and control of an aircraft in the presence of control surface failures has been addressed. Control of the aircraft is maintained via nonlinear dynamic inversion control (a form of feedback linearization) in conjunction with three different outer loop control laws: adaptive control, sliding mode control, and adaptive robust control. Each of these outer loop control techniques offers different benefits. Adaptive control is able to guarantee that the steady state tracking error of the system will decay to zero when the source of aircraft modelling errors is purely "parameterized" uncertainty. However, no such guarantee can be made in the presence of unstructured uncertainty (under the right circumstances, the adaptive law can be proven to be bounded in the mean-squared sense). In addition, when the persistence of excitation condition is not met, there are no transient performance guarantees for the adaptive law. When a pilot is trying to perform precision maneuvers in an aircraft, there is a substantial difference between the tracking error asymptotically decaying to zero and exponentially decaying to zero. The inability of adaptive control to guarantee exponential stability is a large drawback in terms of aircraft performance (especially for fighter aircraft). A second outer loop control technique considered is sliding mode control. Sliding mode control is able to guarantee exponential decay of tracking error to zero, which is extremely important in aircraft control. However, this exponential decay requires the control law to be discontinuous. Such a control law is not practical, and leads to chattering behavior when coupled with control surface rate limits. To prevent this, a continuous approximation is used in practice. The result is that the tracking error does not decay to zero, but to some boundary layer region around zero. Because of the surface rate limits, the boundary layer region must be widened to keep the control gain low in the linear region. This results in steady state error that can be quite large depend-

ing on the size of the disturbance. The final outer loop control methodology considered is termed adaptive robust control [21]. The control combines the adaptive and sliding mode control methodologies into one control law. This allows the control law to retain the transient tracking error performance benefits of sliding mode control, while adding the steady state error guarantess of adaptive control.

Each of the control methodologies was tested in the presence of several failure types, including loss-of-surface effectiveness, actuator hard-over, and floating actuator failures. The most extensive testing was performed for the hard-over failure condition. Each control methodology was implemented on a linearized pitch axis model of the F-15, a full nonlinear model of the F-15 IFCS aircraft (from NASA Dryden), and a nonlinear model of the F-5A. All failure cases were tested on the linearized aircraft. Hard-over testing was performed primarily on the nonlinear F-15 aircraft, while loss-of-surface and floating actuator testing was performed on the F-5. The testing revealed that over a wide range of command amplitudes and failure types, ARC was able to retain the tracking benefits of SMC, but remove the steady state errors as well. A form of the $\mathcal{L}_2$ norm was defined to perform an assessment of the tracking error responses based on performance criteria that would a pilot be testing. This measure utilizes a frequency weighting on the error response to penalize high-frequency behavior (specifically at frequencies above the desired handling qualities specifications). The measure also penalizes errors based on the aggressiveness of the command input. Error is penalized more severely for smaller, slower command inputs than for larger more quickly varying inputs. For the nonlinear simulations involving multiple command axes, the aggressiveness of the command inputs in other axes is considered as well.

Of the three failure types, loss-of-surface effectiveness failures present the simplest case for the control methodologies to handle. For loss-of-surface effectiveness failures, ARC and SMC perform much better than adaptive control. This type of failure tests the

ability of each controller to track in the presence of model mismatch only. As more surface effectiveness is lost, each control technique has a more difficult time tracking, however the changes in ARC and SMC are much smaller than those for adaptive control. The loss of effectiveness failure case demonstrates that the addition of the adaptive control law to the sliding mode control law reduces the tracking performance only a very small amount. Varying the command amplitude showed that tracking performance varied only a small amount with command amplitude.

The hard-over failure condition was the most widely tested of the three failure types. Three performance characteristics were analyzed for this failure condition: transient, tracking, and steady state performance. The transient and tracking performance analysis shows that adaptive robust control retains the ability of sliding mode control to perform well in the presence of large uncertainty. The steady state performance analysis shows that sliding mode control retains large steady state errors and that the error increases as disturbance size (failure amplitude) increases. To relate these characteristics a form of the frequency weighted $\mathcal{L}_2$ norm was utilized to gauge the overall error response. In general, this analysis showed that at low failure amplitudes, SMC and ARC perform similarly, but as failure amplitude becomes large, the performance of SMC becomes very poor. This is due to the steady state error and the requirement that SMC function near saturation. As command amplitude is increased and as the maneuvers become more aggressive, the ability of each control methodology to maintain performance levels declines. In general, ARC is less sensitive to both command amplitude and aggressive maneuvers. For very aggressive maneuvers the performance of ARC breaks down because of the relative performance of each axis and control surface limitations.

Finally, the floating actuator failure mode was addressed. This failure mode revealed the limitations of each control method to maintain performance in the face of parameter varying disturbances. While ARC and SMC were able to perform relatively well in general

(with ARC performing slightly better in general), the performance was poor with respect to the hard-over failure mode. This failure type demonstrates the limitations of each control methodology. It also opens the door to discussion about rate and position limitations and their effects on the control problem. The rate limits of the aircraft surfaces and to a lesser extent, the position limits severely limit what can be accomplished through outer loop control. This is because the outer loop control techniques attempt to use "brute force" to allow the aircraft to overcome DI mismatch. If the control laws could reconfigure the DI law to account for the change in control effectiveness, the outer loop controls would be much more effective.

The advantages of using adaptive control over adaptive control in this application come in the form of performance gains. As shown in the simulation examples, the use of ARC provides exponential convergence of tracking error. This prevents the necessity of the persistence of excitation condition being satisfied in order to obtain this type of performance (as is the case for adaptive control). With respect to sliding mode control, ARC has the advantage of eliminating steady state error in the presence of disturbances. This benefit can also serve to be a disadvantage to using ARC. If a failure occurs with ARC, the disturbances are eliminated and the plane returns to "normal" flight. Once this occurs, the pilot has no indication of how drastic the failure may be until he/she attempts a maneuver. As a result, the pilot may attempt to perform maneuvers that may be physically impossible. For SMC, when a failure occurs, there is a resulting steady state error as well. This helps the pilot assess how drastic the failure is, and that if it persists. The pilot can then make adjustments to his or her flying based on the knowledge that there is a failure.

On the whole, adaptive robust control allows an aircraft under dynamic inversion control to preserve its performance and maneuverability in the presence of various failures. The performance of the aircraft under adaptive robust control is similar to that of a healthy aircraft. This is accomplished without any control reconfiguration or online fault detection

algorithms. The performance is maintained for large failure amplitudes and for aggressive maneuvers.

CHAPTER XV

RECOMMENDATIONS FOR FUTURE WORK

The discussion presented thus far in the thesis has centered around implementation of adaptive robust control as an outer loop to dynamic inversion control. While this implementation performs well in the face of modelling uncertainties and actuator failures, there are many further developments that can be pursued to improve the response of the aircraft. The control allocation scheme is one area where the control could be improved. As mentioned previously, much can be accomplished by altering the control allocation. Currently, no adaptation is being performed with respect to the impact that the control has on the state evolution of the system. Any deviation from the nominal performance is treated as a disturbance and lumped with unstructured uncertainty. If the control allocation were able to be reconfigured in the face of failures, the control authority could be applied to the actuators in such a way as to eliminate the parametric uncertainties and reduce the problem to one of disturbance rejection. This could be applied in the inner loop or the outer loop. Further work is necessary to include the adaptation of the control authority (in the outer loop) into ARC. Future work is also needed to lessen the requirements needed for ARC to ensure exponential tracking error convergence. ARC requires that the adaptation parameter be bounded above and below by some value for the performance to be guaranteed. In particular, when there is no guarantee of PE, this can be a very restrictive condition. It also means that for the adaptive bounds to be extended, the gains of the sliding mode portion of the control must be higher. Further research into the removal of these bounds is important to extend the convergence properties of the adaptive portion of the ARC control law and to lessen the restrictions of the control law needed to provide good exponential tracking performance.

REFERENCES

[1] S. Bennani, R. van der Sluis, G. Schram, and J.A. Mulder, "Control law reconfiguration using robust linear parameter varying control," in *AIAA Guidance, Navigation, and Control Conference and Exhibit*, Portland, OR, 1999, pp. 977–987, AIAA.

[2] Andy Packard and Michael Kantner, "Gain scheduling the lpv way," in *Proceedings of the 35th Conference on Decision and Control*, Kobe, Japan, 1996, pp. 3938–3941, IEEE.

[3] Jennifer Georgie and John Valasek, "Evaluation of longitudinal desired dynamics for dynamic inversion controlled generic re-entry vehicles," *Journal of Guidance, Control, and Dynamics*, vol. 26, no. 5, pp. 811–819, 2003.

[4] Honeywell Technology Center, Lockheed Martin Skunk Works, and Lockheed Martin Tactical Aircraft Systems, "Application of multivariable control theory to aircraft control laws: Final report: Multivariable control design guidelines, flight dynamics directorate," Tech. Rep. WL-TR-96-3099, Wright Lab, Wright-Patterson AFB, OH, 1996.

[5] John J. Burken, Ping Lu, and Zhenglu Wu, "Reconfigurable flight control designs with applications to the x-33 vehicle," in *AIAA Guidance, Navigation, and Control Conference and Exhibit*, Portland, OR, 1999, pp. 951–965, AIAA.

[6] Flavio Nardi and Anthony J. Calise, "Robust adaptive nonlinear control using single hidden layer neural networks," in *Proceedings of the 39th IEEE Conference on Decision and Control*, Sydney, Australia, 2000, pp. 3825–3830, IEEE.

[7] R. Rysdyk, F. Nardi, and A. J. Calise, "Robust adaptive nonlinear flight control using

neural networks," in *Proceedings of the American Control Conference*, San Diego, CA, 1999, pp. 2595–2599, IEEE.

[8] R. Rysdyk, F. Nardi, and A. J. Calise, "Nonlinear adaptive flight control using neural networks," *Control Systems Magazine*, vol. 18, no. 6, pp. 14–25, 1998.

[9] Michael B. McFarland and Anthony J. Calise, "Robustness analysis for a neural network based adaptive control scheme," in *Proceedings of the American Control Conference*, Philadelphia, PA, 1998, pp. 2158–2162, IEEE.

[10] Ki-Seok Kim, Keum-Jin Lee, and Youdan Kim, "Reconfigurable flight control system design using direct adaptive method," *Journal of Guidance, Control, and Dynamics*, vol. 26, no. 3, 2003.

[11] Sahjendra N. Singh, Marc Steinberg, and Anthony B. Page, "Adaptive control of high-performance aircraft with multiple control effectors," in *AIAA Guidance, Navigation, and Control Conference and Exhibit*, Portland, OR, 1999, pp. 1642–1652, AIAA.

[12] M. D. Tandale and John Valasek, "Structured adaptive model inversion control to simultaneously handle actuator failure and actuator saturation," in *AIAA Guidance, Navigation, and Control Conference and Exhibit*, Austin, TX, 2003, pp. 3938–3941, AIAA.

[13] R.A. Hess and S.R. Wells, "Sliding mode control applied to reconfigurable flight control design," *Journal of Guidance, Control, and Dynamics*, vol. 26, no. 3, 2003.

[14] Y. Shtessel, J. Buffington, M. Pachter, P. Chandler, and S. Banda, "Reconfigurable flight control on sliding modes addressing actuator deflection and deflection rate saturation," in *AIAA Guidance, Navigation, and Control Conference and Exhibit*, Boston,

MA, 1998, pp. 127–137, AIAA.

[15] Y. Shtessel, J. Buffington, and S. Banda, "Multiple time scale flight control using re-configurable sliding modes," in *Proceedings of the 37th IEEE Conference on Decision and Control*, Tampa, FL, 1998, pp. 4196–4201, IEEE.

[16] Yuri Shtessel, James Buffington, and Siva Banda, "Tailless aircraft flight control using multiple time scale reconfigurable sliding modes," *IEEE Transactions on Control Systems Technology*, vol. 10, no. 2, pp. 288–296, 1998.

[17] R.A. Hess and S.R. Wells, "Multi-input/multi-output sliding mode control for a tailless fighter aircraft," *Journal of Guidance, Control, and Dynamics*, vol. 26, no. 3, 2003.

[18] S.R. Wells and R.A. Hess, "Mimo sliding mode control for a tailless fighter aircraft, an alternative to reconfigurable architectures," in *AIAA Guidance, Navigation, and Control Conference and Exhibit*, Monterey, CA, 1998, pp. 1–13, AIAA.

[19] Jean-Jacques E. Slotine and Weiping Li, *Applied Nonlinear Control*, Prentice Hall, Englewood Cliffs, New Jersey, 1991.

[20] Petros A. Ioannou and Jing Sun, *Robust Adaptive Control*, Prentice Hall, Upper Saddle River, New Jersey, 1996.

[21] Bin Yao, "Adaptive robust control of nonlinear systems with applications to control of mechanical systems," Ph.D. dissertation, University of California at Berkeley, 1996.

[22] S. Sastry and M. Bodson, *Adaptive Control: Stability, Convergence, and Robustness*, Prentice Hall, Englewood Cliffs, New Jersey, 1989.

[23] I.L. Ashkenas, H.R. Jex, and D.T. McRuer, "Pilot-induced oscillations: Their cause and analysis," Tech. Rep. NOR-64-143, Norair Report, 1964.

[24] J.Q. Gong and Bin Yao, "Adaptive robust control without knowing bounds of parameter variations," in *Proceedings of the IEEE Conference on Decision and Control*, Phoenix, AZ, 1999, pp. 3334–3339, IEEE.

[25] C. Rohrs, L. Valavani, M. Athans, and G. Stein, "Robustness of continuous-time adaptive control algorithms in the presence of unmodeled dynamics," *IEEE Transactions on Automatic Control*, vol. 30, no. 9, pp. 881–889, 1985.

[26] Hassan K. Khalil, *Nonlinear Systems*, Prentice Hall, Upper Saddle River, New Jersey, 3rd edition, 1996.

[27] A.J. Krener, "On the equivalence of control systems and the linearization of nonlinear systems," *SIAM Journal of Optimal Control*, vol. 11, pp. 670–676, 1973.

[28] R. W. Brockett, "Feedback invariants for nonlinear systems," in *Procedings of th 6th IFAC World Congress*, Helsinki, Finland, 1978, vol. 6, pp. 1115–1120.

[29] A. Isidori, A. Krener, A.J. Gori, and S. Monaco, "Nonlinear decoupling via feedback: A differential geometric approach," *IEEE Transactions on Automatic Control*, vol. 26, pp. 331–345, April 1981.

[30] L. R. Hunt, R. Su, and G. Meyer, "Global transformations of nonlinear systems," *IEEE Transactions on Automatic Control*, vol. 28, no. 1, pp. 24–31, January 1988.

[31] Bernard Etkin, *Dynamics of Flight, Stability, and Control*, John Wiley and Sons, New York, 2nd edition, 1982.

VITA

James Robert Fisher received his Bachelor's degree from Texas A&M University in May 2001. Since that time he has become interested in nonlinear controls with specific interest in adaptive systems. He has been supported by the NASA Graduate Student Research Program and has worked with Dryden Flight Research Center. He has done work in dynamics and control of robotics at Johnson Space Center as well as in dynamics and control of aircraft at Dryden. He is currently beginning his PhD at Texas A&M University in Aerospace Engineering.